This is a repository copy of *Pattern, style and timing of British–Irish Ice Sheet advance and retreat over the last 45 000 years: evidence from NW Scotland and the adjacent continental shelf*.

White Rose Research Online URL for this paper:
https://eprints.whiterose.ac.uk/174135/

Version: Published Version

Article:
Bradwell, T., Fabel, D., Clark, C.D. orcid.org/0000-0002-1021-6679 et al. (16 more authors) (2021) Pattern, style and timing of British–Irish Ice Sheet advance and retreat over the last 45 000 years: evidence from NW Scotland and the adjacent continental shelf. Journal of Quaternary Science, 36 (5). pp. 871-933. ISSN 0267-8179

https://doi.org/10.1002/jqs.3296

Reuse
This article is distributed under the terms of the Creative Commons Attribution (CC BY) licence. This licence allows you to distribute, remix, tweak, and build upon the work, even commercially, as long as you credit the authors for the original work. More information and the full terms of the licence here:
https://creativecommons.org/licenses/

Takedown
If you consider content in White Rose Research Online to be in breach of UK law, please notify us by emailing eprints@whiterose.ac.uk including the URL of the record and the reason for the withdrawal request.

eprints@whiterose.ac.uk
https://eprints.whiterose.ac.uk/

JOURNAL OF QUATERNARY SCIENCE (2021) 1–63 ISSN 0267-8179. DOI: 10.1002/jqs.3296

JQS Journal of Quaternary Science QRA Quaternary Research Association

Pattern, style and timing of British–Irish Ice Sheet advance and retreat over the last 45 000 years: evidence from NW Scotland and the adjacent continental shelf

TOM BRADWELL,[1,2]* DEREK FABEL,[3] CHRIS D. CLARK,[4] RICHARD C. CHIVERRELL,[5] DAVID SMALL,[6] RACHEL K. SMEDLEY,[5] MARGOT H. SAHER,[7] STEVEN G. MORETON,[8] DAYTON DOVE,[2] S. LOUISE CALLARD,[9] GEOFF A. T. DULLER,[10] ALICIA MEDIALDEA,[4,11] MARK D. BATEMAN,[4] MATTHEW J. BURKE,[5] NEIL MCDONALD,[1] SEAN GILGANNON,[4] SALLY MORGAN,[12] DAVID H. ROBERTS[6] and COLM Ó COFAIGH[6]

[1]University of Stirling, UK
[2]British Geological Survey, Edinburgh, UK
[3]University of Glasgow/Scottish Universities Environmental Research Centre (SUERC), East Kilbride, UK
[4]University of Sheffield, UK
[5]University of Liverpool, UK
[6]Durham University, UK
[7]University of Bangor, UK
[8]NERC Radiocarbon Lab, East Kilbride, UK
[9]University of Newcastle, UK
[10]Aberystwyth University, UK
[11]National Research Centre on Human Evolution (CENIEH), Burgos, Spain
[12]University of Leicester, UK

Received 28 July 2020; Revised 9 February 2021; Accepted 12 February 2021

ABSTRACT: Predicting the future response of ice sheets to climate warming and rising global sea level is important but difficult. This is especially so when fast-flowing glaciers or *ice streams,* buffered by ice shelves, are grounded on beds below sea level. What happens when these ice shelves are removed? And how do the ice stream and the surrounding ice sheet respond to the abruptly altered boundary conditions? To address these questions and others we present new geological, geomorphological, geophysical and geochronological data from the ice-stream-dominated NW sector of the last British–Irish Ice Sheet (BIIS). The study area covers around 45 000 km^2 of NW Scotland and the surrounding continental shelf. Alongside seabed geomorphological mapping and Quaternary sediment analysis, we use a suite of over 100 new absolute ages (including cosmogenic-nuclide exposure ages, optically stimulated luminescence ages and radiocarbon dates) collected from onshore and offshore, to build a sector-wide ice-sheet reconstruction combining all available evidence with Bayesian chronosequence modelling. Using this information we present a detailed assessment of ice-sheet advance/retreat history, and the glaciological connections between different areas of the NW BIIS sector, at different times during the last glacial cycle. The results show a highly dynamic, partly marine, partly terrestrial, ice-sheet sector undergoing large size variations in response to sub-millennial-scale climatic (Dansgaard–Oeschger) cycles over the last 45 000 years. Superimposed on these trends we identify internally driven instabilities, operating at higher frequency, conditioned by local topographic factors, tidewater dynamics and glaciological feedbacks during deglaciation. Specifically, our new evidence indicates extensive marine-terminating ice-sheet glaciation of the NW BIIS sector during Greenland Stadials 12 to 9 – prior to the main 'Late Weichselian' ice-sheet glaciation. After a period of restricted glaciation, in Greenland Interstadials 8 to 6, we find good evidence for rapid renewed ice-sheet build-up in NW Scotland, with the Minch ice-stream terminus reaching the continental shelf edge in Greenland Stadial 5, perhaps only briefly. Deglaciation of the NW sector took place in numerous stages. Several grounding-zone wedges and moraines on the mid- and inner continental shelf attest to significant stabilizations of the ice-sheet grounding line, or ice margin, during overall retreat in Greenland Stadials 3 and 2, and to the development of ice shelves. NW Lewis was the first substantial present-day land area to deglaciate, in the first half of Greenland Stadial 3 at a time of globally reduced sea-level c. 26 ka BP, followed by Cape Wrath at c. 24 ka BP. The topographic confinement of the Minch straits probably promoted ice-shelf development in early Greenland Stadial 2, providing the ice stream with additional support and buffering it somewhat from external drivers. However, c. 20–19 ka BP, as the grounding-line migrated into shoreward deepening water, coinciding with a marked change in marine geology and bed strength, the ice stream became unstable. We find that, once underway, grounding-line retreat proceeded in an uninterrupted fashion with the rapid loss of fronting ice shelves – first in the west, then the east troughs – before eventual glacier stabilization at fjord mouths in NW Scotland by ~17 ka BP. Around the same time, ~19–17 ka BP, ice-sheet lobes readvanced into the East Minch – possibly a glaciological response to the marine-instability-triggered loss of adjacent ice stream (and/or ice shelf) support in the Minch trough. An independent ice cap on Lewis also experienced margin oscillations during mid-Greenland Stadial 2, with an ice-accumulation centre in West Lewis existing into the latter part of Heinrich Stadial 1.

*Correspondence: Tom Bradwell, as above.
Email: tom.bradwell@stir.ac.uk

© 2021 The Authors. *Journal of Quaternary Science* Published by John Wiley & Sons Ltd
This is an open access article under the terms of the Creative Commons Attribution License, which permits use, distribution and reproduction in any medium, provided the original work is properly cited.

Final ice-sheet deglaciation of NW mainland Scotland was punctuated by at least one other coherent readvance at c. 15.5 ka BP, before significant ice-mass losses thereafter. At the glacial termination, c. 14.5 ka BP, glaciers fed outwash sediment to now-abandoned coastal deltas in NW mainland Scotland around the time of global Meltwater Pulse 1A. Overall, this work on the BIIS NW sector reconstructs a highly dynamic ice-sheet oscillating in extent and volume for much of the last 45 000 years. Periods of expansive ice-sheet glaciation dominated by ice-streaming were interspersed with periods of much more restricted ice-cap or tidewater/fjordic glaciation. Finally, this work indicates that the role of ice streams in ice-sheet evolution is complex but mechanistically important throughout the lifetime of an ice sheet – with ice streams contributing to the regulation of ice-sheet health but also to the acceleration of ice-sheet demise via marine ice-sheet instabilities. © 2021 The Authors. *Journal of Quaternary Science* Published by John Wiley & Sons Ltd

KEYWORDS: Bayesian modelling; ice stream; marine ice-sheet instability; palaeoglaciology; Weichselian

Introduction

Predicting the future response of ice sheets to climate warming and rising global sea level is important but difficult owing to the currently unquantified dynamical response of large fast-flowing glaciers or *ice streams* grounded on beds below sea level. These marine ice-sheet sectors, exemplified in the Weddell Sea and Amundsen Sea Embayments of West Antarctica, are thought to be most vulnerable to future warming; observations and some models are predicting a step-change acceleration in glacier flow rate and subsequent ice-mass loss to the ocean following the removal of supporting ice shelves in the near future (e.g. Golledge *et al.*, 2015; De Conto and Pollard, 2016; Pattyn *et al.*, 2018). The dynamic phenomena inherent to marine ice sheets currently produce unquantified uncertainties in numerical ice-sheet models, hampering our ability to confidently predict ice-sheet behaviour over the next 50–500 years (IPCC, 2018).

Recent reconstructions of the last British–Irish Ice Sheet (BIIS) (Bradwell *et al.*, 2008a, Sejrup *et al.*, 2009; Clark *et al.*, 2012) suggest it was considerably larger than previously thought (cf. Bowen *et al.*, 2002, Boulton *et al.*, 2001), and predominantly marine-based with numerous marine-influenced palaeo-ice streams terminating on the continental shelf discharging ice into the North Atlantic Ocean and North Sea Basin (e.g. Clark *et al.*, 2012; Bradwell and Stoker, 2015a, Sejrup *et al.*, 2016; Small *et al.*, 2017; Callard *et al.*, 2018; Scourse *et al.*, 2019). At its maximum, around 24 000–27 000 years ago, the BIIS covered approximately 850 000 km^2 – around half the size of the present-day Greenland Ice Sheet – with an ice volume equivalent to 2.5 m of global sea level (Hubbard *et al.*, 2009; Clark *et al.*, 2012). In its NW sector, a large ice stream, fed from ice-sheet accumulation areas in northern and western Scotland, operated periodically at times of more extensive Pleistocene glaciation [i.e. Marine Isotope Stage (MIS) 2–16] (Stoker and Bradwell, 2005; Bradwell *et al.*, 2007). Known as the Minch Ice Stream (MnIS), the trunk of this fast-flow corridor occupied the submarine trough, now a 40-km-wide seaway, between mainland Scotland and the Outer Hebrides, with ice-stream tributaries extending 10–100 km inland. The total drainage area of the MnIS was c. 15 000 km^2 during times of maximal glaciation. Over the last 15 years, the Quaternary geology and glacial geomorphology of the MnIS have been studied in some detail. These studies have focused on: the landform evidence of ice streaming onshore (Bradwell *et al.*, 2007, 2008a: Hughes *et al.*, 2014); the submarine sediment and landform record (Bradwell *et al.*, 2008a; Stoker *et al.*, 2009; Bradwell and Stoker, 2015a, 2016); the evidence for thermal zonation and tributary flow (Ballantyne, 2010; Fabel *et al.*, 2012; Bradwell, 2013); and most recently the submarine geological record and chronology of grounding-line retreat (Bradwell *et al.*, 2019). In addition to this, numerical modelling has shown the MnIS to be a dynamic yet quasi-stable feature that dominated flow geometry in the ice sheet's NW sector (Boulton and Hagdorn, 2006; Hubbard *et al.*, 2009; Gandy *et al.*, 2019). Higher order modelling work, focusing on the MnIS catchment, has highlighted the importance of subglacial bed slope, trough width and ice-shelf buttressing in controlling the retreat rate and overall stability of the ice stream (Gandy *et al.*, 2018) – a finding also emphasized in recent empirical work (Bradwell *et al.*, 2019).

Although much is now known about the former MnIS, many questions still remain. Perhaps the most pertinent relate to its mode of operation over time, its discharge flux and frontal fluctuation history, as well as the response of adjacent non-streaming ice-sheet sectors. Moreover, relatively little research has been undertaken on the glacial history of Lewis, the evidence for ice-sheet termini here and the evolution of an independent ice cap on the Outer Hebrides. This is somewhat surprising given its location in the north-western periphery of the BIIS and situated at the western lateral margin of the former MnIS. Another unresolved issue relates to the precise timing and maximal extent of the ice stream on the Hebrides continental shelf during the last glacial cycle. Did the ice sheet reach the continental shelf edge (or shelfbreak) in the NW sector? And if so, when and by what mechanism? Was shelf-edge glaciation restricted to earlier Pleistocene glacial stages (pre-MIS 4), as proposed by some (Stoker *et al.*, 1993; Stoker and Bradwell, 2005; Bradwell and Stoker, 2015b)? Or did shelf edge glaciation occur more recently, as others have surmised, during the Last Glacial Maximum (in MIS 2; e.g. Bradwell *et al.*, 2008a; Chiverrell and Thomas, 2010; Clark *et al.*, 2012; Sejrup *et al.*, 2016)? Was the ice sheet terminus grounded (as an ice stream) or partially floating in the form of an ice shelf? These questions are important as they help to define not only the lateral extent, thickness and style of ice-sheet glaciation but also the mechanism of sediment delivery to the extra-glacial continental shelf and slope, and the potential for ice-free land areas during periods of full glaciation and greatly lowered sea levels.

Ice shelf formation around the former BIIS has been hypothesized (e.g. Peters *et al.*, 2015, 2016) but until recently was a largely unexplored topic. The seafloor of the Minch and Malin Sea are relatively unusual in a British and Irish context for exhibiting large grounding-zone wedges (GZWs) (Callard *et al.*, 2018; Bradwell *et al.*, 2019) akin to those seen on deglaciated continental shelves in polar latitudes (Batchelor and Dowdeswell, 2015). Did ice shelves form in the Minch as the submarine geomorphology would strongly suggest? And if so, what was their role in buttressing or protecting the MnIS from rapid change? Importantly, what happened when these ice shelves no longer provided ice stream restraint? And finally, how and when did ice streaming in NW Scotland cease? Recent work has shown that MnIS recession rates were temporally variable and occurred in stepped phases, with rapid losses separated by stabilizations probably governed by

bathymetric/topographic controls rather than purely external forcing factors (Bradwell *et al.*, 2019). Final ice-stream collapse appears to have been rapid, perhaps even catastrophic (Gandy *et al.*, 2018; Bradwell *et al.*, 2019). But what was the wider impact of ice-stream collapse on the configuration, mass balance and flow geometry of the ice sheet in this sector?

This paper seeks to address these research questions, specifically relating to Minch ice-stream decay and the ice-sheet deglaciation of NW Scotland more generally. By doing so we generate new temporal and spatial constraints for the advance, maximum extent and subsequent deglaciation of the BIIS's NW sector, using a multi-proxy dating approach [accelerator mass spectrometry (AMS) radiocarbon, optically simulated luminescence (OSL) and cosmogenic-nuclide analyses] on glacial deposits both onshore and offshore. The research forms part of a larger consortium project, called Britice-Chrono, with three main objectives: (i) to greatly improve the existing chronological database for a whole ice-sheet complex, i.e. the BIIS; (ii) to better understand the long-term behaviour of the BIIS – as an analogue for contemporary marine-terminating ice sheets; and (iii) to generate robust empirical constraints for numerical experiments seeking to validate model output with greater confidence [Clark *et al.*, (foreword) this issue; and other papers in this issue]. This article constitutes an end-of-project overview, bringing together all results from several terrestrial field campaigns and a dedicated scientific marine cruise, with laboratory analyses and data interpretations, conducted by a team of researchers over 6 years.

Study area

This study concerns the NW sector of the former BIIS. The study area comprises a total land and seafloor area of approximately 45 000 km^2 centred on the Minch (Fig. 1), a 30-to 40-km-wide seaway or strait separating NW mainland Scotland from the Outer Hebrides (Gaelic: *Eilean nan t-Siar*), but also includes the adjacent land areas and a large area of submarine continental shelf. The Minch and its bathymetric continuation as a cross-shelf trough acted as the main flow path of a former ice stream that drained much of the NW sector of the BIIS during Late Pleistocene glaciations (Stoker and Bradwell, 2005; Bradwell *et al.*, 2007; Bradwell and Stoker, 2015a, 2016). The study area also includes the coastal fringes of NW mainland Scotland (north of 57.2°N); the Isle of Lewis, but not Harris; parts of the Isle of Skye, Raasay and other islands close to NW Scotland, as well as those small uninhabited islands and skerries much further offshore (e.g. Flannan Islands, North Rona, Sula Sgeir). Numerous bathymetric highs and shallow banks also occur closer inshore and on the mid- to outer continental shelf. In the central portion of the Minch at ~58°N, ~6°W a large bathymetric high – known on hydrographic maps as 'East Shiant Bank', but referred to here simply as the Mid-Trough Bedrock High (MTBH), rises to within 35 m of present-day mean sea level (Figs. 1 and 2). The study area is bounded to the west at 7.75°W and to the east at 4.75°W, where it abuts the adjacent Britice-Chrono transect area: Shetland and northern North Sea sector (Transect 1) (Bradwell *et al.*, 2019, this issue). The NW extent of the study area is arbitrarily defined by the 1000-m water depth contour (Fig. 1). For convenience, the whole study area is referred to as Britice-Chrono Transect 8 (T8).

Previous work and existing geochronology

The glacial history and Quaternary geology of NW Scotland, including the Minch and the surrounding continental shelf, have been the focus of many studies over the past 50 years. Much pioneering work on the stratigraphy of Quaternary deposits on the Hebrides Shelf, in the Minch and on the seafloor around the Inner Hebrides was carried out by the British Geological Survey during the UK Continental Shelf mapping programme (1970–1990). This information sets out a broad stratigraphic framework of Late Quaternary erosional and depositional events, and inferred ice-sheet changes, based largely on the interpretation of numerous seismic (sub-bottom) profiles, geological boreholes and shallow seabed cores (Fyfe *et al.*, 1993; Stoker *et al.*, 1993; Ritchie *et al.*, 2011) and the formal stratigraphic overview documents (McMillan *et al.*, 2011; Stoker *et al.*, 2011). However, these stratigraphic sub-divisions are underpinned by relatively few absolute ages.

Building on this work, more recent mapping compilations based on best-available bathymetry data have brought the seabed landscape into sharp focus and enhanced the record of Late Weichselian deglaciation in the NW sector of the BIIS (Bradwell and Stoker, 2015a, b). In addition to these works, two excellent, wide-ranging reviews on the glacial history of Scotland from a largely terrestrial perspective have recently been published (Ballantyne and Small, 2019; Merritt *et al.*, 2019).

The study area (Transect 8) possesses an unusual level of landscape diversity in a British Isles context, within a relatively restricted terrestrial area (<20 000 km^2) (Figs. 1 and 2). The landscapes of NW Scotland include former ice-sheet *core* areas – the main centres of ice-mass accumulation; a major palaeo-ice-stream land system, including its tributaries and catchments; as well as ice-sheet *peripheral* areas – where glaciation(s) has been much less marked and less prevalent. Typically core areas exhibit some preserved pre-glacial sediments and landforms due to limited subglacial erosion in predominantly cold-based (frozen-bed) regions (e.g. Kleman and Borgstrom, 1996; Kleman and Glasser, 2007). However, few pre-glacial sediment sequences are known from the generally alpine and fjordic scenery of NW Scotland and Skye, with the exception of mountain summit regolith blankets and blockfields (Ballantyne and Hall, 2008; Fabel *et al.*, 2012; Merritt *et al.*, 2019). On lower ground east and west of the present-day watershed in NW Scotland, probable pre-glacial sediments have been recorded, but none are dated or in secure stratigraphic settings (e.g. Krabbendam and Bradwell, 2014). Further away from the ice-mass centres, in the geographical extremities of the Outer Hebrides, rare but important pre-glacial sediments and landforms have been preserved with good stratigraphic integrity in an ice-sheet peripheral setting (Peacock, 1984; Gordon and Sutherland, 1993). Thought to relate to higher sea levels in MIS 5, and non-glacial cold phases in the build-up to Late Weichselian glaciation (Gordon and Sutherland, 1993), pre-MIS 2 sediments in NW Lewis, although not yet dated, remain some of the most controversial terrestrial sequences in Scotland (e.g. Sutherland and Walker, 1984; Gordon and Sutherland, 1993; Merritt *et al.*, 2019).

This landscape diversity continues on the submerged continental shelf, with well-preserved landforms and sediment sequences in key locations, from the fjords to the upper continental slope (Stoker *et al.*, 1993; Bradwell and Stoker, 2016) (Figs. 1 and 2). Although the Quaternary sediments and landforms are less accessible and, as a result, have been less intensely studied, there is good evidence, recovered from boreholes, of pre-MIS 2 glacial and non-glacial sediment sequences preserved on the mid- and outer shelf (Stoker *et al.*, 1993; Ritchie *et al.*, 2011) – both within the former MnIS track and adjacent to it. During cold periods of the last glacial cycle, the Outer Hebrides nourished a glaciologically independent ice mass (Gordon

© 2021 The Authors. *Journal of Quaternary Science* Published by John Wiley & Sons Ltd

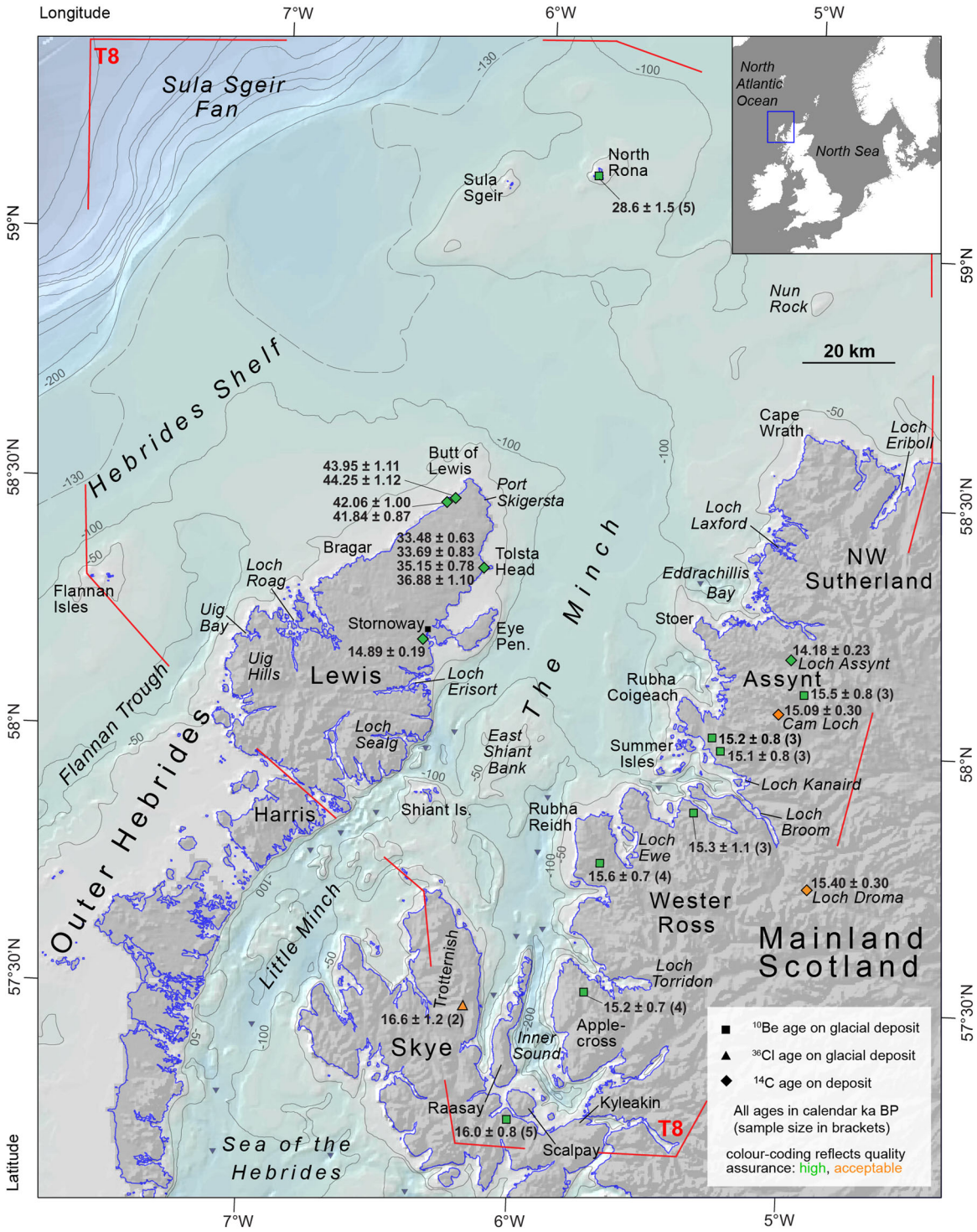

Figure 1. Location map showing study area in NW Scotland and the adjacent continental shelf. Places referred to in the text are labelled; terrestrial locations in roman font; hydrographic features in *italic* font. Inset box shows location in NW Europe. Red dashed line defines study area, referred to as Britice-Chrono Transect 8 (or T8). Isobaths at 50, 100, 130 (=MIS 2 eustatic sea-level minimum; not GIA corrected) and 200 m vertical intervals on shelf; with 100-m isobaths beyond shelf. Bathymetry data from British Geological Survey and GEBCO 2014 sources. Topographic data from NERC Earth Observation Data Centre. Key pre-existing age assessments (onshore and offshore) also shown, taken from Britice database (Hughes *et al.*, 2011); colour coding relates to quality assurance (green = robust; amber = acceptable; red = unreliable) after Small *et al.* (2017). All published TCN surface-exposure ages are re-calculated using Lm scaling (CRONUS-Earth calculator; Balco *et al.*, 2008) and Loch Lomond Production rate (LLPR; Fabel *et al.*, 2012). An erosion rate of 1 mm ka^{-1} is assumed. All ages are presented in calendar kiloyears (ka) before present. [Color figure can be viewed at wileyonlinelibrary.com].

and Sutherland, 1993; Stone and Ballantyne, 2006) which, at certain times, contributed to the MnIS (Bradwell *et al.*, 2007). No evidence currently exists for ice-sheet accumulation centres on the continental shelf to the north or west of Lewis, despite the extensive bedrock platform at < 50 m below present-day sea level (Fig. 2), providing ample room for ice to accumulate.

Existing geochronological constraints on the **advance** of the last BIIS in NW Scotland are based on a small number of radiocarbon dates in terrestrial settings, supported by iceberg-rafted sediments in deep-water NE Atlantic Ocean cores with chronological control. By contrast, existing timing data on ice-sheet **retreat** comes from a relatively large number of cosmogenic-nuclide exposure ages ($n = 36$) clustered on a

© 2021 The Authors. *Journal of Quaternary Science* Published by John Wiley & Sons Ltd

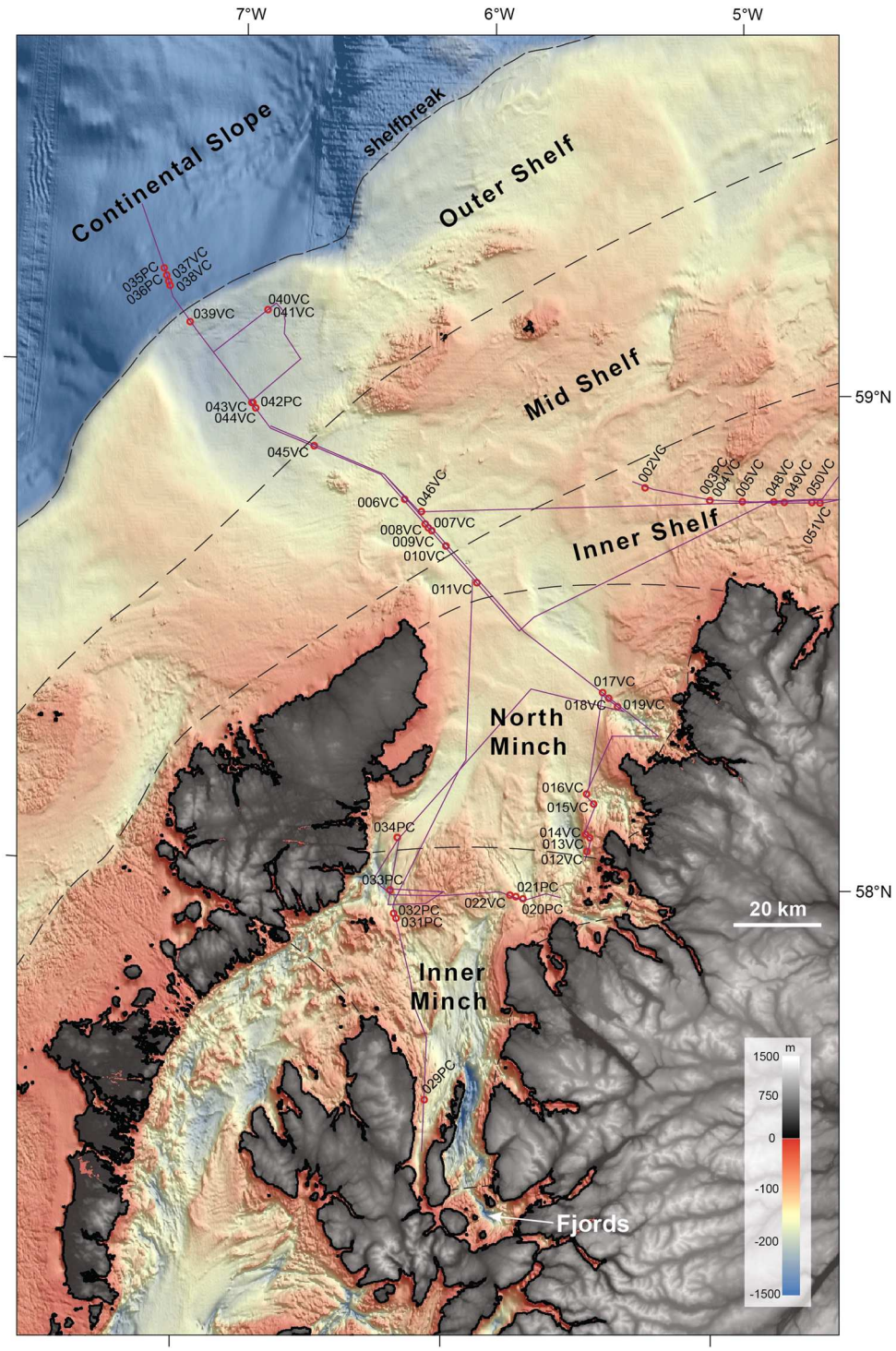

Figure 2. Regional present-day bathymetry of the study area showing offshore sample sites. Merged and re-gridded EMODnet 2018 data (EMODnet Bathymetry Consortium, 2018). DTM lit from the NE/045 to generate hillshade model. Note: colour palette stretched to highlight continental shelf water depths (mainly < 200 m). Greyscale onshore DEM generated from elevation data accessed via NERC Earth Observation Data Centre. Thin magenta line shows JC123 offshore data collection transects (ship's track) with core sites (red circles) labelled. Informal names of offshore/shelf regions used in this study shown with dashed lines indicating boundaries. Continental shelfbreak approximated by 200-m isobath. [Color figure can be viewed at wileyonlinelibrary.com].

few ice-sheet moraines and mountain tops, supported by radiocarbon dates in spatially disparate localities (Ballantyne and Small, 2019) (see Fig. 1). All absolute dating constraints relating to the last BIIS were compiled and collated in a geographical information system (GIS) prior to the start of the Britice-Chrono project (Hughes *et al.*, 2011) and updated in 2014 (Small *et al.*, 2017). All numerical ages were systematically re-calculated (if appropriate) and quality-checked using a semi-quantitative 'traffic light' system – where green denotes reliable, robust ages; amber denotes acceptable with caveats; and red denotes unreliable or poor context dates. The existing deglacial age assessments (prior to the Britice-Chrono project) for the NW sector are shown in Fig. 1. In addition, we have added the small number of reliable dates related to ice-sheet advance < 50 ka cal BP (Fig. 1). These are all briefly discussed below.

Late Weichselian BIIS advance in NW Scotland is currently constrained by one key site at Tolsta Head in eastern Lewis, and supported by two others: Dell Sands (Suainebost), NW Lewis, and the Inchnadamph 'Bone Caves' in Assynt. Strong

© 2021 The Authors. *Journal of Quaternary Science* Published by John Wiley & Sons Ltd

evidence comes from organic sediments beneath over-consolidated glacial diamict (ice-stream till) in a lee-side cliff-top setting at Tolsta Head. The organic sediments have been AMS ^{14}C dated to 38–33 cal ka BP, when calibrated (Whittington and Hall, 2002). These ages, and the fragmentary pollen spectra preserved, indicate cool ice-free interstadial conditions in NE Lewis, and by inference, the North Minch during Greenland Interstadial 8 (GI-8) to GI-6 (or GI-5) (Whittington and Hall, 2002). The dates constrain the timing of ice-sheet advance across northern Lewis and the continental shelf to sometime after this.

The lowest exposed subglacial till at Dell Sands/Traigh Chumail, NW Lewis, yielded four finite conventional radiocarbon ages from reworked shells ranging between 40.5 and 44.3 ka cal BP, when calibrated (Sutherland, 1986; Hughes *et al.*, 2011). These ages support the Tolsta Head chronology and also indicate that, prior to ice-sheet advance across Northern Lewis from the south-east, open-water marine conditions existed at least periodically in the (North) Minch probably until c. GI-9 (~40 ka BP).

The third important site, located 20 km inland from the Minch, provides a wealth of uranium-series and radiocarbon dates that have been used to demonstrate ice-free conditions at various times in the mountains of the NW Highlands over the last ~100 ka (Lawson, 1995, 2010; Lawson *et al.*, 2014). Numerous radiocarbon dates on faunal remains and U-series dates from speleothems in the karstic cave systems near Inchnadamph indicate predominantly ice-free conditions between ~57 ka and ~38 ka cal BP (and possibly c. 30 ka cal BP), appearing to place the onset of Late Weichselian glaciation in the mountains of NW Scotland after GI-8 (and possibly after GI-5) (Lawson *et al.*, 2014). However, the complex stratigraphic settings, limestone-bedrock-induced 'hard-water effect' and dating uncertainties (10–20% on U-series ages) complicate the interpretation of these ages. Furthermore, some of the younger (MIS 2) radiocarbon dates suggesting ice-free conditions here c. 25–29 ka cal BP are strongly at odds with the wider deglacial chronology and offshore Late Weichselian stratigraphy (Stoker *et al.*, 1993; Bradwell *et al.*, 2008a; Everest *et al.*, 2013; Ballantyne and Small, 2019; Merritt *et al.*, 2019).

Other constraints on ice-sheet advance such as ice-rafted debris (IRD) in marine cores are multi-factorial and do not *demonstrate* ice-sheet advance but have been used to *infer* periods of more extensive, marine-terminating glaciation in the NE Atlantic (e.g. Knutz *et al.*, 2002; Scourse *et al.*, 2009; Hibbert *et al.*, 2010). Careful geochemical provenancing of IRD has been used to relate debris to particular geological provinces (e.g. NW British Isles Palaeogene Igneous Province), thus strongly implicating a NW BIIS origin. Importantly, detailed study of BIIS-diagnostic IRD grains in piston core MD04-2822 (Hibbert *et al.*, 2010) recorded a pulse in BIIS debris c. 41–39 ka BP followed by a marked absence of debris from c. 38 to c. 35 ka BP, followed by a gradual increase in IRD flux from 35 to 30 ka BP, suggesting extensive ice-sheet glaciation after the Tolsta (or Alesund) Interstadial (GI-8 to GI-5). The reconstructed IRD flux adjacent to the BIIS includes a step-change, ten-fold, increase in IRD flux from c. 29.0 to c. 27.4 ka BP taken to indicate extensive shelf-edge glaciation west of Scotland (Hibbert *et al.*, 2010). This general pattern from core MD04-2822 accords with IRD fluxes reconstructed at other core sites nearby (MD95-2006: Knutz *et al.*, 2001; MD04-2829: Scourse *et al.*, 2009) and ~400 km further south (MD01-2461: Peck *et al.*, 2007). However, the link between IRD peaks and ice-sheet advances is still uncertain, especially at distal deep-water sites receiving sediment from numerous sources. Prominent IRD peaks in these cores are now thought to indicate short-lived mass-loss events – such as ice-front collapses or massive calving events – as well as gradual ice-sheet mass increases. Hence, no simple mechanistic model of IRD generation currently exists (Scourse *et al.*, 2009; Hibbert *et al.*, 2010).

The BIIS-wide dating database (Hughes *et al.*, 2011; Small *et al.*, 2017) shows that dated deglacial sites are more common in NW Scotland. Most of these relate to moraines of the Wester Ross Readvance (WRR) – a prominent former ice-sheet oscillation that affected NW mainland Scotland from 57°N to 58°N. Twenty-two terrestrial cosmogenic-nuclide (TCN) exposure ages from this moraine, sampled in several localities by two separate studies (Bradwell *et al.*, 2008b; Ballantyne *et al.*, 2009), yield re-calculated ages tightly clustered around 15.3 ± 0.7 ka BP (Ballantyne and Small, 2019). This revised chronology demonstrates that the ice-sheet margin in NW Scotland readvanced to a fjord-mouth setting prior to 15.3 ka BP, and was already in retreat several centuries *before* the dramatic warming at the end of MIS 2 (14.7 ka BP; Lowe *et al.*, 2008). TCN ^{10}Be exposure ages have allowed the geographical extent of WRR-equivalent ice-sheet oscillations to be extended south to Skye (Small *et al.*, 2012) and north to Assynt (Bradwell *et al.*, 2008b), showing a broadly coeval ice-sheet response (16.0–15.0 ka BP) over > 100 km (Fig. 1).

Other important TCN age constraints on ice-sheet recession in NW Scotland are from deglaciated high-elevation sites and mountain summits. Several individual dates from Harris (Outer Hebrides) indicate ice-free conditions by 17.3-16.5 ka BP (Stone and Ballantyne, 2006); whilst those from the mountains of Wester Ross (mainland) demonstrate ice-free conditions above 500 m asl by ~16 ka BP, indicating considerable ice-sheet thinning in the preceding millennia (Fabel *et al.*, 2012). Two ^{36}Cl exposure ages from bedrock at 450 m asl in Trotternish, Skye (Stone *et al.*, 1998), support this chronology, when recalculated, suggesting deglaciation here by 16–17 ka BP (Ballantyne and Small, 2019) (Fig. 1).

Robust deglaciation constraints on final ice-sheet disappearance during MIS 2 are still surprisingly rare in NW Scotland (Fig. 1). The Lateglacial chronology is complicated by the regrowth and readvance of mountain ice masses in NW mainland Scotland, Skye and Lewis during Greenland Stadial 1 (GS-1) (known in Britain as the 'Loch Lomond Readvance'). Although the geographical extent and chronology of GS-1 glaciers in Scotland are now relatively firmly constrained and well understood (e.g. Golledge *et al.*, 2008; Golledge, 2010; Ballantyne, 2012; Macleod *et al.*, 2011; Bickerdike *et al.*, 2018; Lowe *et al.*, 2019) – though the chronology is strongly contested by Bromley *et al.* (2014, 2018) – the final stages of ice-sheet waning, after the WRR and into GI-1 (15.0–13.0 ka BP), are not well constrained. The three, most-often cited, Lateglacial sites in mainland NW Scotland constraining final ice-sheet wastage are: Loch Droma (Kirk and Godwin, 1963), Cam Loch (Pennington *et al.*, 1972) and Loch Assynt (Boomer *et al.*, 2012) (Fig. 1). However, Loch Droma and Cam Loch were analysed before the routine use of AMS dating techniques, and all three sites have their own site-specific difficulties. Only one Lateglacial site in Lewis with good stratigraphic context is included in the dating database (Hughes *et al.*, 2011) (Fig. 1). AMS radiocarbon dates from organic sediments overlying marine clays near Stornoway, at 15 m asl, indicate deglaciation some time before ~14.9 ka cal BP (Hedges *et al.*, 1989).

Methods

Onshore and offshore data for this study were collected in several complementary field campaigns. Onshore fieldwork took place in 2013 and 2014 on Skye, NW mainland

© 2021 The Authors. *Journal of Quaternary Science* Published by John Wiley & Sons Ltd

Scotland and Lewis (Outer Hebrides). Offshore fieldwork constituted one-third of a 30-day scientific cruise (JC123) onboard the *RRS James Cook* in July 2015. Legacy data analysis and revised glacial landform mapping was undertaken prior to the onshore fieldwork and offshore cruise. This was supplemented, interpreted and revisited during and after the respective data-collection campaigns. The numerous methods and datasets used in this research are described below.

Terrestrial cosmogenic-nuclide exposure-age dating

Eleven sampling sites in NW Scotland were identified to optimally constrain the wider ice-sheet pattern in Lewis and on either side of the Minch. Clear and unambiguous glacially transported boulders in geographically important localities were targeted, as well as specific glacial landforms (e.g. recessional moraines) where appropriate. In the field, glacially transported boulders were chosen based on their specific lithological suitability (quartz-bearing), morphological setting (to avoid local shielding) and large size (to avoid potential disturbance). Samples were collected from the top surface of boulders using a hammer and chisel. Boulders exhibiting unusual surface weathering or potential signs of pre-glacial exposure were avoided. Precise locations, detailed site-specific descriptions and topographic shielding were recorded for each sample (Tables 1 and 2). At least three separate samples were collected from each site. We assumed that samples at each site, typically collected within a 500-m radius, would share a common deglaciation history and therefore common exposure age (Applegate *et al.*, 2012; Small *et al.*, 2017).

All samples were prepared and processed at the University of Glasgow (School of Geographical and Earth Sciences). For ^{10}Be analysis, quartz was separated from the 250–500-μm fraction using standard mineral separation techniques (Kohl and Nishiizumi, 1992) and purified by ultrasonification in 2% HF/HNO_3 to remove remaining contaminants, mainly feldspars and meteoric ^{10}Be. The purity of the leached samples was assessed by aluminium content using flame atomic absorption spectrometry with bulk Al content considered a proxy for the presence of feldspars. Be extraction was carried out at two independent laboratories housed at the Scottish Universities Environmental Research Centre (SUERC): the NERC Cosmogenic Isotope Analysis Facility and the SUERC Cosmogenic Nuclide Laboratory, using established procedures (Child *et al.*, 2000).

For ^{36}Cl analysis, whole rock samples were crushed and sieved to 250–710 μm. An initial ~100-g aliquot of the sample was etched overnight in 2 M HNO_3 and 40% HF to remove meteoric Cl and contaminants, losing ~60% of the sample during the process. Afterwards a ~5-g etched split was taken for major element analysis by inductively coupled plasma optical emission spectrometry (ICP-OES) and an additional ~25 g for AMS target preparation. The samples and two blanks were dissolved in HF with a ^{35}Cl-enriched spike (~99%). Samples were then prepared according to Marrero (2012). Chlorine was extracted and purified to produce an AgCl target for AMS analysis. For the purpose of determining the effect of including trace elemental concentrations we recalculated the oldest and the youngest age obtained in this study using minimum and maximum concentrations for trace elements (Gale *et al.*, 2013) and indicative U and Th values (Larsen and Gottfried, 1960). The variations in calculated ages are entirely within the calculated age uncertainties.

The ^{10}Be/^{9}Be, ^{37}Cl/^{35}Cl and ^{36}Cl/^{35}Cl ratios of all samples were measured on the 5-MV AMS pelletron at SUERC (Xu *et al.*, 2010). ^{10}Be and ^{36}Cl measurements were normalized to NIST27900 [^{10}Be/^{9}Be = 2.79×10^{-11}] and Z93-0005 [^{36}Cl/^{35}Cl = 1.2×10^{-12}], respectively. Measured ratios were converted to concentrations. Blank corrections were propagated in quadrature with attendant carrier and AMS analytical uncertainties ranging from 1.2 to 10.3% for ^{10}Be and 1.4 to 4.7% for ^{36}Cl (Tables 3 and 4).

We calculate ^{10}Be exposure ages using the CRONUS-Earth calculator (Developmental version; Wrapper script 2.3, Main calculator 2.1, constants 2.2.1, muons 1.1; http://hess.ess.washington.edu/math/al_be_v22/al_be_calibrate_v22.php; accessed 18 July 2016; Balco *et al.*, 2008) and ^{36}Cl exposure ages using the CRONUScalc calculator (http://web1.ittc.ku.edu:8888/2.0/html; accessed 2 June 2016; Marrero *et al.*, 2016). Ages calculated in the CRONUS-Earth calculator (Balco *et al.*, 2008) were calibrated using a local production rate to reduce scaling uncertainties and to improve agreement with other geochronological techniques (e.g. Balco *et al.*, 2009; Putnam *et al.*, 2010; Kaplan *et al.*, 2011; Young *et al.*, 2013; Phillips *et al.*, 2016). Two independently calibrated local production rates are available from the British Isles, the Loch Lomond (LLPR) and the Glen Roy production rate (GRPR) (Small and Fabel, 2015). These production rates agree within uncertainties. We adopt the most securely calibrated local ^{10}Be (LLPR; Fabel *et al.*, 2012) in all calculations (4.02 ± 0.18 atoms g^{-1}), noting that this is almost identical to the global mean ^{10}Be production rate calculated from the CRONUS-Earth primary dataset (Borchers *et al.*, 2016). For a discussion of the LLPR with respect to other production rates see Small and Fabel (2016). All TCN ages in this study are presented rounded to the nearest 0.1 ka with full external uncertainties at ± 1 sigma, unless otherwise stated (Tables 5 and 6).

Exposure-age distributions for each sample were plotted as probability density functions and visually compared, to identify any obvious outliers, before statistical treatments were applied. We calculated the uncertainty-weighted mean and associated uncertainties for exposure ages at each site. A two-tailed generalized extreme Studentized deviate test (gESD) – a tool within the iceTEA online interface (Jones *et al.*, 2019) – was used to check for and remove outliers. To test for similarity and goodness of fit in multiple samples from the same feature (or in close proximity) we used the Reduced Chi-squared statistic (χ^2), as done by others (e.g. Balco *et al.*, 2008; Heyman *et al.*, 2016; Small *et al.*, 2017), whereby a reduced-χ^2 value ≈1 (typically < 2, when $n = 4$) indicates that the scatter can be explained by measurement uncertainty (at 95% confidence). A value >>1 indicates an additional source of variance in the dataset (e.g. Balco *et al.*, 2008; Jones *et al.*, 2019) usually related to geological or post-depositional factors. These tests were performed iteratively to ensure optimal data reduction at each site. To build the final geochronology we constructed a uniform-phase Bayesian sequence model using OxCal 4.3 (Bronk Ramsey, 2013) (see Supporting Information).

Optically stimulated luminescence dating

To support the TCN chronology we also sought material for OSL dating during terrestrial field campaigns in 2014. Six suitable sites, hosting glaciofluvial sand-grade material, were sampled for OSL analysis using opaque 30-mm-diameter plastic tubes hammered into the sediment facies. Samples were capped and labelled and kept in dark conditions at all times during analysis to prevent exposure to sunlight. For each OSL sample, the external gamma dose-rates were determined using *in situ* gamma spectrometry, with external beta dose-rates calculated from U, Th and K concentrations determined using inductively coupled plasma mass spectrometry (ICP-MS). Appropriate conversion and attenuation factors were used to

© 2021 The Authors. *Journal of Quaternary Science* Published by John Wiley & Sons Ltd

Table 1. TCN sample locations and physical properties (beryllium isotope analyses only). Note: a density of 2.6 g cm^{-3} was used for all samples.

Sample	Location	Region	Latitude (°N)	Longitude (°W)	Elevation (m OD)	Sample lithology	Sample thickness (mm)	Shielding correction
T8ABB01	Ard Bheag Bhragar	W Lewis	58.35084	6.64852	28	Quartz vein in Lewisian gneiss (bedrock)	2.5	1.0000
T8ABB02	Ard Bheag Bhragar	W Lewis	58.35099	6.64874	27	Lewisian gneiss	2.5	1.0000
T8ABB03	Ard Bheag Bhragar	W Lewis	58.33901	6.65788	33	Lewisian gneiss (bedrock)	2.5	1.0000
T8ABB04	Ard Bheag Bhragar	W Lewis	58.33901	6.65788	33	Lewisian gneiss	2.5	1.0000
T8AIR01	Airigh na Gaoithe	N Lewis	58.45799	6.22627	108	Torridon Group sandstone	2.5	1.0000
T8AIR02	Airigh na Gaoithe	N Lewis	58.45807	6.22646	105	Lewisian gneiss	2.5	1.0000
T8AIR03	Airigh na Gaoithe	N Lewis	58.45770	−6.22628	109	Lewisian gneiss	3.26	0.9989
T8AIR04	Airigh na Gaoithe	N Lewis	58.45162	−6.21942	110	Lewisian gneiss	2.8	1.0000
T8BRA01	Bragar	W Lewis	58.33179	−6.65158	47	Lewisian gneiss	2.5	1.0000
T8BRA02	Bragar	W Lewis	58.33321	−6.65127	39	Lewisian gneiss	3	1.0000
T8BRA03	Bragar	W Lewis	58.33345	−6.65036	36	Lewisian gneiss	2.8	1.0000
T8CLA01	Clashnessie	Assynt (NW Mainland)	58.22205	−5.33787	83	Lewisian gneiss	0.65	1.0000
T8CLA02	Clashnessie	Assynt (NW Mainland)	58.22339	−5.33601	93	Lewisian gneiss	3.41	1.0000
T8CLA03	Clashnessie	Assynt (NW Mainland)	58.22400	−5.33539	99	Lewisian gneiss	2.5	1.0000
T8GEI02	Geireadha Mor	NE Lewis	58.37526	−6.21429	64	Lewisian gneiss	2.5	0.9665
T8GEI03	Geireadha Mor	NE Lewis	58.37485	−6.21415	57	Lewisian gneiss	4	0.9987
T8GEI05	Geireadha Mor	NE Lewis	58.37406	−6.22187	60	Lewisian gneiss	3.5	0.9665
T8ISL02	Islibhig	W Lewis	58.13979	−7.10636	51	Lewisian gneiss	1	0.9999
T8ISL03	Islibhig	W Lewis	58.14827	−7.10254	69	Lewisian gneiss	2	0.9996
T8ISL04	Islibhig	W Lewis	58.14800	−7.10300	62	Lewisian gneiss	2	0.9987
T8RAA01	North Raasay	Raasay	57.47645	−6.00351	231	Torridon Group sandstone	2.85	0.9999
T8RAA02	North Raasay	Raasay	57.47804	−6.00384	242	Torridon Group sandstone	2.52	0.9926
T8RAA03	North Raasay	Raasay	57.47821	−6.00396	250	Torridon Group sandstone	1.68	0.9958
T8RAB01	Central Raasay	Raasay	57.38691	−6.05940	134	Torridon Group sandstone	1.87	0.9982
T8RAB02	Central Raasay	Raasay	57.38699	−6.05912	140	Torridon Group sandstone	0.94	0.9982
T8RAB03	Central Raasay	Raasay	57.38735	−6.05923	136	Torridon Group sandstone	1.05	0.9982
T8RAI01	Rainish	E Lewis	58.13439	−6.39124	43	Lewisian gneiss	1	1.0000
T8RAI02	Rainish	E Lewis	58.13454	−6.39109	44	Lewisian gneiss	2.7	1.0000
T8RAI04	Rainish	E Lewis	58.13488	−6.39079	50	Lewisian gneiss	2.26	0.9989
T8RUB01	Rubha Linish	W Lewis	58.18058	−7.02084	42	Lewisian gneiss	2.33	0.9998
T8RUB02	Rubha Linish	W Lewis	58.18034	−7.02105	41	Lewisian gneiss	4.57	0.9998
T8RUB05	Rubha Linish	W Lewis	58.18117	−7.01895	32	Lewisian gneiss	1.5	0.9998
T8RUB06	Rubha Linish	W Lewis	58.18135	−7.01889	40	Lewisian gneiss	2.4	0.9999
T8STO01	Stoer	Assynt (NW Mainland)	58.24495	−5.36691	95	Lewisian gneiss	2.23	0.9999
T8STO02	Stoer	Assynt (NW Mainland)	58.24463	−5.36307	78	Lewisian gneiss	2.8	1.0000
T8STO03	Stoer	Assynt (NW Mainland)	58.24232	−5.36110	74	Conglomeratic sandstone (Stoer Group?)	3.39	1.0000
T8WRA01	Cape Wrath	Sutherland (NW Mainland)	58.62135	−4.99896	141	Quartz vein in Lewisian gneiss	2.5	0.9997
T8WRA02	Cape Wrath	Sutherland (NW Mainland)	58.62072	−4.99873	149	Lewisian gneiss	3.38	0.9997
T8WRA03	Cape Wrath	Sutherland (NW Mainland)	58.61884	−4.99747	173	Lewisian gneiss	1.9	1.0000
T8WRA04	Cape Wrath	Sutherland (NW Mainland)	58.61883	−4.99593	175	Lewisian gneiss	2.44	1.0000

© 2021 The Authors. *Journal of Quaternary Science* Published by John Wiley & Sons Ltd

Table 2. TCN sample locations and physical properties (chlorine isotope analyses only). Note: a density of 2.6 g cm^{-3} was used for all samples.

Sample	Location	Region	Latitude (°N)	Longitude (°W)	Elevation (m OD)	Sample lithology	Sample thickness (mm)	Shielding correction
T8TRT01	Ben Volovaig	N Trotternish (Skye)	57.70258	6.30859	96	Dolerite (boulder)	1.79	0.9999
T8TRT02	Ben Volovaig	N Trotternish (Skye)	57.70155	6.30562	115	Dolerite (bedrock)	3.78	0.9997
T8TRT03	Ben Volovaig	N Trotternish (Skye)	57.70128	6.30358	96	Dolerite (boulder)	2.17	0.9993
T8TRT04	Ben Volovaig	N Trotternish (Skye)	57.70128	6.30358	96	Dolerite (bedrock)	3.46	0.9994

calculate the final total dose rate, applying an assumed moisture of 23% for partially saturated samples and 27% for saturated samples (Table 7).

Eight OSL samples were analysed at the University of Aberystwyth using the 212–250-μm quartz grain fraction mounted into 10 by 10 grids of 300-μm-diameter holes in a 9.8-mm-diameter aluminium single-grain disc. All luminescence measurements were performed using a Risø TL/OSL DA-15 automated single-grain system equipped with a $^{90}Sr/^{90}Y$ beta source. A green laser was used to stimulate the grains for 1 s and OSL signal was detected through a 2.5-mm-thick U-340 filter and convex quartz lens in front of the photomultiplier tube. A preheat plateau test performed on 5-mm aliquots of sample T8SKIG02 was used to determine the preheat temperature (220 °C for 10 s), with a cut-heat of 160°C for the single aliquot regenerative dose (SAR) protocol. OSL stimulation was performed at 125°C for 1 s; the initial and background OSL signals were summed over the first 0.1 s and final 0.2 s, respectively.

Five OSL samples were measured at the University of Sheffield using the 212–250-μm quartz grain fraction mounted on small multi-grain aliquots each with approximately 20 grains. These were stimulated using a blue (470 ± 30 nm) light-emitting diode array providing a stimulation power of ~80 mW/cm^2 at the sample position. Luminesce signal was detected through a 735-mm Hoya U-340 filter. Equivalent doses (D_e) were measured using the single aliquot regeneration procedure with a pre-heat of 220 °C for 10 s.

Bathymetric data compilation and geomorphological mapping

Existing bathymetric datasets covering the study area were compiled to form a seamless elevation model of the submarine landscape around NW Scotland (Fig. 2). Most of the bathymetry data are available via the European Marine Observation and Data Network (EMODnet) Digital Terrain Model (EMODnet Bathymetry Consortium, 2018). This new submarine landform mapping is presented in Bradwell *et al.* (2019), along with further details on the methodology employed. A revised summary of the offshore glacial geomorphology is shown in Fig. 3.

Marine geophysical data

Continuous MBES data were collected on scientific cruise JC123 using a Kongsberg EM710 system operating at 70–100 kHz. To determine the sub-seabed Quaternary stratigraphy, continuous high-frequency (Chirp) hydro-acoustic sub-bottom profiler (SBP) data were collected. The Chirp SBP system used a sweep frequency of 2.5–6.5 kHz, with a depth resolution of 0.3 ms and a ping interval of 500 ms. Data were continuously logged in *seg* and *raw* form as well as visualized on a digital echogram. The hydro-acoustic SBP data were imported into IHS Kingdom Suite software to interpret the shallow sub-seabed stratigraphy and determine geological core sites. Two-way travel times were converted to sediment depths using an average velocity derived from p-wave measurements of sediment cores (see below). Existing lower frequency (sparker, airgun) analogue profiles acquired by the BGS between 1970 and 1995 were also used for interpretation purposes.

Marine geology and sedimentology

Forty-two sediment cores were taken from the seabed within the study area (T8) during scientific cruise JC123 on *RRS James Cook*: 31 vibrocores (VC) and 11 piston cores (PC) from five sub-transects. Seabed cores were taken using the BGS

© 2021 The Authors. *Journal of Quaternary Science* Published by John Wiley & Sons Ltd

Table 3. TCN beryllium isotope AMS analytical data for all samples from T8. ^{10}Be analyses were conducted at SUERC AMS Laboratory, East Kilbride. Errors include laboratory procedural uncertainties and individual AMS measurement errors.

Sample name	^{9}Be carrier (µg)	Quartz mass dissolved (g)	AMS ID	^{10}Be/^{9}Be[a] (×10^{-15})	Process blank ^{10}Be[b] (×10^{4} atoms)	^{10}Be[c] (×10^{4} atom g^{-1})
T8ABB01	210 ± 1.5	47.191	b7925	373.3 ± 8.51	4.19 ± 1.33	10.98 ± 0.27
T8ABB02	209.9 ± 1.5	24.044	b7926	162.94 ± 5.91	4.19 ± 1.33	9.26 ± 0.36
T8ABB03	210.7 ± 1.5	19.007	b7927	122.48 ± 8.62	4.19 ± 1.33	8.76 ± 0.65
T8ABB04	211 ± 1.5	21.714	b7928	136.99 ± 3.43	4.19 ± 1.33	8.62 ± 0.25
T8AIR01	257.9 ± 1.8	21.48	b8607	150.94 ± 3.43	6.95 ± 1.39	11.55 ± 0.31
T8AIR02	240.8 ± 1.7	11.311	b9696	86.21 ± 2.64	3.63 ± 0.7	11.75 ± 0.4
T8AIR03	257.6 ± 1.8	16.185	b8608	131.41 ± 4.35	6.95 ± 1.39	13.23 ± 0.5
T8AIR04	240.5 ± 1.7	28.456	b9698	298.81 ± 6.19	3.63 ± 0.7	16.67 ± 0.37
T8BRA01	224.8 ± 3.2	8.713	b10388	47.43 ± 1.84	3.4 ± 0.73	7.57 ± 0.36
T8BRA02	228.2 ± 3.2	11.957	b10510	65.57 ± 1.95	2.44 ± 0.63	8.05 ± 0.29
T8BRA03	225.2 ± 3.2	17.886	b10391	105.74 ± 3.01	3.4 ± 0.73	8.6 ± 0.29
T8CLA01	256.9 ± 1.8	22.925	b8605	109.09 ± 3.54	6.95 ± 1.39	7.64 ± 0.29
T8CLA02	260 ± 1.8	22.788	b8606	98.77 ± 2.82	6.95 ± 1.39	7 ± 0.25
T8CLA03	228 ± 3.2	17.018	b10507	89.28 ± 2.6	2.44 ± 0.63	7.77 ± 0.26
T8GEI02	227.7 ± 3.8	17.4942	b8574	114.67 ± 4.19	5.89 ± 1.04	9.46 ± 0.41
T8GEI03	227.7 ± 3.8	19.6676	b9658	124.43 ± 3.6	5.8 ± 0.78	9.18 ± 0.33
T8GEI05	188.5 ± 3.2	19.8244	b9659	156.24 ± 3.96	5.8 ± 0.78	9.48 ± 0.31
T8ISL02	227.2 ± 3.8	19.6227	b9660	104.63 ± 3.96	5.8 ± 0.78	7.64 ± 0.34
T8ISL03	228 ± 3.8	14.4543	b9662	82.03 ± 2.76	5.8 ± 0.78	8.04 ± 0.34
T8ISL04	230.4 ± 3.9	14.72	b10783	80.91 ± 4.66	4.52 ± 0.71	7.99 ± 0.51
T8RAA01	237 ± 1.6	20.371	b7932	112.16 ± 3.26	2.32 ± 0.67	8.54 ± 0.27
T8RAA02	235.6 ± 1.6	19.233	b7933	106.86 ± 3.12	2.32 ± 0.67	8.56 ± 0.27
T8RAA03	234.5 ± 1.6	19.998	b7934	94.58 ± 2.9	2.32 ± 0.67	7.23 ± 0.24
T8RAB01	209 ± 1.4	21.421	b7446	116.06 ± 4.38	3.96 ± 0.91	7.31 ± 0.3
T8RAB02	208.5 ± 1.4	21.48	b7447	118.58 ± 3.79	3.96 ± 0.91	7.43 ± 0.26
T8RAB03	207.9 ± 1.4	17.043	b7448	102.95 ± 3.32	3.96 ± 0.91	8.06 ± 0.29
T8RAI01	258.4 ± 1.8	39.261	b8611	194.18 ± 4.91	6.95 ± 1.39	8.23 ± 0.23
T8RAI02	242.5 ± 1.7	26.268	b9699	127.5 ± 3.74	3.63 ± 0.7	7.64 ± 0.24
T8RAI04	257.4 ± 1.8	13.179	b8612	67.24 ± 2.25	6.95 ± 1.39	7.86 ± 0.35
T8RUB01	255.8 ± 1.8	40.384	b8613	193.91 ± 4.46	6.95 ± 1.39	7.91 ± 0.21
T8RUB02	256.3 ± 1.8	20.394	b8614	95.14 ± 2.67	6.95 ± 1.39	7.4 ± 0.26
T8RUB05	257.9 ± 1.8	25.488	b8616	113.55 ± 3.18	6.95 ± 1.39	7.2 ± 0.24
T8RUB06	240.7 ± 1.7	15.302	b9700	69.75 ± 2.36	3.63 ± 0.7	6.95 ± 0.26
T8STO01	208.4 ± 1.4	19.776	b7449	104.63 ± 4.77	3.96 ± 0.91	7.08 ± 0.35
T8STO02	209.5 ± 1.5	15.078	b7451	72.54 ± 4.49	3.96 ± 0.91	6.37 ± 0.43
T8STO03	208.7 ± 1.4	19.817	b7452	116.06 ± 5.52	3.96 ± 0.91	7.89 ± 0.4
T8WRA01	208.9 ± 1.4	22.494	b7453	191.39 ± 5.38	3.96 ± 0.91	11.63 ± 0.35
T8WRA02	208.5 ± 1.4	23.511	b7454	199.49 ± 6.5	3.96 ± 0.91	11.59 ± 0.4
T8WRA03	239.8 ± 1.7	26.44	b9701	193.63 ± 4.3	3.63 ± 0.7	11.52 ± 0.28
T8WRA04	258.6 ± 1.8	27.589	b8617	180.51 ± 3.96	6.95 ± 1.39	10.87 ± 0.27

[a] Final AMS ^{10}Be/^{9}Be ratio from weighted mean of repeat measurements.
[b] All AMS ratios were corrected for full chemistry procedural blank and calibrated against NIST-4325 AMS ^{10}Be/^{9}Be standard reference material with a nominal value of 27 900 × 10^{-15}.
[c] ^{10}Be concentration derived from final mean ^{10}Be/^{9}Be ratio. Uncertainty based on final AMS ^{10}Be/^{9}Be error and 2% error in ^{9}Be spike value.

vibrocorer (6 m long barrel; internal diameter 9 cm) and NOC/NMFSS piston corer (9-m and 12-m barrels; internal diameter 12 cm), depending on the nature of the seabed and sub-seabed sediment. Cores were numbered sequentially followed by either the suffix VC or PC to denote the type of corer used (i.e. JC123-002VC, JC123-003PC, etc). Following recovery, all cores were labelled, measured, cut and capped in 1-m-long sections. Whole (round) sediment cores were geophysically scanned onboard the research vessel at 2-cm downcore intervals using a Geotek multi-sensor core logger (MSCL-S). The physical sediment properties measured included magnetic susceptibility, gamma-ray attenuation (GRA) or bulk density, electrical resistivity and p-wave velocity. Each core was then split lengthways, photographed and logged, with detailed (mm-to-cm scale) information on sedimentary structures, colour, grain size, sorting, bedding contacts and macrofaunal content recorded. Sediment shear strengths in kPa were recorded using a hand-operated Torvane. Selected cores were X-rayed using a Geotek XCT X-radiographic core scanner (in Daventry, UK). X-radiographs were captured at 100-µm resolution and output as 16-bit greyscale images.

Radiocarbon dating

Marine shells (articulated, single or broken valves) at key stratigraphic horizons within cores were identified from X-radiography images or from visual inspection and subsequently sampled. Where no macrofossil shells could be identified, cold-water carbonate microfossils (foraminifera) were sampled from mud- (silt/clay) grade material. Radiocarbon analyses were performed on shells and foraminifera at NERC Radiocarbon Laboratory, East Kilbride, Scotland. The outer 20% by weight of the shells was removed by controlled hydrolysis with dilute HCl, but foraminifera samples were not etched. All samples were then rinsed in deionized water, dried and homogenized. A known weight of the pretreated sample was hydrolysed to CO_2 using 85% orthophosphoric acid at room temperature. The CO_2 was converted to graphite by

© 2021 The Authors. *Journal of Quaternary Science* Published by John Wiley & Sons Ltd

Table 4. Chemical composition of etched whole rock, including concentrations of ^{36}Cl target elements Ca, K, Ti and Fe, and chlorine isotope AMS analytical data for four samples from T8. ^{36}Cl analyses were conducted at SUERC AMS Laboratory, East Kilbride. Errors include laboratory procedural uncertainties and individual AMS measurement errors.

Sample	Sample (g)	TiO_2 (wt%)	Al_2O_3 (wt%)	Fe_2O_3 (wt%)	CaO (wt%)	K_2O (wt%)	Spike mass (mg)	^{36}Cl/Cl ($\times 10^{15}$)[a]	Bulk rock Cl[b] (ppm)	^{36}Cl[c] (10^4 atoms g^{-1})
T8TRT01	24.5082	5.91 ± 0.07	2.85 ± 0.02	24.06 ± 1.83	9.86 ± 0.33	0.61 ± 0.01	1.2796	167.77 ± 5.19	0 ± 0.37	14.71 ± 0.48
T8TRT02	24.0769	4.41 ± 0.09	2.22 ± 0.03	17.77 ± 1.25	6.05 ± 0.02	0.77 ± 0.02	1.2753	217.87 ± 6.6	0.15 ± 0.38	19.59 ± 0.62
T8TRT03	24.1481	6.42 ± 0.89	3.54 ± 0.3	24.64 ± 2.42	9.08 ± 0.3	0.68 ± 0.04	1.2764	146.19 ± 4.26	0 ± 0.37	12.91 ± 0.4
T8TRT04	26.0075	4.12 ± 0.19	5.92 ± 0.14	17.39 ± 1.23	15.28 ± 0.84	0.76 ± 0.02	1.2709	228.43 ± 6.77	0.21 ± 0.36	18.99 ± 0.59

[a]Normalized to standard Z93-0005 produced at Prime Lab (Purdue University) with a nominal ^{36}Cl/Cl ratio of 1.2E-12.
[b]Stable Cl concentrations were calculated by AMS isotope dilution. All samples were spiked with non-natural Cl with a ^{35}Cl/^{37}Cl ratio of 20.2 ± 0.07 atoms/atom.
[c]Procedural blank ^{36}Cl/Cl = 3.12 ± 0.55 × 10^{-15}. Blank corrections for ^{36}Cl concentrations ranged from 1.4 to 4.7%.

Fe/Zn reduction. AMS analyses were conducted at SUERC, East Kilbride. Very small samples (<5 μg) were measured at Keck C Cycle AMS Lab, University of California (UCIAMS).

Radiocarbon ages from marine carbonates were calibrated using OxCal 4.3 (Bronk Ramsey, 2013) and Marine13 (Reimer *et al.*, 2013). Calibrated ages are presented in calendar years BP (i.e. before 1950 CE) as the median of the two-sigma uncertainty (Table 8). The calibration includes the standard global marine-reservoir correction of 400 years. Owing to uncertainties surrounding the magnitude, timing and duration of fluctuations in the marine reservoir effect around the NE Atlantic (Stern and Lisiecki, 2013, and references therein), we use a value of $\Delta R = 0$ when calibrating ^{14}C ages. Sensitivity of these results to different assumed ΔR values (300 and 700 years) is, however, also explored (Table 9) (and see Results).

Results

The following sections present a new database of 104 age assessments from the Minch, adjacent land areas and continental shelf to the north and northwest (Figs. 2 and 4–10; Tables 1–9). We report all of these dating results, provide site-specific information, and outline the geological/stratigraphic and geomorphological context. Terrestrial sites are presented first (Scottish mainland sites from north to south, then the islands of Raasay and Lewis, with sites listed from east to west); followed by marine sites (anticlockwise from north by sub-transect). Note that 25 of the TCN-exposure ages and three of the OSL ages have been previously presented by Bradwell *et al.* (2019). However, the TCN exposure ages presented here differ slightly from those in Bradwell *et al.* (2019) owing to minor differences in ^{10}Be production-rate calculations and statistical treatments.

TCN geochronology

Cape Wrath

Cape Wrath is the northwestern extremity of mainland Scotland, 58°38′N, 5°W, and rises to 163 m above present-day sea level (asl) with vertical cliffs along its north and west coasts. This remote rugged headland is composed of Archaean-age Lewisian orthogneiss unconformably overlain in places by Neoproterozoic Torridonian Group sandstone rocks. Numerous large moraines have been mapped on the seabed to the north and west of Cape Wrath (Fig. 3), indicating ice-sheet retreat generally from west to east perpendicular to the north coast of mainland Scotland (Bradwell and Stoker, 2015b). However, no expression of these moraines has been found onshore in the Cape Wrath area, although their radiating fan-shaped pattern offshore suggests that the Cape acted as an important topographic pinning point during ice stream and/or ice sheet retreat (Fig. 3) (Bradwell and Stoker, 2015b; Bradwell *et al.*, 2019).

Four glacially transported boulders (each > 1 m^3) near the summit of Donan Mor, at 140–175 m asl, were sampled in May 2013 (T8WRA01-04). All four were Lewisian gneiss boulders resting directly on Lewisian gneiss bedrock (Fig. 4). Torridon Group sandstone erratic boulders were also noted in the same vicinity. Peat cover on Donan Mor is thin (<1 m) and patchy. No disturbance of the boulders is likely since deposition. These samples were presented in Bradwell *et al.* (2019).

The Cape Wrath samples have exposure ages of 25.0 ± 1.3, 24.9 ± 1.4, 23.8 ± 1.2 and 22.5 ± 1.2 ka, with overlapping uncertainties (Table 5, Figs. 4–6). Collectively, the four ages have a reduced-Chi squared (χ^2) value of 3.28 indicating that they are probably not drawn from a single (larger) population with a normal distribution (at 95% confidence level).

© 2021 The Authors. *Journal of Quaternary Science* Published by John Wiley & Sons Ltd

Table 5. TCN ^{10}Be exposure ages for all samples from T8. Derived using CRONUS-Earth calculator (Developmental version; Wrapper script 2.3, Main calculator 2.1, constants 2.2.1, muons 1.1; Balco *et al.*, 2008) and CRONUScalc v2.0 (http://web1.ittc.ku.edu:8888/2.0/html; accessed 2 June 2016; Marrero *et al.*, 2016) with Lm scaling. Internal uncertainties (±1σ) reflect analytical uncertainties on ^{10}Be measurements only. External uncertainties (±1σ) incorporate additional uncertainties in the calculation and scaling procedure. 1 mm ka^{-1} erosion rate assumed. Adoption of different erosion rates (≤3 mm ka^{-1}) has very little effect on mean ages of samples (<1.5% difference). UWM = uncertainty-weighted mean (per location). Ages in bold are those used to calculate UWM ages (see text for details). Underlining in final column relates to quality-control scheme used throughout (underline = green = robust; no-underline = amber = acceptable).

Sample data		Surface exposure age						
Sample	Location	CRONUS 2.3 with LLPR LM (ka)	Internal uncert. (ka)	External uncert. (ka)	CRONUScalc v2.0 LM (ka)	Internal uncert. (ka)	External uncert. (ka)	UWM (ka)
T8ABB01	Ard Bheag Bhragar	26.6	0.6	1.4	26.6	0.7	2.2	
T8ABB02	Ard Bheag Bhragar	**22.3**	0.9	**1.3**	22.0	0.9	2.0	
T8ABB03	Ard Bheag Bhragar	**21.0**	1.6	**1.8**	21.0	1.6	2.3	**21.1 ± 1.0**
T8ABB04	Ard Bheag Bhragar	**20.6**	0.6	**1.1**	20.7	0.6	1.8	
T8AIR01	Airigh na Gaoithe	**26.0**	0.7	**1.4**	26.1	0.7	2.2	
T8AIR02	Airigh na Gaoithe	**26.2**	0.9	**1.5**	26.2	0.9	2.3	**26.1 ± 1.3**
T8AIR03	Airigh na Gaoithe	30.2	1.2	1.8	30.2	1.2	2.7	
T8AIR04	Airigh na Gaoithe	37.5	0.9	1.9	37.6	0.9	3.2	
T8BRA01	Bragar	**17.8**	0.9	**1.2**	17.8	0.9	1.7	
T8BRA02	Bragar	**19.2**	0.7	**1.1**	19.2	0.7	1.7	**19.3 ± 0.9**
T8BRA03	Bragar	**20.3**	0.7	**1.1**	20.3	0.7	1.8	
T8CLA01	Clashnessie (Stoer)	**17.1**	0.7	**1.0**	17.1	0.7	1.5	
T8CLA02	Clashnessie (Stoer)	**15.8**	0.6	**0.9**	15.8	0.6	1.4	
T8CLA03	Clashnessie (Stoer)	**17.3**	0.6	**1.0**	17.4	0.6	1.5	**16.5 ± 0.8***
T8STO01	Stoer	**15.8**	0.8	**1.0**	15.8	0.8	1.5	
T8STO02	Stoer	**14.5**	1.0	**1.2**	14.5	1.0	1.5	
T8STO03	Stoer	**18.2**	0.9	**1.2**	18.2	0.9	1.7	
T8GEI02	Geireadha Mor	**22.7**	1.0	**1.4**	22.8	1.0	2.1	
T8GEI03	Geireadha Mor	**21.7**	0.8	**1.3**	21.8	0.8	1.9	**22.4 ± 1.1**
T8GEI05	Geireadha Mor	**22.8**	0.8	**1.3**	23.0	0.8	2.0	
T8ISL02	Islibhig	**17.7**	0.8	**1.1**	17.7	0.8	1.6	
T8ISL03	Islibhig	**18.4**	0.8	**1.1**	18.4	0.8	1.7	**18.1 ± 1.0**
T8ISL04	Islibhig	**18.5**	1.2	**1.5**	18.5	1.2	1.9	
T8RAA01	North Raasay	**16.7**	0.5	**0.9**	16.8	0.5	1.4	
T8RAA02	North Raasay	**16.7**	0.5	**0.9**	16.7	0.5	1.4	**16.7 ± 0.9**
T8RAA03	North Raasay	13.8	0.5	0.8	13.8	0.5	1.2	
T8RAB01	Central Raasay	**15.7**	0.6	**0.9**	15.7	0.6	1.4	
T8RAB02	Central Raasay	**15.8**	0.5	**0.9**	15.9	0.6	1.4	**16.2 ± 0.8**
T8RAB03	Central Raasay	**17.2**	0.6	**1.0**	17.3	0.6	1.5	
T8RAI01	Rainish	**19.3**	0.6	**1.0**	19.3	0.6	1.6	
T8RAI02	Rainish	**18.1**	0.6	**1.0**	18.1	0.6	1.6	**18.6 ± 0.9**
T8RAI04	Rainish	**18.4**	0.8	**1.2**	18.5	0.8	1.7	
T8RUB01	Rubha Linish	**18.7**	0.5	**1.0**	18.7	0.5	1.6	
T8RUB02	Rubha Linish	**17.8**	0.6	**1.0**	17.8	0.6	1.6	**17.6 ± 0.9**
T8RUB05	Rubha Linish	**17.1**	0.6	**1.0**	17.1	0.6	1.5	
T8RUB06	Rubha Linish	**16.4**	0.6	**1.0**	16.4	0.6	1.5	
T8WRA01	Cape Wrath	**25.0**	0.7	**1.3**	25.0	0.8	2.1	
T8WRA02	Cape Wrath	**24.9**	0.9	**1.4**	24.9	0.9	2.2	**23.8 ± 1.1**
T8WRA03	Cape Wrath	**23.8**	0.6	**1.2**	24.0	0.6	2.0	(*24.4 ± 1.1*)
T8WRA04	Cape Wrath	**22.5**	0.6	**1.2**	22.5	0.6	1.9	

*All samples from Stoer and Clashnessie used for age calculation (UWM; $n = 6$).

However, none of the samples can be statistically identified as an outlier using the gESD test (Jones *et al.*, 2019). A smaller reduced-χ^2 value (0.97) is returned if the youngest sample is excluded (i.e. T8WRA04). This may indicate that the youngest exposure age was affected by enhanced weathering or transient sediment cover, resulting in a TCN exposure-age which underestimates the true timing of boulder deposition. However, without firm statistical or geomorphological grounds to exclude this sample, we consider the uncertainty-weighted mean (UWM) age of all four samples (23.8 ± 1.1 ka) to be a fair and faithful representation of the deglacial exposure age for this site. (For comparison, the UWM age of the older three samples is 24.4 ± 1.1 ka). These TCN ages from Cape Wrath constrain the timing of ice-sheet retreat from the surrounding continental shelf to first 'landfall' in the NW extremity of mainland Scotland by ~24 ka BP, with deglaciation of the Cape shortly thereafter.

Stoer Peninsula

The Stoer peninsula is a rocky headland projecting into the eastern Minch at c. 58°15′N (Fig. 1). The headland is composed of Mesoproterozoic and Neoproterozoic sedimentary rocks of the Stoer and Torridon Groups, unconformably lying on Lewisian gneiss basement rocks which outcrop to the southeast. Numerous glacially transported Lewisian boulders are found scattered across the Stoer peninsula, many resting directly on glaciated Torridon and Stoer Group bedrock slabs indicating former ice flow from SE to NW.

© 2021 The Authors. *Journal of Quaternary Science* Published by John Wiley & Sons Ltd

Table 6. TCN ^{36}Cl exposure ages for four samples from T8. Derived using CRONUScalc v2.0 (http://web1.ittc.ku.edu:8888/2.0/html; accessed 2 June 2016; Marrero *et al.*, 2016) with Lm scaling. Internal uncertainties (±1σ) reflect analytical uncertainties on ^{36}Cl measurements only. External uncertainties (±1σ) incorporate additional uncertainties in the calculation and scaling procedure. 1 mm ka^{-1} erosion rate assumed. Adoption of different erosion rates (≤3 mm ka^{-1}) has very little effect on mean ages of samples (<1.5% difference).

Sample data		Surface exposure age			
Sample	Location	CRONUScalc v2.0 LM (ka)	Internal uncert. (ka)	External uncert. (ka)	UWM (ka)
T8TRT01	Ben Volovaig	26.5	0.9	2.1	
T8TRT02	Ben Volovaig	49.4	1.7	3.6	n/a
T8TRT03	Ben Volovaig	24.1	0.8	1.8	
T8TRT04	Ben Volovaig	24.0	0.8	2.0	

Six large (1–5 m^3) glacially transported boulders were sampled at two different localities (Stoer and Clashnessie) only 2.5 km apart (Fig. 4). Five of the boulders were Lewisian gneiss erratics (T8STO01, T8STO02, T8CLA01–03), and one was a coarse conglomeratic (Stoer or Torridon Group) sandstone boulder (STO03). No disturbance of these boulders is likely since deposition. These samples were presented in Bradwell *et al.* (2019).

The Stoer samples have exposure ages of 15.8 ± 1.0, 14.5 ± 1.2 and 18.2 ± 1.2 ka. The Clashnessie samples have exposure ages of 17.1 ± 1.0, 15.8 ± 0.9 and 17.3 ± 1.0 ka, with overlapping analytical uncertainties (Table 5, Figs. 5 and 6). Owing to their close spatial proximity on the same headland within the same deglacial landsystem, and without any clear geomorphological evidence to the contrary, the six exposure ages are considered together. The six exposure ages have a reduced-χ^2 value of 2.53, which slightly exceeds the critical value (at 95% confidence) of 2.26 for a population with 5 degrees of freedom. This indicates some influence of geological uncertainty within the data set. However, as no ages can be statistically identified as outliers and the reduced reduced-χ^2 value only slightly exceeds the critical value, we consider the UWM age of all six samples (16.5 ± 0.8 ka) to be a robust representation of the true exposure age (Table 5, Fig. 5). The Stoer peninsula TCN ages therefore constrain the timing of ice-sheet retreat from the Minch onshore to the coastal fringes of Assynt, NW mainland Scotland, by ~16.5 ka BP.

North Raasay

Raasay is situated at the head of the Inner Minch between the mountains of Applecross and Skye, and separated from them by the deep waters of Inner Sound and the Sound of Raasay (Figs. 1 and 2). The 20-km-long island, together with the smaller island of Rona to the north, exhibits strongly streamlined bedrock terrain with a general north–south or NNW–SSE lineation, especially on low ground (Bradwell *et al.*, 2007) – evidence of intense subglacial erosion by powerful fast-flowing ice.

Two glacially transported boulders (each > 0.5 m^3) and one glacially transported cobble (a-axis: < 256 mm) were sampled on high ground c. 230–250 m asl near the summit of Beinn na h-Iolaire, northern Raasay (T8RAA01-03) (Fig. 4). All three were fine- to medium-grained gritty Torridon sandstone erratics resting directly on ice-worn Lewisian gneiss bedrock. The nearest equivalent sandstone outcrops are ~5 km to the SSW on Raasay, 8 km due east on Applecross, or 18 km to the SSE on Scalpay. Scalpay is immediately upstream of Raasay and Rona in the direction of former ice-stream flow, as deduced from independent landform evidence (Bradwell *et al.*, 2007). Disturbance of the boulder/cobble debris since deposition is possible but unlikely. These samples were presented in Bradwell *et al.* (2019).

The north Raasay samples have exposure ages of 16.7 ± 0.9, 16.7 ± 0.9 and 13.8 ± 0.8 ka (Table 5, Figs. 5 and 6). The youngest sample is shown to be an outlier by a gESD test and we therefore exclude it from our age calculations hereafter. Goodness-of-fit statistics cannot be performed on datasets when $n < 3$. However, the exact correspondence between the two ages indicates that they are from a single population. We consider the UWM age of the two samples (16.7 ± 0.9 ka) to be a robust representation of the true deglacial exposure age (in this case, identical to the arithmetic mean age).

Central Raasay

The southern half of Raasay comprises a complex of Jurassic sedimentary rocks and Palaeogene intrusive (granitic bodies) and extrusive (basalt lavas) igneous rocks. Three glacially transported boulders (each > 0.5 m^3) were sampled from within a densely boulder-strewn area, approximately 0.7 km^2, on the western flanks of Meall Daimh at 130–140 m asl (T8RAB01-03) (Fig. 4). All three boulders chosen were fine- to medium-grained gritty Torridon sandstone erratics, within a mainly (>90%) granitic boulder field deposited on Palaeogene Raasay granite bedrock. The abundance of similar-sized glacially derived boulders in this locality is unusual but is strongly resemblant of 'boulder moraine' belts seen elsewhere in the NW Scottish Highlands [e.g. Strollamus moraine in Skye (Small *et al.*, 2012); Wester Ross moraine near Gairloch, and also in Coigach (Bradwell *et al.*, 2008b; Ballantyne *et al.*, 2009)]. Disturbance of these boulders since deposition is unlikely. These samples were presented in Bradwell *et al.* (2019).

The three mid-Raasay samples yield exposure ages of 15.7 ± 0.9, 15.8 ± 0.9 and 17.2 ± 1.0 ka (Table 5, Figs. 5 and 6). A reduced-χ^2 value of 1.94 indicates that ages are from a single population. We therefore consider the UWM of all three exposure ages to be a robust representation of the true deglacial exposure age in central and southern Raasay (i.e. 16.2 ± 0.8 ka).

Rubha Hunish (northern Skye)

Two samples were taken from basaltic boulders and two from basalt bedrock on the Rubha Hunish headland at the northern tip of Skye (Table 2) – a key site to potentially constrain deglaciation in the central part of the inner Minch (Fig. 1). These four whole rock samples were processed and analysed for ^{36}Cl nuclides. The results are complex, do not conform with the remainder of the ages in our TCN dataset and therefore cannot be easily interpreted at face value. Apparent exposure ages range from 24.0 to 49.4 ka (Table 4, Fig. 6). We conclude that all four ages suffer from varying degrees of cosmogenic-nuclide inheritance and may not have experienced sufficient glacial erosion, as such the ages are not deemed useful for constraining ice-sheet retreat. Consequently, they are not discussed further in this work.

© 2021 The Authors. *Journal of Quaternary Science* Published by John Wiley & Sons Ltd

Table 7. Results from OSL dating for all samples in T8, including the environmental dose-rates to grains of quartz, determined using ICP-MS and ICP-AES analysis and field gamma spectrometry. The chemical concentrations are presented to the appropriate decimal places according to the associated detection limit. The grain size for all samples was 212–250 µm. The water contents are expressed as a percentage of the mass of dry sediment.

Sample	K (%)	Rb (ppm)	U (ppm)	Th (ppm)	Beta dose-rate (Gy ka^{-1})	Gamma dose-rate (Gy ka^{-1})	Cosmic dose-rate (Gy ka^{-1})	Total dose-rate (Gy ka^{-1})	n	OD (%)	Age model	D_e (Gy)	Age (ka)
T8GALS01	1.5 ± 0.2	48.2 ± 4.8	0.48 ± 0.05	6.7 ± 0.7	1.0 ± 0.1	0.5 ± 0.0	0.2 ± 0.0	1.7 ± 0.1	29	50	MAM	24.0 ± 3.9	14.0 ± 2.5
T8GABB01	1.8 ± 0.2	64.5 ± 6.5	0.74 ± 0.07	4.3 ± 0.4	1.2 ± 0.1	0.6 ± 0.0	0.2 ± 0.0	2.0 ± 0.1	49	20	CAM	39.4 ± 1.6	20.2 ± 1.6
T8GABB02	1.1 ± 0.1	37.5 ± 3.8	0.37 ± 0.04	1.6 ± 0.2	0.7 ± 0.1	0.3 ± 0.0	0.1 ± 0.0	1.0 ± 0.1	34	32	MAM	41.0 ± 5.0	39.6 ± 5.5
T8SKIG01	1.5 ± 0.2	42.8 ± 4.3	0.67 ± 0.07	2.6 ± 0.3	1.0 ± 0.1	0.5 ± 0.0	0.2 ± 0.0	1.6 ± 0.1	70	39	MAM	37.4 ± 2.4	23.1 ± 2.3
T8SKIG02	1.5 ± 0.2	45.3 ± 4.5	0.54 ± 0.05	2.3 ± 0.2	0.9 ± 0.1	0.5 ± 0.0	0.1 ± 0.0	1.5 ± 0.1	81	27	CAM	33.0 ± 1.2	22.4 ± 2.1
T8SUAI01	1.3 ± 0.1	39.6 ± 4.0	0.57 ± 0.06	1.9 ± 0.2	0.8 ± 0.1	0.4 ± 0.0	0.1 ± 0.0	1.3 ± 0.1	76	39	MAM	48.1 ± 4.8	37.4 ± 4.3
T8SUAI02	1.4 ± 0.1	42.7 ± 4.3	0.51 ± 0.05	2.0 ± 0.2	0.9 ± 0.1	0.4 ± 0.0	0.1 ± 0.0	1.4 ± 0.1	97	36	MAM	55.4 ± 5.0	41.1 ± 4.4
T8SUAI03	1.4 ± 0.1	43.4 ± 4.3	0.39 ± 0.04	1.4 ± 0.1	0.9 ± 0.1	0.4 ± 0.0	0.1 ± 0.0	1.3 ± 0.1	60	24	MAM	59.8 ± 5.9	44.5 ± 5.1
T8LKAN01	1.8 ± 0.1	59.3 ± 5.9	1.51 ± 0.15	5.4 ± 0.6	1.2 ± 0.1	0.6 ± 0.0	0.1 ± 0.0	1.9 ± 0.1	62	78	IEU	26.5 ± 2.1	13.7 ± 1.3
T8LKAN02	1.8 ± 0.1	58.8 ± 5.9	1.51 ± 0.15	5.0 ± 0.6	1.2 ± 0.1	0.7 ± 0.0	0.2 ± 0.0	2.1 ± 0.1	60	93	IEU	30.6 ± 2.4	14.6 ± 1.4
T8LKAN03	1.9 ± 0.1	61.6 ± 6.2	2.59 ± 0.26	6.0 ± 0.6	1.4 ± 0.1	0.6 ± 0.0	0.1 ± 0.0	2.1 ± 0.1	46	96	IEU	30.7 ± 3.5	14.8 ± 1.9
T8SKYE01	1.8 ± 0.1	57.0 ± 5.8	1.12 ± 0.12	4.5 ± 0.5	1.1 ± 0.1	0.7 ± 0.0	0.2 ± 0.0	2.0 ± 0.1	94	88	IEU	25.8 ± 1.3	13.0 ± 1.0
T8SKYE02	1.9 ± 0.1	58.2 ± 5.9	1.06 ± 0.11	4.5 ± 0.6	1.2 ± 0.1	0.6 ± 0.0	0.2 ± 0.0	2.0 ± 0.1	50	110	IEU	20.6 ± 2.0	10.3 ± 1.2

Rainish (East Lewis)

The small rocky headland of Rainish is located on the east coast of Lewis, 9 km south of Stornoway (Fig. 1). In the rugged Lewisian gneiss 'cnoc and lochan' topography, around Loch Erisort, glacially streamlined ice-worn bedrock outcrops, such as crag and tails, are common and clearly visible in digital elevation models (Bradwell *et al.*, 2007). On an outcrop scale, roches moutonnées and whalebacks indicate east to west ice flow across the Rainish headland, consistent with a powerful ice-stream tributary feeding into the northerly flowing MnIS (Bradwell *et al.*, 2007). Three glacially transported Lewisian gneiss boulders perched on ice-worn bedrock outcrops were sampled for TCN analysis (T8RAI01, 02, 04) (Fig. 4). All three were within a 50-m radius of one another and between 40 and 50 m asl. Disturbance of these boulders since deposition is unlikely. These samples were presented in Bradwell *et al.* (2019).

The Rainish samples have exposure ages of 19.3 ± 1.0, 18.1 ± 1.0 and 18.4 ± 1.2 ka (Table 5, Fig. 6), with overlapping analytical uncertainties. A reduced-χ^2 value of 1.13 indicates that the spread of ages can be accounted for by measurement uncertainty and that they are from a single population (Fig. 5). We consider the UWM of all three exposure ages (18.6 ± 0.9 ka) to be an accurate and robust representation of their true exposure age. These TCN ages constrain deglaciation of this coastal region of east Lewis by ~18.6 ka BP and therefore, importantly, also the timing of ice-stream retreat in the western Minch.

Geireadha Mor (NE Lewis)

Much of northern Lewis, north of a line from Stornoway to Bragar, is covered in thick peat obscuring bedrock outcrops and Quaternary glacigenic deposits. Along the northeast coast of Lewis from Tolsta Head to Cellar Head, however, glacially transported boulders are common perched on strongly abraded, plucked and dislocated bedrock outcrops. Almost all the boulders are of locally sourced Lewisian gneiss, although rare erratic lithologies and Jurassic fossils have been found in coastal till sections around Tolsta Head (Peacock, 1984).

We sampled three glacially transported Lewisian gneiss boulders for TCN analysis (T8GEI02, 03, 05), 4 km NW of Tolsta Head, at Geireadha Mor at 55–70 m asl (Fig. 4). The boulders were resting directly on glaciated bedrock surfaces, with little or no till present. They do not form part of a moraine or boulder belt but, given their spatial proximity and close association with other onshore glacial deposits in the vicinity of Tolsta Head and submarine glacial landforms in the western Minch, they can be clearly linked with ice-sheet (ice stream) deglaciation in this part of eastern Lewis. These samples were presented in Bradwell *et al.* (2019).

The three samples have exposure ages of 22.7 ± 1.4, 21.7 ± 1.3 and 22.8 ± 1.3 ka (Table 5, Figs. 5 and 6), with overlapping analytical uncertainties. The tight clustering is reflected in a small reduced-χ^2 value of 0.55, indicating that the spread can be accounted for by measurement uncertainty and that the ages are from a single population. We consider the UWM of all three exposure ages (22.4 ± 1.1 ka) to be an accurate and robust representation of the true exposure age. These ages constrain deglaciation of this part of northeast Lewis by ~22.4 ka BP and, thereby, also the timing of ice-stream retreat in the north Minch.

Airigh na Gaoithe (North Lewis moraine)

A distinctive, non-bedrock-controlled, broad sediment ridge occurs in North Lewis trending in a SSE–NNW direction (Fig. 1). The gently arcing ridge is 4.3 km long, 200–600 m

© 2021 The Authors. *Journal of Quaternary Science* Published by John Wiley & Sons Ltd

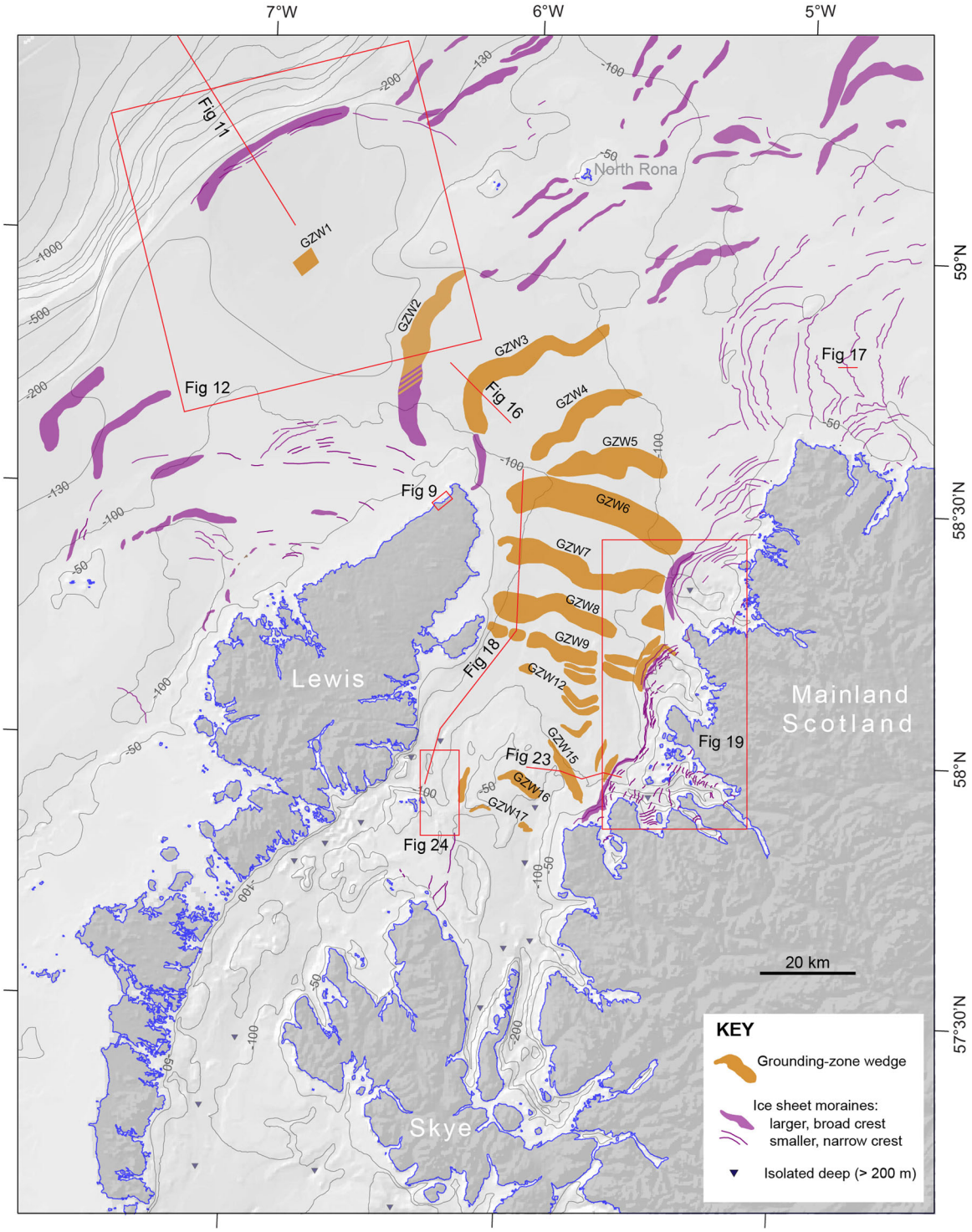

Figure 3. Mapped seabed moraines and grounding-zone features within the study area (modified from Bradwell *et al.*, 2019). Red boxes denote locations of other Figures. [Color figure can be viewed at wileyonlinelibrary.com].

wide and c. 10–20 m high for much of its length with a wide subdued crest. This ridge was previously mapped as glacial sand and gravel by Peacock (1984). However, large glacially transported boulders are present on its crest and a pit mechanically excavated to c. 2 m depth revealed poorly sorted, relatively well-consolidated, sandy diamicton-grade sediments. Further natural exposures within the ridge confirmed the presence of glacial diamicton more widely with an abundance of sub-rounded to sub-angular striated clasts. Many cobble and gravel clasts of fine- to medium-grained red sandstone were identified, with strong affinity to the Torridon Group sandstones of mainland NW Scotland. One Torridon Group sandstone boulder was also identified on the ridge crest. Consequently, we interpret this conspicuous depositional ridge as an ice-sheet moraine, possibly shear-margin moraine (which we term the North Lewis moraine) with boulders deposited by ice sourced from NW Mainland Scotland and the seafloor of the Minch. This glacial configuration, with the MnIS crossing the northern extremity of Lewis, is entirely consistent with the scenario previously suggested by others on the basis of clast provenance within tills and the regional Quaternary geology and geomorphology of northernmost Lewis (Peacock, 1984; Sutherland, 1984; Fyfe *et al.*, 1993; Bradwell *et al.*, 2007).

© 2021 The Authors. *Journal of Quaternary Science* Published by John Wiley & Sons Ltd

Table 8. Locations, sample data and radiocarbon dates from marine cores in this study.

Core JC-123-	Sample ID	Latitude (°N)	Longitude (°W)	Water depth (m)	Sample depth (cm)[a]	Sample type (identification) and/or condition (mass indicated for small samples)	Conventional radiocarbon age (^{14}C a BP)	±1σ	Calibrated age[b] (cal a BP)	±2σ
006VC	T8-006VC-173	58.75785	6.27485	121	172–174	gastropod + barnacle	17 369	41	20 458	169
008VC	T8-008VC-274	58.70503	6.17478	120	271–276	cold water foraminifera (96 mg)	17 046	45	20 076	178
010VC	T8-010VC-526	58.66957	6.10917	123.5	526–536	cold water foraminifera	15 270	45	18 071	171
011VC	T8-011VC-160	58.59487	5.97565	112	160–169	cold water foraminifera	17 640	60	20 786	204
012VC	T8-012VC-170	58.06561	5.51390	70	170	articulated shell (*Mya truncata*?)	11 101	38	12 628	80
012VC	T8-012VC-178	58.06561	5.51390	68.1	178	small single valve (*Macoma* sp)	11 138	38	12 649	84
013VC	T8-013VC-356	58.09382	5.50862	67	356	barnacle fragments	13 955	39	16 326	186
015VC	T8-015VC-200	58.16218	5.50133	119.5	200	largely intact shell fragment	13 704	40	15 991	178
017VC	T8-017VC-364	58.38603	5.48132	118	363–365	shell articulated when sampled	10 969	35	12 533	104
018VC	T8-018VC-451	58.37602	5.45453	113	451	single valve (*Hiatella arctica*)	13 851	41	16 178	169
029PC	T8-029PC-703	57.55758	6.09682	90	703	single valve (articulated when found); species?	12 502	39	13 983	135
029PC	T8-029PC-721	57.55758	6.09682	90	721	single valve (articulated when found); uncertain species	12 546	39	14 027	131
029PC	T8-029PC-734	57.55758	6.09682	90	734	juvenile articulated shells; species?	12 805	38	14 470	316
035PC	T8-035PC-535	59.19552	7.24887	525	535–544	cold water foraminifera	25 330	140	28 972	355
035PC	T8-035PC-619	59.19552	7.24887	525	614–624	cold water foraminifera (32 mg)	42 880	1090	out of range	n/a
036PC	T8-036PC-353	59.18482	7.24497	490	348–358	benthic foraminifera (polyspecific)	28 290	108	31 590	310
036PC	T8-036PC-497	59.18482	7.24497	490	495–502	cold water foraminifera (35 mg)	37 880	610	41 879	896
039VC	T8-039VC-231	59.09388	7.14055	183	231–234	cold water foraminifera	18 080	52	21 384	239
039VC	T8-039VC-393	59.09388	7.14055	183	390–395	benthic foraminifera (monospecific *N. labradorica*)	18 291	50	21 677	202
040VC	T8-040VC-413	59.12550	6.84353	175	413	shell (*Macoma* sp?)	13 786	39	16 100	167
040VC	T8-040VC-506	59.12550	6.84353	175	506	single valve; species uncertain	19 560	53	23 086	251
040VC	T8-040VC-594	59.12550	6.84353	175	594–597	cold water foraminifera	20 797	60	24 498	272
043VC	T8-043VC-421	58.93720	6.88790	171	421	broken gastropod; species?	16 126	48	18 963	135
044VC	T8-044VC-220	58.92675	6.86902	162	220	cold water benthic foraminifera: *N. labradorica* (0.0128 g)	11 191	37	12 682	94
044VC	T8-044VC-240	58.92675	6.86902	162	240	cold water benthic foraminifera: n. labradorica (0.0140 g)	11 290	37	12 757	114
044VC	T8-044VC-260	58.92675	6.86902	162	260	cold water benthic foraminifera: *N. labradorica* (0.0098g)	11 232	38	12 712	104
044VC	T8-044VC-280	58.92675	6.86902	162	280	cold water benthic foraminifera: *N. labradorica* (0.0114 g)	11 407	36	12 858	133
044VC	T8-044VC-300	58.92675	6.86902	162	300	cold water benthic foraminifera: *N. labradorica* (0.0116 g)	11355	38	12810	123
044VC	T8-044VC-312	58.92675	6.86902	162	312	double valve (*Macoma* sp)	10 694	38	12 088	210
044VC	T8-044VC-313	58.92675	6.86902	162	313	double valve (*Macoma* sp)	10 678	37	12 051	198
044VC	T8-044VC-320	58.92675	6.86902	162	320	cold water benthic foraminifera: *N. labradorica* (0.0129 g)	11 200	38	12 688	96
044VC	T8-044VC-340	58.92675	6.86902	162	340	cold water benthic foraminifera: *N. labradorica* (0.0144 g)	11 094	38	12 624	80
044VC	T8-044VC-347	58.92675	6.86902	162	347–350	cold water foraminifera	11 419	38	12 872	139
044VC	T8-044VC-360	58.92675	6.86902	162	360	cold water benthic foraminifera: *N. labradorica* (0.0118g)	12 866	39	14 613	353

(*Continued*)

© 2021 The Authors. *Journal of Quaternary Science* Published by John Wiley & Sons Ltd

Table 8. (*Continued*)

Core JC-123-	Sample ID	Latitude (°N)	Longitude (°W)	Water depth (m)	Sample depth (cm)[a]	Sample type (identification) and/or condition (mass indicated for small samples)	Conventional radiocarbon age (^{14}C a BP)	±1σ	Calibrated age[b] (cal a BP)	±2σ
044VC	T8-044VC-380	58.92675	6.86902	162	380	cold water benthic foraminifera: *N. labradorica* (0.0087 g)	12 175	38	13 623	147
044VC	T8-044VC-400	58.92675	6.86902	162	400	cold water benthic foraminifera: *N. labradorica* (0.0110 g)	12 650	37	14 146	153
044VC	T8-044VC-420	58.92675	6.86902	162	420	cold water benthic foraminifera: *N. labradorica* (0.0187 g)	11 558	38	13 033	137
044VC	T8-044VC-440	58.92675	6.86902	162	440	cold water benthic foraminifera: *N. labradorica* (0.0201 g)	12 085	38	13 529	135
044VC	T8-044VC-466	58.92675	6.86902	162	465–467	cold water foraminifera (228 mg)	13 611	38	15 875	169
044VC	T8-044VC-468	58.92675	6.86902	162	468	shell fragments	18 686	51	22 147	220
045VC	T8-045VC-424	58.85708	6.63305	142.5	424	broken shell; species uncertain	14 375	43	16 947	220
045VC	T8-045VC-445	58.85708	6.63305	142.5	445	broken but articulated shell; species uncertain	14 196	41	16 679	235
045VC	T8-045VC-491	58.85708	6.63305	142.5	491–494	cold water foraminifera (163 mg)	15 501	42	18 346	165
048VC	T8-048VC-098	58.85708	6.63305	142.5	98	gastropod shell; species uncertain	15 096	43	17 879	163
048VC	T8-048VC-099	58.85708	6.63305	142.5	99	single valve; species uncertain	15 162	42	17 954	155
049VC	T8-049VC-065	58.78002	4.80542	86.5	65–74	cold water foraminifera	16 345	50	19 230	204
050VC	T8-050VC-105	58.77997	4.70482	82	105	shell (*Hiatella arctica*?)	13 712	38	16 002	176

[a]Sample depth = depth in core (in cm), assuming that zero is seabed. 'Shoe' refers to the geological sample (<10 cm long) recovered from foot of vibrocorer, not included in the core barrel; 'catcher' refers to the geological sample recovered in core-catcher mechanism at base of vibrocore core barrel. Depths for shoe and core-catcher samples are approximate.
[b]Radiocarbon dates from marine carbonate (shells) converted from conventional radiocarbon years using OxCal 4.3 (Bronk Ramsey, 2013) and MARINE13 (Reimer *et al.*, 2013). Calibrated ages are presented in calendar years BP (i.e. before 1950 CE) as mean of two-sigma uncertainty; local marine-reservoir correction $\Delta R = 0$.

© 2021 The Authors. *Journal of Quaternary Science* Published by John Wiley & Sons Ltd

Table 9. Radiocarbon ages from marine cores in this study presented with a range of ΔR marine reservoir-effect corrections. Blank cell is where no calibration could be performed. For sample-specific metadata see Table 8.

Sample ID	Lab. code	Conventional radiocarbon age (^{14}C a BP)	± 1σ	Calibrated age (cal a BP) $\Delta R = 0$ years	± 2σ	Calibrated age (cal a BP) $\Delta R = 300$ years	± 2σ	Calibrated age (cal a BP) $\Delta R = 700$ yrs	± 2σ
T8-006VC-173	SUERC-64113	17369	41	**20458**	169	20103	174	19640	174
T8-008VC-274	SUERC-66652	17046	45	**20076**	178	19729	196	19231	196
T8-010VC-526	UCIAMS-176373	15270	45	**18071**	171	17749	176	17250	198
T8-011VC-160	UCIAMS-176374	17640	60	**20786**	204	20420	204	19945	214
T8-012VC-170	SUERC-64114	11101	38	**12628**	80	12282	218	11487	249
T8-012VC-178	SUERC-67432	11138	38	**12649**	84	12343	212	11551	257
T8-013VC-356	SUERC-64115	13955	39	**16326**	186	15928	172	15328	190
T8-015VC-200	SUERC-67433	13704	40	**15991**	178	15547	220	14956	229
T8-017VC-364	SUERC-64116	10969	35	**12533**	104	12031	186	11256	114
T8-018VC-451	SUERC-67434	13851	41	**16178**	169	15796	186	15187	145
T8-029PC-703	SUERC-67438	12502	39	**13983**	135	13653	151	13278	104
T8-029PC-721	SUERC-67439	12546	39	**14027**	131	13704	147	13315	102
T8-029PC-734	SUERC-67440	12805	38	**14470**	316	13987	133	13551	139
T8-035PC-535	UCIAMS-176375	25330	140	**28972**	355	28661	314	28261	359
T8-035PC-619	UCIAMS-170252	42880	1090					45429	2174
T8-036PC-353	SUERC-71556	28290	108	**31590**	310	31352	204	31142	178
T8-036PC-497	UCIAMS-170253	37880	610	**41879**	896	41639	960	41301	1045
T8-039VC-231	SUERC-68228	18080	52	**21384**	239	20964	212	20470	186
T8-039VC-393	SUERC-71557	18291	50	**21677**	202	21252	233	20729	184
T8-040VC-413	SUERC-64117	13786	39	**16100**	167	15687	206	15096	182
T8-040VC-506	SUERC-67441	19560	53	**23086**	251	22711	214	22343	161
T8-040VC-594	SUERC-68229	20797	60	**24498**	272	24156	210	23721	231
T8-043VC-421	SUERC-67442	16126	48	**18963**	135	18689	118	18245	180
T8-044VC-220	SUERC-73100	11191	37	**12682**	94	12433	178	11657	270
T8-044VC-240	SUERC-73101	11290	37	**12757**	114	12551	96	11885	188
T8-044VC-260	SUERC-73102	11232	38	**12712**	104	12490	141	11759	259
T8-044VC-280	SUERC-73103	11407	36	**12858**	133	12631	78	12115	208
T8-044VC-300	SUERC-73104	11355	38	**12810**	123	12601	82	12003	188
T8-044VC-312	SUERC-67443	10694	38	**12088**	210	11474	247	10980	163
T8-044VC-313	SUERC-67444	10678	37	**12051**	198	11444	241	10959	165
T8-044VC-320	SUERC-73105	11200	38	**12688**	96	12446	172	11678	274
T8-044VC-340	SUERC-73106	11094	38	**12624**	80	12271	220	11474	247
T8-044VC-347	SUERC-68230	11419	38	**12872**	139	12638	82	12141	216
T8-044VC-360	SUERC-73110	12866	39	**14613**	353	14047	131	13614	147
T8-044VC-380	SUERC-73111	12175	38	**13623**	147	13339	102	12942	151
T8-044VC-400	SUERC-73112	12650	37	**14146**	153	13827	131	13397	102
T8-044VC-420	SUERC-73113	11558	38	**13033**	137	12732	110	12377	204
T8-044VC-440	SUERC-73114	12085	38	**13529**	135	13263	102	12837	129
T8-044VC-466	SUERC-66653	13611	38	**15875**	169	15416	200	14750	343
T8-044VC-468	SUERC-67448	18686	51	**22147**	220	21779	192	21245	235
T8-045VC-424	SUERC-67451	14375	43	**16947**	220	16487	221	15953	180
T8-045VC-445	SUERC-67452	14196	41	**16679**	235	16241	180	15704	208
T8-045VC491	SUERC-66654	15501	42	**18346**	165	17996	155	17546	171

(*Continued*)

© 2021 The Authors. *Journal of Quaternary Science* Published by John Wiley & Sons Ltd

Table 9. *(Continued)*

Sample ID	Lab. code	Conventional radiocarbon age (^{14}C a BP)	± 1σ	Calibrated age (cal a BP) $\Delta R = 0$ years	± 2σ	Calibrated age (cal a BP) $\Delta R = 300$ years	± 2σ	Calibrated age (cal a BP) $\Delta R = 700$ yrs	± 2σ
T8-048VC-098	SUERC-67453	15096	43	**17879**	163	17540	172	16981	216
T8-048VC-099	SUERC-67454	15162	42	**17954**	155	17626	182	17087	206
T8-049VC-65	UCIAMS-176376	16345	50	**19230**	204	18880	118	18510	147
T8-050VC-105	SUERC-64118	13712	38	**16002**	176	15560	218	14971	221

Four glacially transported boulders at 105–100 m asl on the crest of the North Lewis moraine were sampled for ^{10}Be TCN analysis (Fig. 4). Three were from Lewisian gneiss boulders of undetermined provenance and transport path (T8AIR02-04), and one was from a far-travelled Torridon Group sandstone erratic boulder (T8AIR01). These samples were presented in Bradwell *et al*. (2019).

The four samples have exposure ages of 26.0 ± 1.4, 26.2 ± 1.5, 30.2 ± 1.8 and 37.5 ± 1.9 ka (Table 5, Figs. 5 and 6), with only two ages overlapping within analytical uncertainties. The lack of clustering suggests that the boulders were not drawn from one statistical population. The older two ages are deemed to be outliers, based on a gESD test – their ages probably reflecting a degree of pre-existing nuclide inheritance rather than the actual timing of boulder deposition. We therefore consider the UWM of the two closely-in-agreement exposure ages to be an accurate and robust representation of the true exposure age at this site (26.1 ± 1.3 ka). These TCN ages constrain the formation, technically the abandonment, of this moraine and thereby date the deglaciation of inland northern Lewis at ~26 ka BP. These ages from the North Lewis moraine also constrain deglaciation of the continental shelf to the NW of Lewis by 26 ka BP, and by inference, ice-stream advance across northern Lewis and the wider Hebrides shelf *prior* to this time (>26 ka BP).

Bragar (NW Lewis)

Three separate locations with different geomorphological contexts were sampled in September 2013, within a 2.5-km^2 area, near Bragar in NW Lewis (ca. 58°20′N, 6°40′W). They are described here in turn.

Ard Bheag Bhragar is a small, low-elevation (20–30 m asl) rocky coastal headland of ice-worn Lewisian gneiss outcrops and scattered glacially transported Lewisian gneiss boulders. We sampled the upper surface of one large boulder and the ice-abraded bedrock surface on which the boulder was resting (Fig. 4). The large boulder (>1 m^3) is unlikely to have been deposited or moved by Atlantic storm waves.

The bedrock sample (T8ABB01) returned an exposure age of 26.6 ± 1.4 ka, whilst the perched Lewisian gneiss boulder (T8ABB02) returned an exposure age of 22.3 ± 1.3 ka (Table 5, Figs. 5 and 6). We interpret the apparent age of the bedrock sample to reflect a degree of pre-existing nuclide inheritance through incomplete or partial (<2 m) erosion of the bedrock surface by glaciation. We cannot be certain that the erratic boulder does not also have a degree of nuclide inheritance, but it is ~4 ka 'younger' than the bedrock sample and generally conforms with the exposure ages from adjacent landforms nearby at Bragar (see below) indicating effective or complete ice-sheet erosion.

Approximately 1 km SW of Ard Bheag Bhragar headland, we sampled a second bedrock-erratic pair on the south side of Loch Eallagro. Ice-abraded bedrock on the stoss (up-glacier) surface of a well-developed roche moutonnèe was sampled along with the upper surface of a glacially transported Lewisian gneiss boulder immediately adjacent to it. Disturbance of this large boulder since deposition is unlikely.

The bedrock sample (T8ABB03) returned an exposure age of 21.0 ± 1.8 ka, whilst the glacially transported boulder (T8ABB04) returned an exposure age of 20.6 ± 1.1 ka (Table 4, Figs. 5 and 6). Both ages agree within analytical uncertainties. We interpret both these ages to reflect the true exposure age and hence sufficient removal of rock (>2 m), and pre-existing cosmogenic nuclides, by an erosive warm-based ice mass. The close agreement between the ages indicates that exposure from beneath ice occurred here at c. 21.0–20.5 ka BP. This age

© 2021 The Authors. *Journal of Quaternary Science* Published by John Wiley & Sons Ltd

assessment broadly agrees, within full uncertainties, with the glacially transported boulder age from Ard Bheag Bhragar ~1 km away (T8ABB02; see above), suggesting that it too reflects the timing of deglaciation (UWM = 21.1 ± 1.0 ka BP; T8ABB02-04) (Table 5, Fig. 5).

A conspicuous boulder moraine complex lies between the communities of Bragar and Shawbost, c. 500 m south of the previous sample site. The main, near-continuous, well-defined ridge is over 500 m long and is 5–8 m high in places. The boulder-dominated slightly arcuate ridge is surrounded by an extensive tract (~1 km^2) of boulder-strewn hummocks, smaller ridge fragments and undulating ground punctuated by occasional streamlined bedrock exposures. We interpret these surficial deposits as an ice-marginal morainic landform assemblage and hereby refer to it as the Bragar Moraine. The moraine represents a retreat stage (or local readvance) of the last ice sheet to cover Lewis. It has not been previously reported or described to our knowledge.

We sampled the upper surface of three large (>1 m^3) glacially transported Lewisian gneiss boulders on the crestline of the Bragar Moraine for TCN analysis (T8BRA01-03) (Fig. 4). All three boulders were firmly lodged within the surrounding morainic debris, meaning that disturbance of these boulders since deposition is unlikely.

The three samples have exposure ages of 17.8 ± 1.2, 19.2 ± 1.1 and 20.3 ± 1.1 (Table 5, Figs. 5 and 6), overlapping within analytical uncertainties. The reduced-χ^2 value of 2.61 indicates that the spread of ages can be explained by stochastic measurement uncertainty (at 95% confidence) and that the ages are from a single population. We therefore consider the UWM of the three ^{10}Be TCN exposure ages (19.3 ± 0.9 ka) to be an accurate and robust representation of the true exposure age. These ages date the formation of the Bragar Moraine, a conspicuous ice-sheet margin stillstand or brief readvance during overall recession, to c. 19.3 ka BP. By inference, the older meaningful dates from Ard Bheag Bhragar (T8ABB02-04), located ~1 km to the north, also constrain deglaciation of the continental shelf offshore NW Lewis to before ~21 ka BP and indicate ice-sheet retreat to the present-day west coast of Lewis by this time.

Rubha Linish (Uig, West Lewis)

West Lewis, west of Loch Roag, has considerably greater relief than northern and eastern Lewis. The geology is similar Archaean Lewisian gneiss but the glaciated bedrock terrain is better exposed as peat cover is generally thin or absent. Located at around 20–50 m asl, at the head of the broad Camas Uig bay, is a complex of depositional glacial landforms relating to deglaciation of the last ice sheet or of an independent Late Weichselian ice cap on Lewis. These features were mapped by Peacock (1984) but their glaciological relationships to former ice masses on the Outer Hebrides have not been previously described. These landforms fall outside the limits of the proposed Younger Dryas (GS-1) glaciation on Lewis (Ballantyne *et al.*, 2008), whilst their large size, low-elevation setting and geomorphological diversity (i.e. moraines, deltas, outwash deposits, etc.) suggest deposition by lobate ice-cap (or ice-sheet) outlet glaciers rather than by small independent mountain glaciers. Four large Lewisian gneiss boulders (T8RUB01, 02, 05, 06), opposite Rubha Linish, on a prominent moraine c. 800 m long and ~20 m high, located ~1.5 km north of Loch Suainaval, were sampled for TCN analysis in May 2013 (Fig. 4).

The four samples have exposure ages of 18.7 ± 1.0, 17.8 ± 1.0, 17.1 ± 1.0 and 16.4 ± 1.0 ka (Table 5, Figs. 5 and 6). The UWM mean of all four samples is 17.6 ± 0.9 ka. A reduced-χ^2 test on all four samples yields a value of 3.11, suggesting that the samples may not be from a single population. The mean exposure age of RUB01 lies + 0.9 ka beyond the age of the next oldest sample (RUB02), but is not distinguished as an outlier at 90% using a gESD test. The youngest sample (RUB06) is also not statistically distinguishable as an outlier in this grouping. Although a stronger fit is returned when using the younger three (reduced-χ^2 = 1.12; UWM = 17.5 ± 0.9 ka), or older three samples (reduced-χ^2 = 2.24; UWM = 18.0 ± 0.9 ka), we have no sound statistical basis for rejecting either RUB01 or RUB06, and, hence, we choose to use the mean of all four ages as the most robust and, on balance, the most faithful representation of exposure age at this locality. These TCN ages date the formation of the Uig moraines (Rubha Linish) and the closely associated glaciofluvial and glaciodeltaic deposits – a significant ice-marginal complex in west Lewis. By inference, these exposure ages also chronologically constrain deglaciation of the Atlantic seaboard of westernmost Lewis by 18.0-17.5 ka BP.

Islibhigh (West Lewis)

On Lewis, 6 km to the SW of Camas Uig and 1 km north of the small community of Islibhig, an unusual spread of large glacially transported boulders (some > 10 m^3) covers an area of c. 0.5 km^2. Many of the boulders are perched directly on stoss–lee or ice-abraded Lewisian gneiss bedrock outcrops. This broad swathe of boulders and finer grade glacial debris, ~500 m wide, trends in a WNW to NW direction, from the steep northern flank of Mealaisbhal hill (570 m asl) to the present-day coastline at Aird Feinis. Three samples (T8ISL02–04) were taken for TCN analysis from the upper surface of three large Lewisian gneiss 'pseudo-erratic' boulders at 50–70 m asl (Fig. 4).

The three samples have exposure ages of 17.7 ± 1.1, 18.4 ± 1.1 and 18.5 ± 1.5 (Table 5, Figs. 5 and 6), with strongly overlapping analytical uncertainties. The tight clustering is reflected in a small reduced-χ^2 value of 0.25, indicating that the spread of ages is well within the range expected from measurement uncertainty and therefore that they are from a single population. We consider the UWM of the three ages (18.1 ± 1.0 ka) to be an accurate and robust representation of the true exposure age at this site. These ages agree well with those on ice-marginal landforms at Uig 6 km to the NW (see above) and hence constrain deglaciation of westernmost Lewis to ~18.0 ka BP, and by inference, deglaciation of the inner continental shelf and the deeper water Flannan Channel to the west of Lewis sometime before this.

OSL geochronology

OSL dating of proglacial and ice-marginal sediments has been used successfully to constrain ice-sheet-margin behaviour and the timing of deglaciation at numerous previous locations around the British Isles (e.g. Smedley *et al.*, 2017a, 2017b). The following section reports 13 new OSL ages, sampled in 2014, from glacigenic sediments at six carefully chosen terrestrial sites in NW Scotland (Table 7) to augment our ^{10}Be TCN dataset (Fig. 6).

Loch Kanaird (Wester Ross)

Located at the head of Loch Kanaird, 5 km north of Ullapool, is a high-level sand and gravel terrace with a gently sloping upper surface at 14–18 m asl (Fig. 7), relating to the final stages of ice-sheet decay in NW mainland Scotland. Lithostratigraphically the sediments are within the Ullapool Gravel

© 2021 The Authors. *Journal of Quaternary Science* Published by John Wiley & Sons Ltd

Formation (Stoker *et al.*, 2009) – glaciofluvial and glacio-deltaic sediments thought to relate to an undated relative sea-level highstand during deglaciation that left extensive evidence along the seaboard of NW mainland Scotland (Bradwell, 2010). A storm-eroded coastal section over 100 m long shows two main sediment facies: lithofacies association (LFA) A composed of planar laminated and ripple laminated silt and fine sand, with an erosional upper bounding surface; overlain by LFA B composed of planar cross-bedded, predominantly clast-supported coarse gravel with occasional boulders. One sample (T8LKAN01) was taken from near the top of LFA A, and a second (T8LKAN03) was taken 0.6 m lower down the sequence in the same unit. A third sample (T8LKAN02) was taken from a thin (0.1 m thick) discontinuous unit of rippled laminated sand within the upper gravel-dominated facies (LFA B).

All three OSL age assessments from Loch Kanaird are similar: 13.7 ± 1.3 ka (T8LKAN01), 14.6 ± 1.4 ka (T8LKAN02) and 14.8 ± 1.9 ka (T8LKAN03), with relatively small (~10%) and overlapping uncertainty terms (Table 7, Figs. 6 and 8). We consider the weighted mean (and standard error) of all three (14.3 ± 0.9 ka) as the most robust and accurate age assessment for the timing of glaciofluvial sediment deposition at this site (following the approach of Smedley *et al.*, 2017a). These ages constrain the final stage of ice-sheet deglaciation in the Summer Isles region of NW Scotland, following the deposition of a conspicuous sequence of well-preserved subaqueous moraines (Fig. 3) during overall tidewater glacier retreat c. 15 ka BP (Stoker *et al.*, 2006; Bradwell *et al.*, 2008b; Ballantyne and Small, 2019).

Kyleakin Quarry (Skye)

This site is located in a disused sand and gravel quarry in the southeast of Skye, 1 km from the Isle of Skye Bridge. The quarry has been excavated into a bench of massive stratified sands and gravels interpreted as glaciofluvial deposits, currently ~50 m asl, thought to relate to final wastage of the ice sheet in the topographic narrows between Skye and mainland Scotland (Fig. 7). Two samples were collected (T8SKYE01 and T8SKYE02), both from within discontinuous units or lenses of horizontally stratified medium-grained sand (0.1–0.3 m thick) contained within a thicker bed of imbricated, clast-supported coarse gravel and boulders.

The samples returned OSL ages of 13.0 ± 1.0 and 10.3 ± 1.2 ka (Table 7; Fig. 6). Although the ages are from the same stratigraphic level, they do not overlap within their uncertainty terms. They are therefore given 'red' quality-control status. For reasons that cannot be fully explained, both ages are considerably younger than expected, with T8SKYE02 being firmly within the Holocene, and not meaningful for constraining ice-sheet deglaciation. These two OSL ages are not considered further.

Suainebost (NW Lewis)

The northwest coast of Lewis between the beaches of Eoropie and Dell exhibits a complex sequence of interbedded and tectonized glacial sediment, up to 20 m thick, and capped in places by windblown sands (Fig. 9). The glacial sediments at Suainebost Sands, Traigh Chumail, Cross Sands and Dell Sands are unusually thick, in an Outer Hebrides context, and have been previously described, albeit briefly, by Baden-Powell (1938), Peacock (1984), Sutherland (1986) and Gordon (1993). The sediment sequences (Fig. 9) are characterized by well-sorted glaciofluvial sands and gravels (LFA 2) sandwiched between two stiff, grey, generally massive, occasionally shelly, glacial diamictons (tills) (LFA 1 and 3), with varying degrees of glacial deformation. The Suainebost to Dell coastal sequences are generally believed to relate to one or more episodes of ice-marginal sedimentation in subaerial, subaqueous and/or subglacial environments (Peacock, 1984; Gordon, 1993). Baden-Powell (1938) related the bedded shelly sands at Suainebost Sands to an 'interglacial marine bed' of unknown age. These coastal sections, comprising variably consolidated Quaternary sediments, are unprotected from Atlantic storm waves and have experienced considerable marine erosion in recent years (since 2010).

All three samples (T8SUAI01-03) at Suainebost (sometimes referred to as Traigh Chumail) were collected from a similar stratigraphic position within the overall sequence (i.e. overlying lower diamict and beneath upper diamict), but were each separated horizontally by ~50 m (Fig. 9). Samples were taken from roughly the middle of the sandy LFA 2 within units of medium to coarse sand, recording subaqueous glaciofluvial and/or glacio-deltaic deposition in shallow water. These waterlain facies all display various degrees of deformation (folding, faulting and compression of laminae), indicating one or more episode(s) of glacio-tectonization following deposition (Fig. 9). No terrestrial organic sediments were found.

The three samples all yielded OSL age assessments falling within MIS 3: 37.4 ± 4.3, 41.1 ± 4.4 and 44.5 ± 5.1 ka (Table 7, Figs. 6 and 8). Although differing by ~3–4 ka, the mean ages overlap within their relatively large uncertainties, and hence neither the lowest nor highest ages can be rejected as outliers. We therefore consider the weighted mean of all three OSL ages (40.6 ± 2.6 ka) to represent a robust and accurate timing of ice-marginal sedimentation at Suainebost in NW Lewis. (For comparison the arithmetic mean is 41.1 ± 2.6 ka). These new OSL ages date ice-marginal or ice-proximal proglacial sedimentation in shallow subaqueous settings (probably lacustrine or lagoonal/low-energy marine) in NW Lewis at c. 41 ka BP. We attribute the glacio-deltaic sands to a period of ice-sheet glaciation on Lewis during one or more pre-Last Glacial Maximum (LGM) cold phases in the latter part of MIS 3.

Port Skigersta (NW Lewis)

Port Skigersta is a rocky cove on the northeast coast of Lewis (Fig. 1), c. 2 km north of the North Lewis Moraine (see above). Coastal sediment exposures here display a complex sequence of interbedded shelly glacial diamictons (tills), cross-bedded sands, silts and gravels interpreted as oscillatory ice-marginal glaciolacustrine and glaciofluvial deposits (Fig. 10). The sediment sequence represents one or more ice-marginal lake environments, with proglacial subaqueous debris fans and deltas, dammed by the former presence of a large ice mass (Peacock, 1984) – probably the MnIS – lying offshore to the north and east. Two samples for OSL dating were taken from the sequence: a lower sample (T8SKIG02) from a horizontally stratified medium–coarse sand unit beneath a thin (<1 m thick) unsorted clast-rich diamicton; and an upper sample (T8SKIG01) from a similarly stratified sand unit immediately overlain by a massive sandy coarse gravel, interpreted as a delta topset prograding into a former ice-dammed lake of undetermined size (Fig. 10).

The upper sample yielded an OSL age assessment of 23.1 ± 2.3 ka, whilst the lower sample returned an age of 22.4 ± 2.1 ka (Table 7, Figs. 6 and 8). Both ages overlap within their uncertainties. We consider the weighted mean of their ages (22.7 ± 1.8 ka) to represent the most robust and accurate timing of ice-marginal sedimentation at Port Skigersta. These two OSL ages, previously reported by

© 2021 The Authors. *Journal of Quaternary Science* Published by John Wiley & Sons Ltd

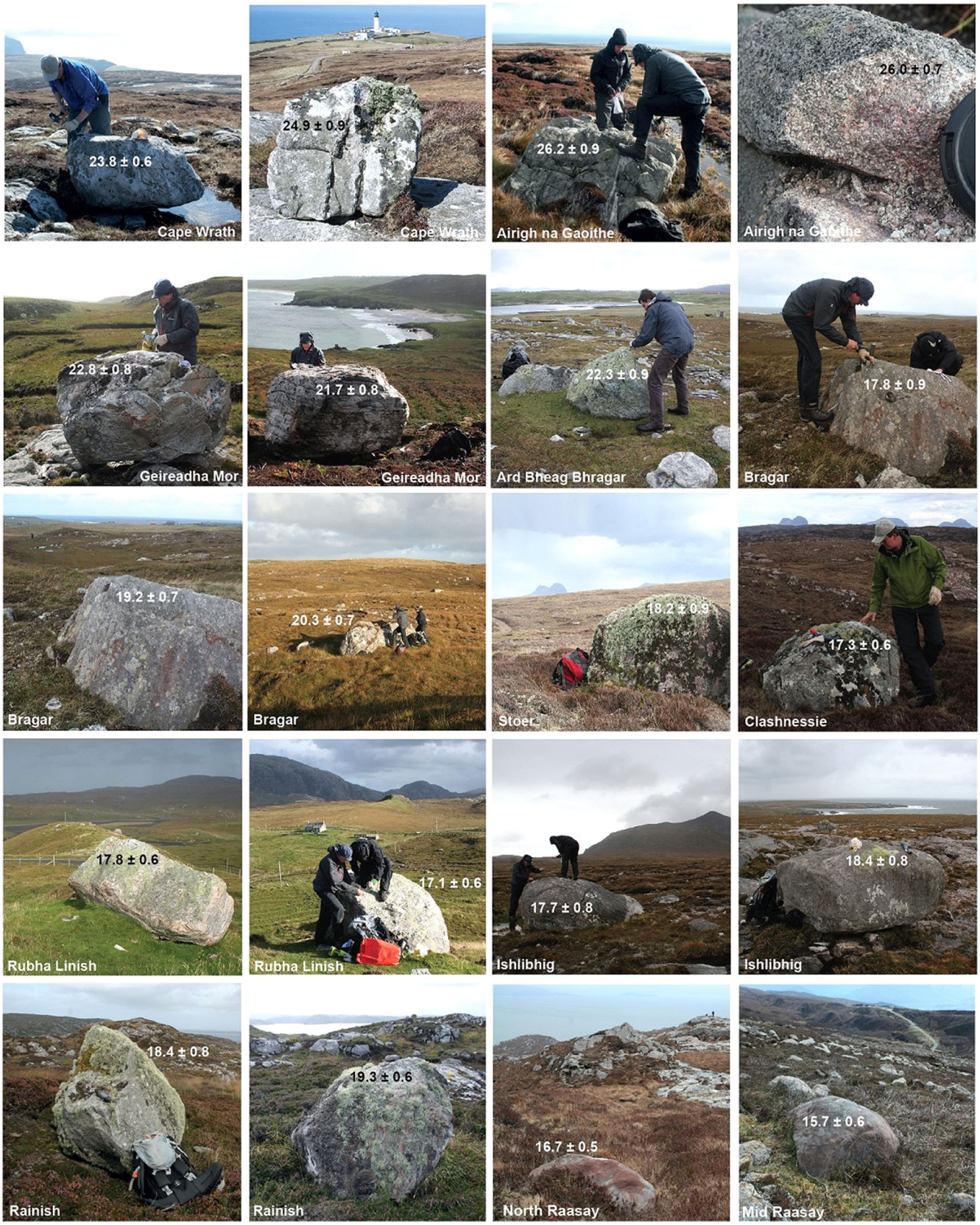

Figure 4. Field photographs and ^{10}Be TCN exposure ages of samples from Lewis, Raasay and mainland NW Scotland, from north to south (down page). Note: all samples, analytical data and age calculations are described in text and presented in Tables 1, 3 and 5. This figure shows only a selection of samples analysed from each site. Apparent exposure ages are in ka (with internal uncertainties). [Color figure can be viewed at wileyonlinelibrary.com].

Bradwell *et al.* (2019), date ice-sheet deglaciation of northern Lewis and, in combination with the TCN ages from NE Lewis (Geireadha Mor) 11 km to the south, constrain retreat of the MnIS from the inner continental shelf into the North Minch straits by ~23 ka BP.

Galson (NW Lewis)

One sample was taken from a lens of fine- to medium-grained sand incorporated within a thin diamicton unit directly overlying cryoturbated raised-beach pebble and cobble gravels of

© 2021 The Authors. *Journal of Quaternary Science* Published by John Wiley & Sons Ltd

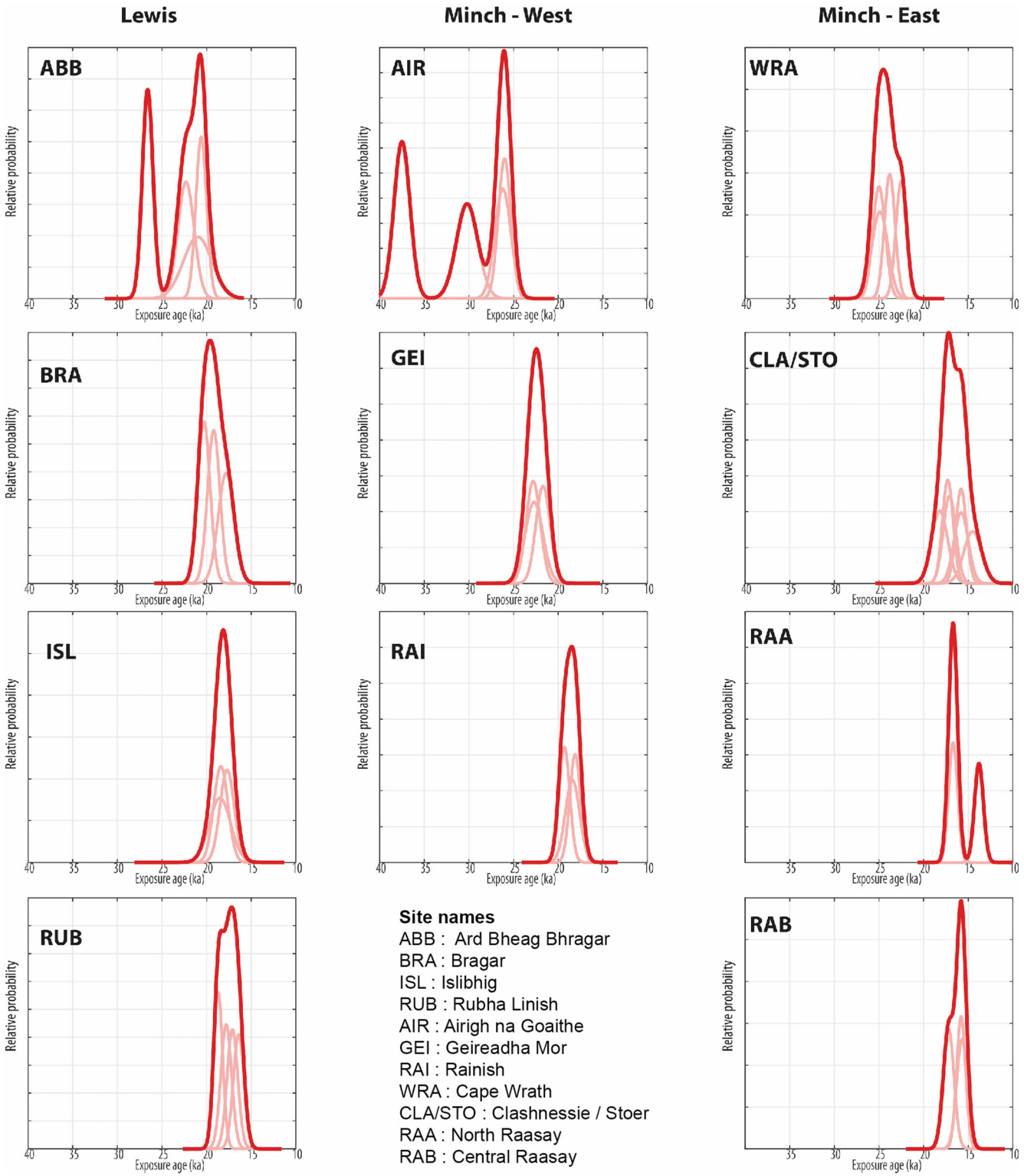

Figure 5. Probability density plots of all ^{10}Be TCN exposure ages described in this study from north to south (down page), west to east (across page). Note: see Tables 1, 3 and 5 for metadata and accompanying analytical data. Note: samples from the Minch (West and East) were presented in Bradwell *et al.* (2019) with slightly different age calculations. [Color figure can be viewed at wileyonlinelibrary.com].

pre-Weichselian age (Fig. 10) – known as the Galson Beach (Peacock, 1984; Gordon, 1993; Hall, 1995). The sample, from an elevation of 5 m asl and a depth of 0.2 m in the sediment profile, returned an OSL age of 14.0 ± 2.5 ka BP (Table 7, Figs. 6 and 8). This single age assessment is very difficult to interpret as it post-dates the timing of deglaciation in NW Lewis by at least 10 000 years, as shown by independent exposure ages in this study (see Results, above). We therefore attribute this anomalously young age to post-glacial sediment disturbance in the uppermost part of the sequence, possibly ice-wedging or cryoturbation during GS-1. Consequently, this single age is assigned 'red' quality-control status, from a deglaciation perspective, and is not considered further.

Garrabost (East Lewis)

Garrabost is located on the Eye (An Rubha) Peninsula, around 15 km south of Tolsta Head, in eastern Lewis (Fig. 1). Here a

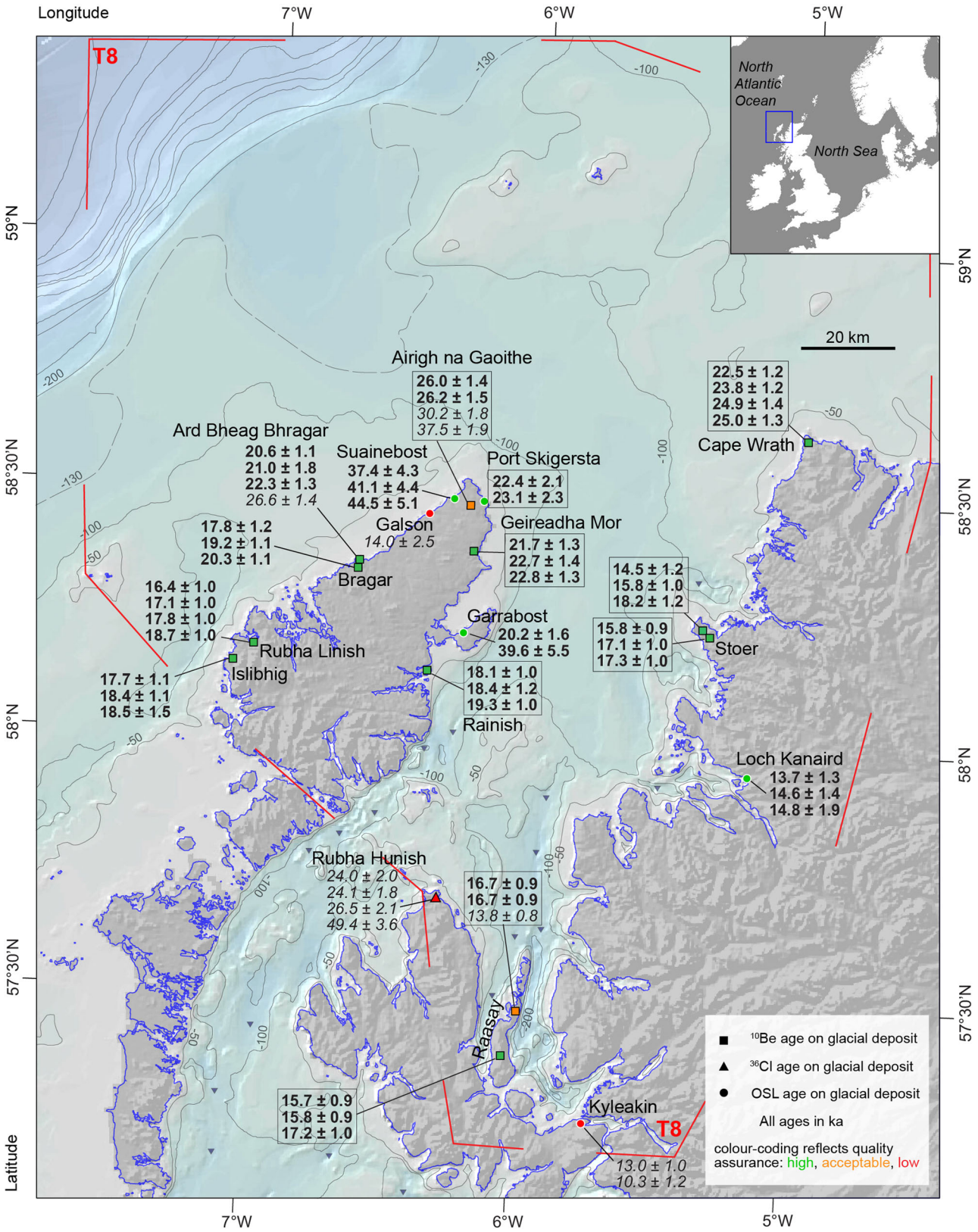

Figure 6. Map showing all new TCN ages with external (full) uncertainties and OSL ages with associated uncertainties. Symbol denotes type of age assessment (see key); colour coding denotes quality assurance of mean 'site-specific' deglacial age. Green = robust, high confidence; amber = acceptable; red = insecure or erroneous, low confidence. Italic font denotes anomalously young or old outliers (see text for details). Those ages in rectangles were presented by Bradwell *et al.* (2019). [Color figure can be viewed at wileyonlinelibrary.com].

15–30-m-thick Quaternary sediment section has been exposed by recent coastal landslipping. From the base upwards, the section shows a relatively simple sequence of structureless dense, over-consolidated grey subglacial diamicton (lower till) with occasional marine shells (LFA A); this is capped by firm, weakly cemented, well-sorted, cross-stratified, medium-grained white sand probably of aeolian origin (LFA B). This, in turn, is overlain by a massive red-brown highly consolidated diamicton (LFA C), with an abundance of Permo-Triassic sandstone clasts characteristic of the Stornoway region of Lewis. This stiff subglacial diamicton (upper till) is separated from an overlying lower-strength fissile morainic diamicton (LFA E) by a thin

© 2021 The Authors. *Journal of Quaternary Science* Published by John Wiley & Sons Ltd

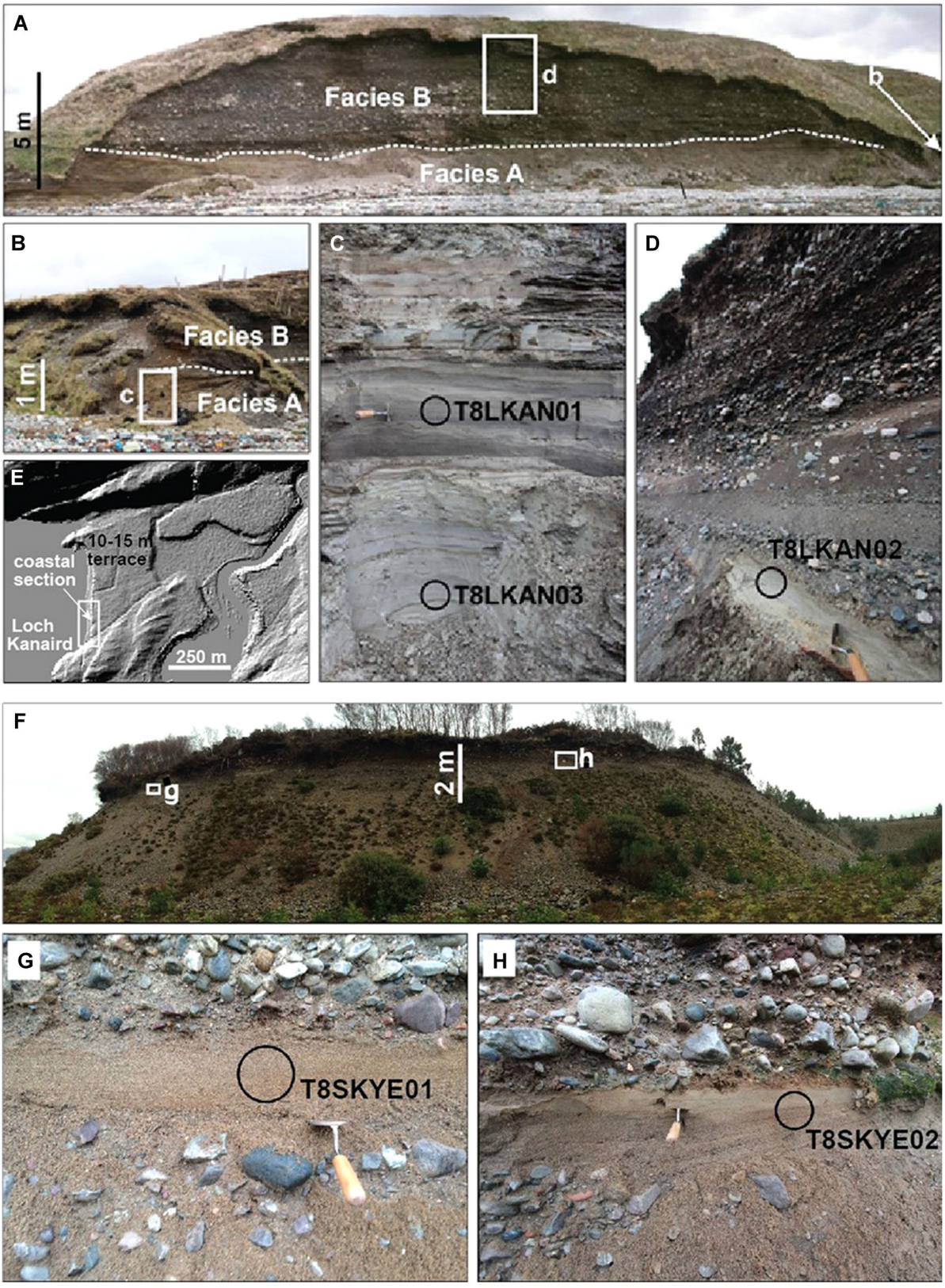

Figure 7. Glacial stratigraphy and OSL sample sites at Loch Kanaird, Wester Ross, and Kyleakin Quarry, Skye. (a) Natural section exposing glaciofluvial and glaciodeltaic sediments in raised coastal terrace adjacent to Loch Kanaird. Note clear division into lower (sand-silt-dominated) and upper (gravel-dominated) lithofacies. (b) Small continuation of natural section, 50 m further south. (c) Close-up of OSL sample sites in rippled laminated fine sand and silt, 1 m above storm beach. (d) OSL sample site in fine sand unit within gravel-dominated facies. (e) Hillshaded NEXTMap elevation model (Intermap Technologies) of Loch Kanaird coastal terraces, showing location of natural section. (f) Disused sand and gravel quarry near Kyleakin, Skye; location of two OSL samples shown. (g,h) Detail of sampled sediment in quarry face. Trowel for scale. [Color figure can be viewed at wileyonlinelibrary.com].

(10–30 cm) unit of planar bedded fine- to coarse-grained glaciofluvial sand (LFA D). One OSL sample was collected from the middle of the lower weakly cemented (aeolian) white sand unit (LFA B) (T8GABB01). A second sample was taken from the diamicton-bounded glaciofluvial sand unit (LFA D) (T8GABB01) (Fig. 10).

We relate the lowest diamicton (LFA A) to an early but significant period of ice streaming across this low ground

© 2021 The Authors. *Journal of Quaternary Science* Published by John Wiley & Sons Ltd

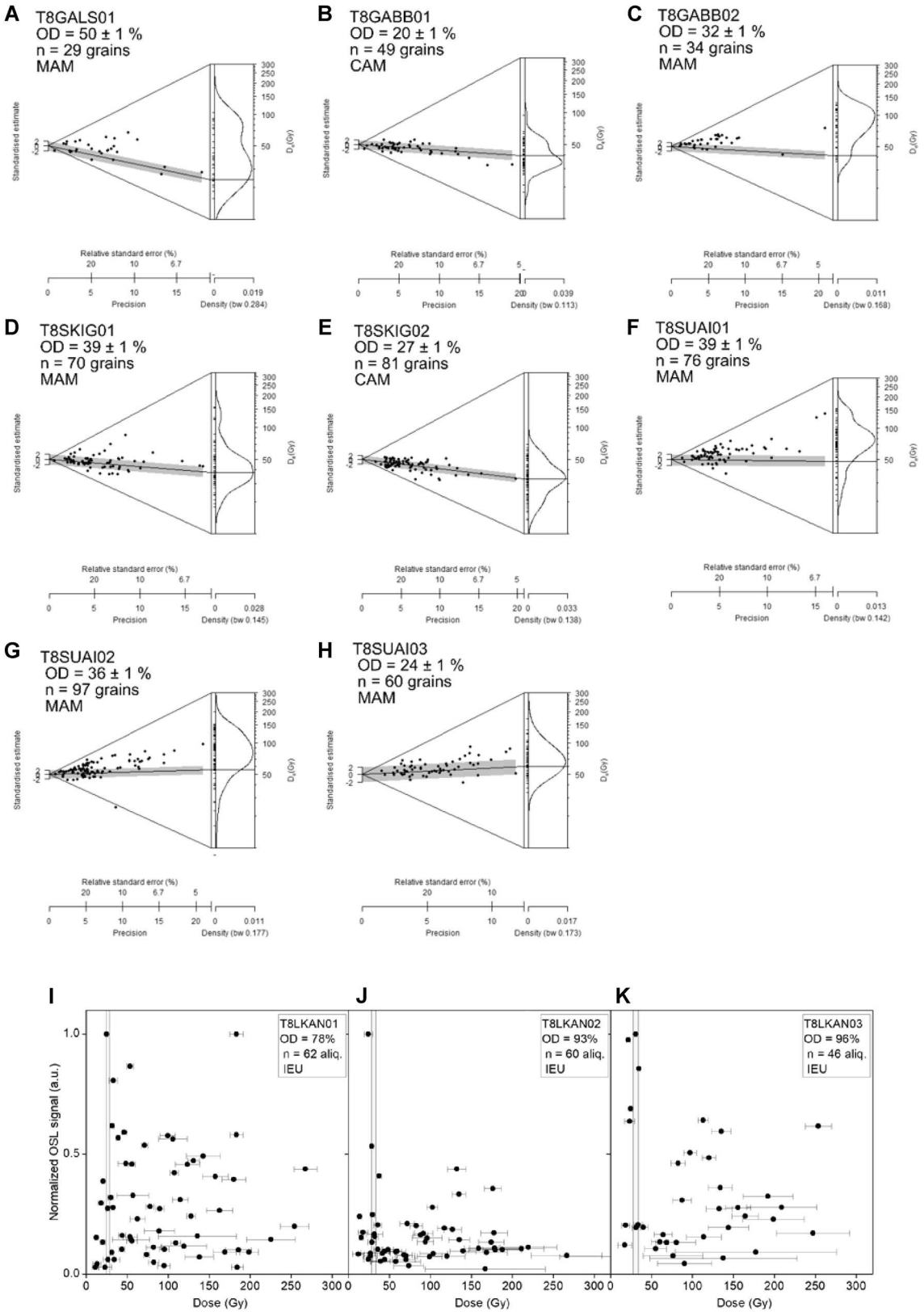

Figure 8. (A–H) Single-grain dose (D_e) distributions (Abanico plots) determined for OSL dating of glaciofluvial sediments. Grey shading shows the CAM or MAM D_e value; '*n*' is number of individual grains analysed in each distribution. (I–K) Small-sample normalized test dose signal as a function of measured dose, with associated errors (1σ). The vertical bars indicate the equivalent dose determined from IEU approach (Thomsen *et al.*, 2005) used in age calculations; '*n*' is number of small multigrains (<20 grains per aliquot) in each distribution. See Table 7 for data.

with a flow direction from the south entraining marine material. The aeolian sands indicate a period of ice-free subaerial conditions with dune development, subsequently overridden by a renewed phase of glaciation. The upper till (LFA C) within this sequence is interpreted as recording later 'tributary' ice-stream flow from Lewis towards the Minch. Ice-marginal sedimentation, represented by the near-surface outwash sands and morainic diamicton (LFA D, E), are consistent with relatively late-stage ice-stream terminus oscillations, or possibly a local Lewis ice-cap advance, during overall ice-stream retreat in the North Minch (Bradwell *et al.*, 2019).

© 2021 The Authors. *Journal of Quaternary Science* Published by John Wiley & Sons Ltd

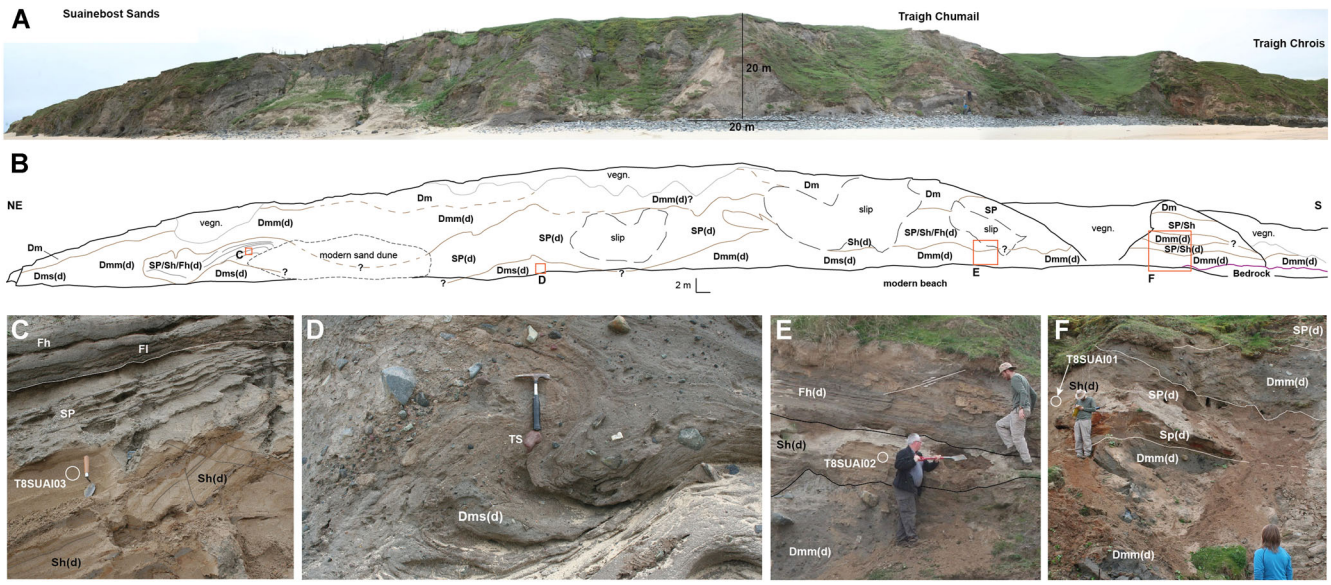

Figure 9. Glacial stratigraphy and OSL sample sites at Suainebost, NW Lewis. (A) Photographic diorama of complex sediment sections (taken May 2014) exposed along coastline between Suainebost and Traigh Chrois. (B) Outline of sediment-stratigraphic relationships in coastal section (interpreted from above). Facies codes after Miall (1988). Locations of sample sites (C, E, F, below) shown as red boxes. (C) Glaciofluvial and glaciodeltaic fine- to coarse-grained thinly bedded sand units with evidence of brittle faulting, overlain by thinly bedded fine sand and silt units with ripple bedding; OSL sample site circled. (D) Recumbent fold, indicating compression, in strongly deformed shelly grey diamicton (lowest unit in sequence). Pre-existing stratification or crude bedding evident in diamicton;?Torridon Group sandstone (TS) clast also highlighted. (E) Planar laminated and thinly bedded glaciofluvial, deltaic and lacustrine fine sand and silt units overlying deformed (basal) grey diamicton; OSL sample site circled. Richard Chiverrell and Matt Burke for scale. (F) Interbedded and weakly deformed sand-and-diamicton sequence at south end of coastal section, partially obscured by slumping; OSL sample site circled. See text and Table 7 for details and data. [Color figure can be viewed at wileyonlinelibrary.com].

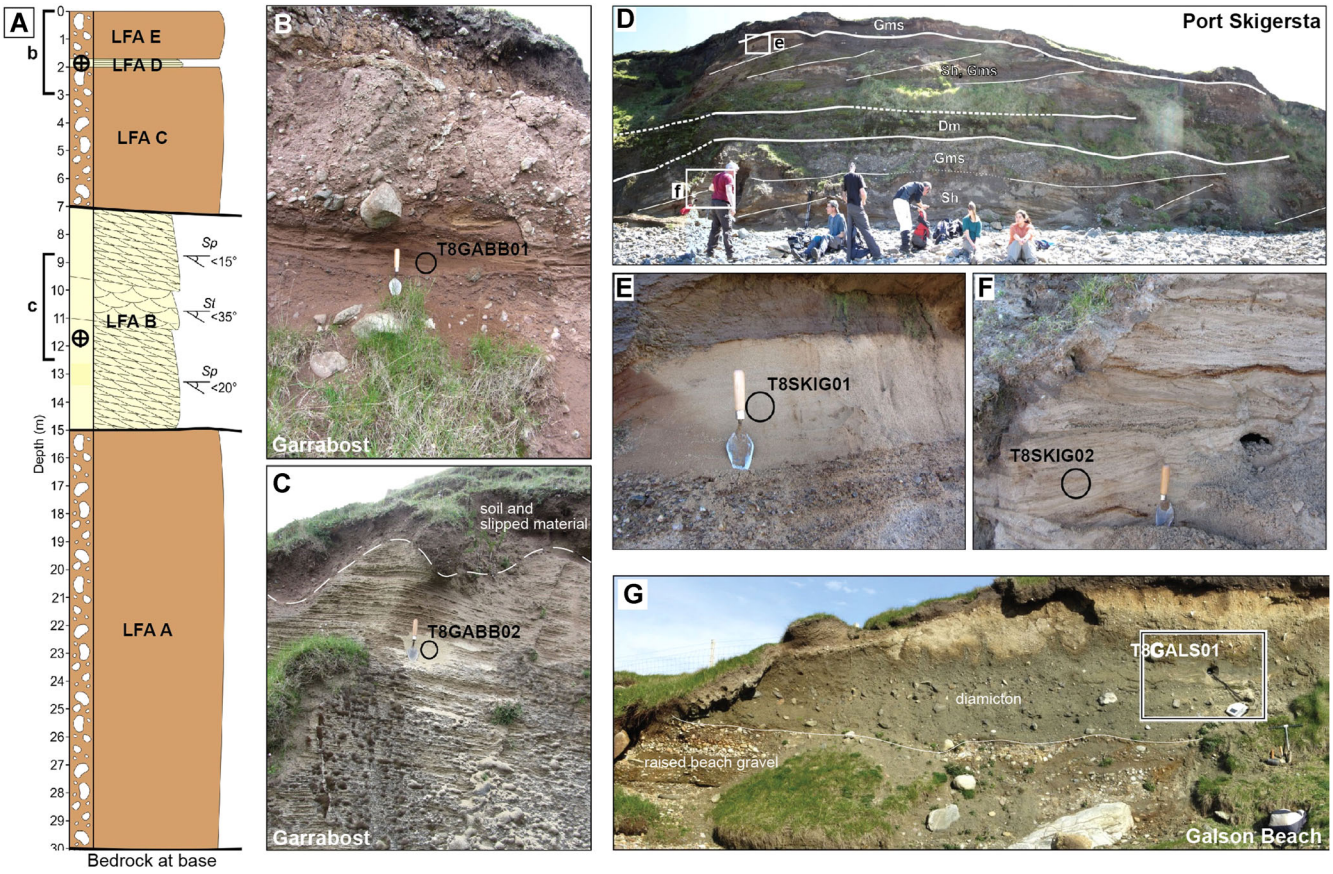

Figure 10. Quaternary stratigraphy and OSL sample sites elsewhere on Lewis: (A–C) Garrabost; (D–F) Port Skigersta; (G) Galson raised beach. Facies codes after Miall (1988). See Table 7 for details and data. [Color figure can be viewed at wileyonlinelibrary.com].

© 2021 The Authors. *Journal of Quaternary Science* Published by John Wiley & Sons Ltd

The stratigraphically lowest OSL sample yielded an age of 39.6 ± 5.5 ka (Table 7, Figs. 6 and 8) indicating windblown dune development and therefore ice-free conditions here at that time. The upper OSL sample at Garrabost has an age of 20.2 ± 1.6 ka constraining an ice-marginal oscillation, and deposition of morainic diamicton, during or immediately after MnIS retreat from the Eye Peninsula. The younger age assessment was previously reported in Bradwell *et al.* (2019).

Submarine glacial geomorphology

Revised seabed landform mapping across the entire T8 study area was undertaken as part of the Britice-Chrono project. Much of this mapping has been recently presented and described by Bradwell *et al.* (2019). We present this glacial landform pattern information here to place our new terrestrial and marine chronological datasets in context (Fig. 3), but in the interest of page space we do not describe the submarine landform record. More information on the glacial geomorphology of the Minch and continental shelf around NW Scotland can be found in several previous publications (Fyfe *et al.*, 1993; Stoker *et al.*, 1993; Ritchie *et al.*, 2011; Bradwell and Stoker, 2015a, 2015b, 2016; Bradwell *et al.*, 2019).

New echosounder bathymetry data (EMODnet Consortium, 2018) has allowed small but important revisions to the existing moraine mapping on the outer continental shelf (Figs. 2 and 3), where the youngest shelfbreak moraines do not continue to the NE [as shown in previous reconstructions (e.g. Clark *et al.*, 2012; Bradwell and Stoker, 2015a, 2015b; Bradwell *et al.*, 2019)], but curve around to the east towards the Sula Sgeir High (Figs. 2 and 3). In addition, moraine patterns on the mid- to outer continental shelf combined with the existing Quaternary stratigraphy strongly suggest that the glacial landforms to the north of the Sula Sgeir/North Rona High (ca. 6°W) date from an earlier (pre-MIS 3) glacial stage (Stoker *et al.*, 1993; Ritchie *et al.*, 2011; Bradwell and Stoker, 2015b).

Marine sedimentology and geochronology

Forty-two successful seabed cores were taken within the study area (T8) during scientific cruise JC123, to validate the Quaternary stratigraphy at key locations and recover material for dating purposes (Fig. 2). This total was made up of 31 vibrocores (VCs) and 11 piston cores (PCs). VCs ranged from 0.86 to 6.06 m long; PCs from 0.47 to 8.89 m long (see Supporting Information Table S1 for core metadata). The marine sedimentological results are presented here in outline form to place our chronological data in context, focusing on key cores that yielded finite dates. The following results section presents all cores and radiocarbon dates by sub-transect, starting furthest offshore. Note, for the sake of brevity, the prefix 'JC123' has been omitted from all core names (i.e. 074VC = JC123-074VC). All depth measurements are from core-top down, to the nearest whole centimetre; all ^{14}C ages

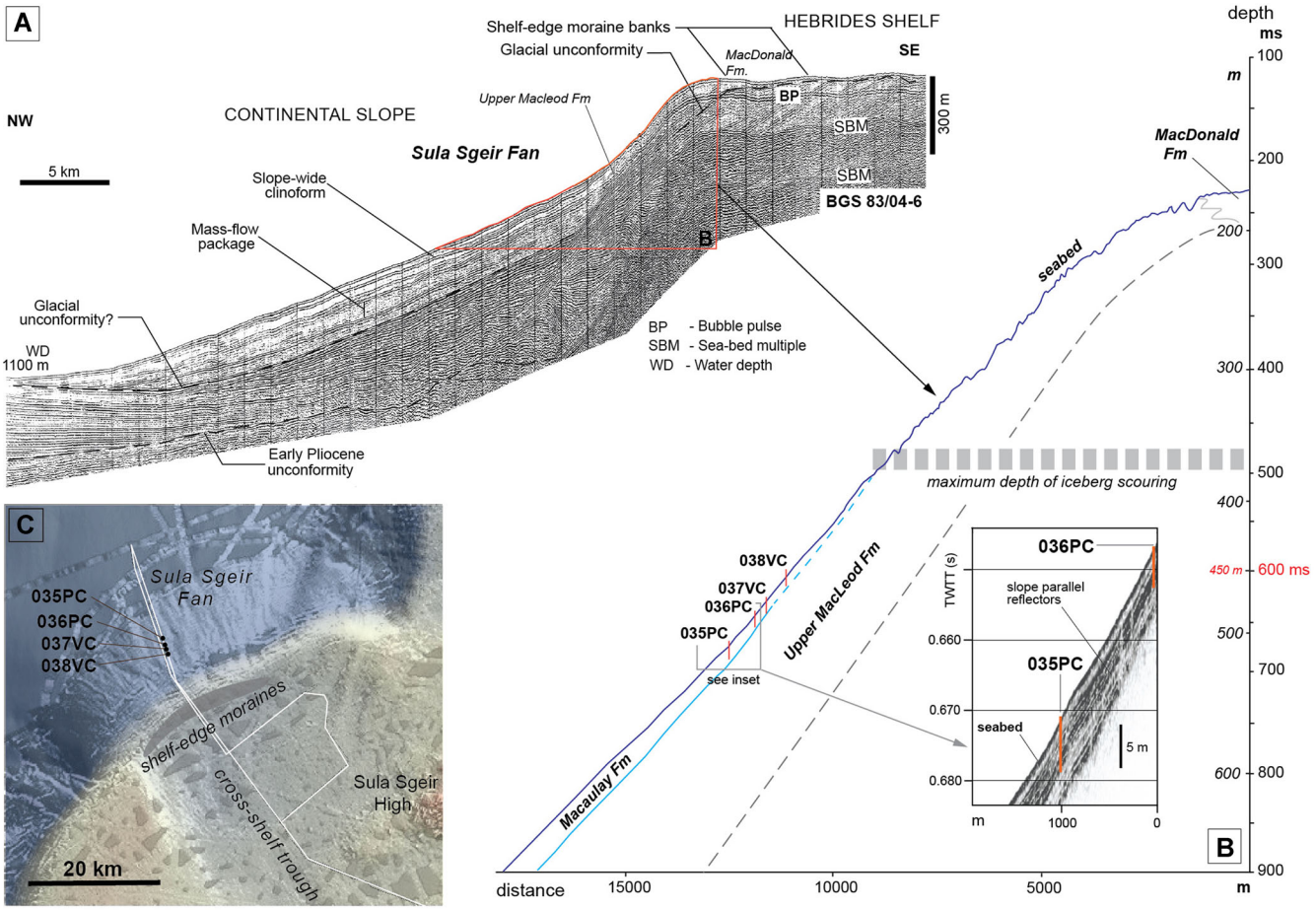

Figure 11. Marine geophysical data from the Sula Sgeir Fan, Continental Slope, offshore NW Scotland. (A) BGS airgun profile across outer Hebrides Shelf and continental slope showing seismic architecture of Sula Sgeir Fan (from Stoker and Bradwell, 2005). Section in panel B highlighted orange. (B) Bathymetric profile of upper Sula Sgeir Fan showing location of cores taken below maximum depth of iceberg scouring on slope. Inset panel shows sub-bottom profile (SBP) data on slope from core sites 035PC and 036PC. TWTT = two-way travel time. A velocity of 1500 m s^{-1} was used to convert TWTT into depth. (C) Singlebeam echosounder bathymetry (Olex dataset) highlighting the macroscale geomorphology of the Sula Sgeir Fan at the mouth of the adjacent cross-shelf palaeo-ice-stream trough. White line is data collection track (JC123); core sites on slope are labelled. [Color figure can be viewed at wileyonlinelibrary.com]

© 2021 The Authors. *Journal of Quaternary Science* Published by John Wiley & Sons Ltd

are presented calibrated (unless otherwise stated) in cal ka BP (see Methods and Tables 8 and 9 for more details of the calibration procedure).

Sub-transect 1 – Sula Sgeir Fan, Outer Shelf and Mid Shelf

The Sula Sgeir Fan is a large (~3750 km^2) wedge-shaped depocentre on the continental slope fronting the cross-shelf trough on the northern Hebrides shelf (Stoker *et al.*, 1993) (Figs. 1, 2). BGS seismic reflection profiles show a marked (Lower Pleistocene) glacial unconformity overlain by laterally continuous slope-parallel reflectors, totalling over 100 m in thickness, on the mid- to lower slope. The whole Pleistocene sequence is divided into three packages on seismostratigraphic grounds: the Lower Macleod, Upper Macleod and Macaulay Formations (Fig. 11). The Lower Macleod Fm is Late Pliocene to Early Pleistocene in age (Stoker *et al.*, 1993; Ritchie *et al.*, 2011). The Upper Macleod Fm comprises glacigenic debris-flow sediments and diamictons, at least in its upper part, thought to be from ice-marginal input during the Early to Mid-Weichselian (MIS 3–5) (Stoker *et al.*, 1993; Ritchie *et al.*, 2011). The overlying Macaulay Fm is undated but is thought to relate to debris flows and hemipelagic sedimentation on the slope after this time (i.e. MIS 2–4). This relatively thin, crudely layered acoustic unit pinches out on the upper slope at around 350–375 m water depth, coinciding with the maximum depth of iceberg scour and seabed disturbance (500 ms) (Fig. 11). We took four cores on the upper- to mid-fan slope in water depths of 450–550 m to prove the sediments in the Macaulay Fm and recover material for dating.

Core 035PC

Piston core 035PC was taken on the Sula Sgeir Fan, ~10 km NW of the continental shelfbreak, in 525 m water depth at 59°11.73'N, 7°14.93'W (Figs. 2 and 11). The core recovered 6.24 m of continuous sediment which is broadly classified into six lithofacies on the basis of visible and X-radiographic sedimentology and geophysical properties (Supporting Information Fig. S1). From the base upwards: Facies I comprises 0.90 m of soft to firm (50–60 kPa) brown, muddy, matrix-supported diamicton with a relatively high proportion of randomly distributed clasts. The clasts are mostly rounded or subrounded, weathered, gneissose, psammitic and arkosic lithologies with NW Highlands and Outer Hebrides affinities. The upper contact with the overlying facies is sharply defined in the geophysical and X-radiographic data, with acoustic velocity, bulk density and CT greyscale values (a proxy for X-ray attenuation or Hounsfield Units) all showing a marked drop at 5.40 m (Fig. S1). The overlying unit, Facies II, is a soft (20–40 kPa) grey-brown mud with occasional scattered small clasts, and faint planar to wispy lower density laminations seen in X-radiographs. This unit grades into the overlying facies (III) at 4.80–4.90 m: a low-strength (20-30 kPa) mud with only rare gravel clasts (>2 mm), less well-defined lamination and evidence of bioturbation. Velocity readings in Facies III are generally uniform at ~1500 ms^{-1} (Fig. S1). This unit is interrupted by Facies IV: 0.35–0.40 m of silty fine sand with occasional gravel clasts, characterized by a peak in velocity, gamma ray attenuation (bulk density) and magnetic susceptibility. The upper 2 m of the core is composed of sediment Facies V with very similar properties to Facies III, with wispy laminations and some bioturbation, but devoid of gravel clasts and showing higher cm-scale variance in geophysical properties. The sequence is capped by 0.10 m of muddy fine sand with occasional shell fragments and small gravel clasts (Facies VI) at, or close to, present-day seabed.

Except for within the surface lag (Facies VI), no macroscopic shells were identified within core 035PC. To provide chronological control on the sediment sequence we AMS-radiocarbon dated two marine carbonate samples of cold-water (not monospecific) bulked foraminifera: one from the diamict at core base, at 6.14–6.24 m, within Facies I – interpreted as a glacigenic subaqueous mass-flow unit or possibly waterlain till; and a second at 5.30–5.35 m, from the low-strength crudely laminated Facies II immediately overlying the diamict (Fig. S1). The lower sample returned a radiocarbon age of 42 880 ± 1090 ^{14}C a BP equivalent to a non-finite or 'background' age (>50 ka BP). The upper sample, from within a mixed unit of ice-rafted sand and gravel debris and muddy hemipelagic sediments, returned a calibrated age of 28.97 ± 0.36 ka cal BP (Table 8).

We deduce that the basal diamict (Facies I), an ice-marginal glacigenic debris flow or waterlain till, stratigraphically within the Macaulay Formation, was deposited when the former BIIS extended to the continental shelfbreak as a grounded ice-sheet ~85 km to the NW of Lewis. We interpret the marked transition, from Facies I to Facies II, as the cessation of primary glacigenic input to the Sula Sgeir Fan slope, above which only glaciomarine sediments, with varying degrees of IRD, and non-glacial hemipelagic sediments have accumulated. There is no evidence of an erosional hiatus or break in sedimentation at this lower facies boundary (Fig. S1). The ^{14}C-dated foraminiferal assemblage at the base of Facies II is therefore a valuable meaningful constraint on the timing of BIIS deglaciation from the shelf edge at ~29.0 ka cal BP, and by inference this date also constrains the most recent ice-sheet maximum in this sector, to *before* 29.0 ka BP. [Note that by applying a ΔR of 300 or 700 years reduces this age marginally (by ~2%) to 28.66 or 28.26 ka BP respectively, but does not change the overall finding, i.e. ice-sheet terminus at the shelfbreak > 28 ka BP].

We have no way of presupposing how much earlier the ice-sheet retreated from its maximal position on the outer shelf. But as core 035PC is from a deeper water continental slope setting, below the maximum depth of iceberg scouring with no obvious erosional breaks in sedimentation, we assume that environmental changes are continuously and systematically reflected in the sediment profile. We thereby place the most likely timing of maximal Late Weichselian ice-sheet extent within the second half of GS-5 (ca. 30.2–29.0 ka BP). We note that this 1200-year period has the most strongly negative $\Delta^{18}O$ values in the Greenland (NGRIP) ice-core record over the last ~50 ka (Rasmussen *et al.*, 2014).

Core 036PC

Taken 1 km further upslope from core 035PC, at 491 m below sea level, piston core 036PC recovered 5.02 m of continuous sediment from the uppermost acoustic facies (i.e. Macaulay Fm) on the Sula Sgeir fan (Fig. 11). The core is stratigraphically similar to core 035PC and can be divided into six main facies, but with some subtle differences (Supporting Information Fig. S2). The lowest unit (Facies I) is a soft to firm (30–40 kPa) grey-brown gravelly mud, with predominantly small gravel clasts widely dispersed within the massive structureless muddy matrix. Above 4.20 m Facies I is more diamictic, becoming more gravel-rich with occasional sandy laminae, and one large cobble-sized clast of gneiss or meta-igneous rock. At ~3.50 m this unit grades upwards into a weakly laminated soft grey mud (Facies II) with occasional isolated gravel clasts and sandy gravel laminae < 10 mm thick (Fig. S2). These two facies are separated by a mixed facies, around 0.40 m thick, with characteristics of both Facies I and II: predominantly less dense weakly laminated soft mud but with occasional denser muddy gravel units (5–10 cm thick), gravel-rich laminae (<10 mm thick) and sand stringers. Facies III

© 2021 The Authors. *Journal of Quaternary Science* Published by John Wiley & Sons Ltd

and Facies IV are both essentially gravel-free muds with some bioturbation (as in core 035PC) interrupted at 1.60 m by a 35-cm-thick muddy fine sand unit with occasional gravel clasts (Facies V). The uppermost unit (Facies VI), at seabed, comprises 0.12 m of muddy fine sand with occasional out-sized gravels and one sandstone cobble (Fig. S2).

We sampled cold-water (not monospecific) foraminifera from the diamictic Facies I (4.90–5.02 m) and the transitional unit Facies I/II (3.50–3.56 m) for marine carbonate ^{14}C analysis (Table 8). Neither sub-sample produced more than 200 micro-fossils in total, and consequently had to be analysed at the small sample AMS lab (UCIAMS). The lower sample, from within a probable glacigenic mass-flow unit or waterlain till, returned a calibrated age of 41.88 ± 0.90 ka cal BP consistent with reworking of subglacial sediment by debris flows from a grounded ice-sheet margin at the continental shelf-break sometime *after* 42 ka BP (see above). The upper age from the mixed facies, calibrated as 31.59 ± 0.31 cal ka BP, is more difficult to interpret (Fig. S2). We view this as probably the product of reworked older foraminifera (i.e. > 35 ka) and *in situ* younger foraminifera (i.e. < 30 ka) being amalgamated within one sample (to generate sufficient mass for analysis). Not a constraining deglaciation age, per se, it is however entirely consistent with this transitional facies being a mixed sediment, containing both an ice-rafted and hemipelagic component – deposited around the time of ice-sheet maximal extent (ca. 30 ka BP). More detailed resolution-specific sampling (sub cm-scale) in the future may be able to extract a more precise dating assessment from this sediment facies.

Cores 037VC and 038VC

Two vibrocores were taken to accompany piston cores 035PC and 036PC on the upper slope section of the Sula Sgeir fan. Core 037VC, taken 350 m upslope of core 036PC in a water depth of 484 m, recovered 4.15 m of continuous sediment. Core 038VC, 600 m further upslope at 457 m bsl, captured 4.80 m of sediment (Fig. 11). Both showed similar downcore geophysical properties and X-ray stratigraphy to cores 035PC and 036PC, with six mud-dominated lithofacies broadly distinguished with varying degrees of gravel clasts and sand. As expected when sampling an up-slope transect through slope-depositional reflectors, the upper facies (II–IV) are thinner in cores 037VC and 038VC than further downslope (in 035PC and 036PC), with core 038VC also capturing significantly more (nearly 3.0 m) of the basal diamict (Facies I) recovered in cores 035PC and 036PC (Fig. 12). No samples were submitted for radiocarbon analysis from either core 037VC or 038VC.

For the purposes of this study, the 'Outer Shelf' region starts at the shelfbreak (maximum change in slope) and extends inshore approximately 45 km to the more varied submarine topography of the 'Mid Shelf' (Fig. 2). We took seven cores on the outer shelf in water depths of 140–180 m to prove the sediments in these Quaternary formations and recover material to constrain ice-sheet retreat.

The acoustic stratigraphy of the Sula Sgeir Basin is well imaged in new SBP survey lines (Fig. 12), with good-quality reflection data to > 70 ms below seabed. The main stratigraphy follows that previously described (Stoker *et al.*, 1993), being a

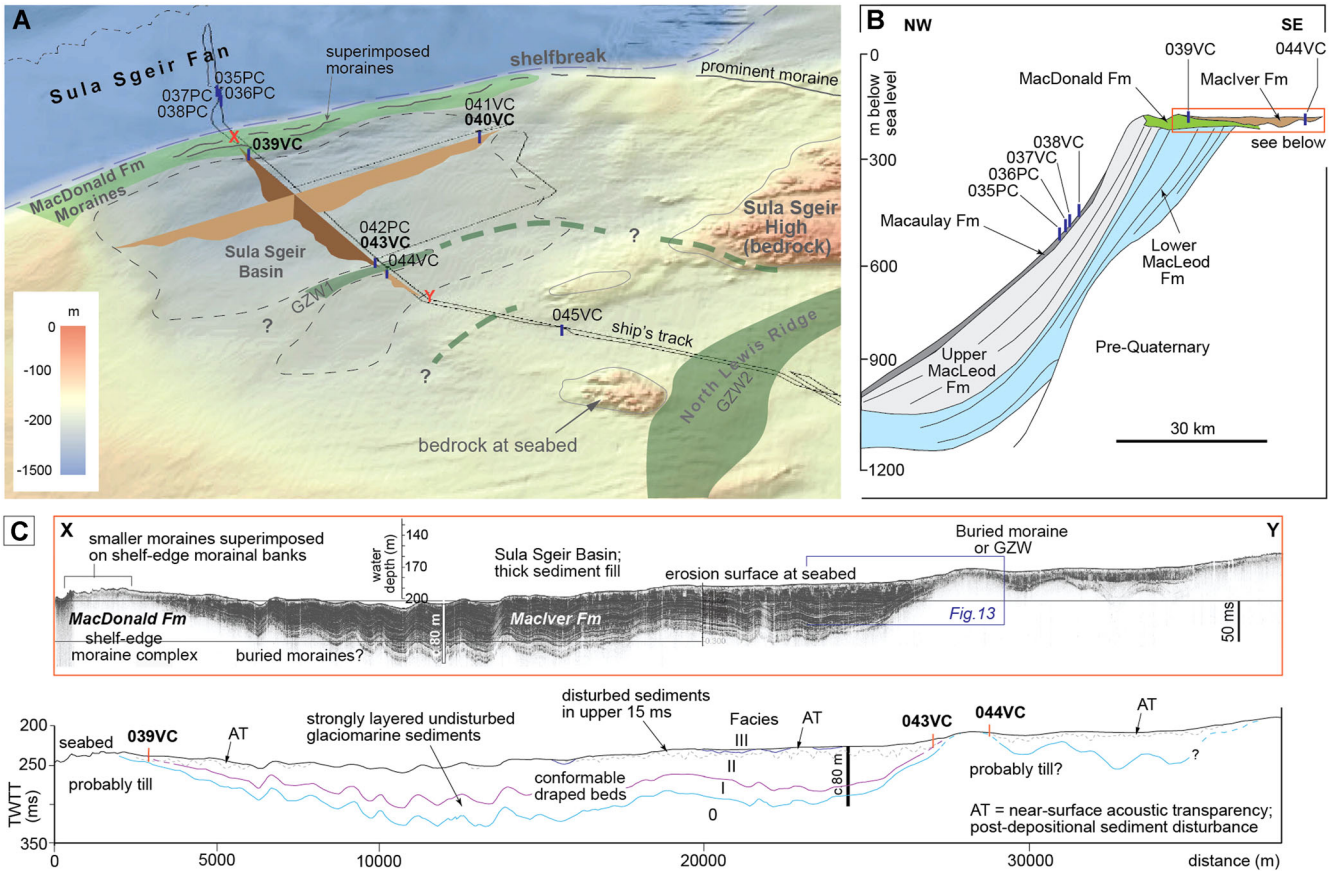

Figure 12. Outer Shelf Late Pleistocene stratigraphy. (A) Perspective view of seabed looking north (EMODnet 2018 bathymetry; DTM lit from NW/315). Outline of Sula Sgeir Basin (layered sediments > 10 m thick) marked with black dashed line; brown profiles show approximate relative sediment thickness across basin; bedrock outcrops in wider area marked with thin grey line. Moraines and grounding-zone wedges (GZWs) shown as green polygons or grey lines (where superimposed). Ship's track and core sites also labelled. (B) Overview stratigraphy of Sula Sgeir Fan and Sula Sgeir Basin showing relationship of main Pleistocene units (after Stoker *et al.*, 1993; Bradwell and Stoker, 2015a). (C) SBP data along line XY (see panel A) highlighting general acoustic stratigraphy and facies sub-division in Sula Sgeir Basin. Formal formation names defined in Stoker *et al.* (1993, 2011). Note zone of near-surface acoustic semi-transparency in shallower parts of basin. [Color figure can be viewed at wileyonlinelibrary.com].

© 2021 The Authors. *Journal of Quaternary Science* Published by John Wiley & Sons Ltd

50–70-m-thick acoustically well-layered high- to low-amplitude sequence of glaciomarine sediment (MacIver Fm), eroded at seabed, proved in BGS boreholes 78/05 and 88/09-10 (Stoker *et al.*, 1993), draped over an acoustically structureless to semi-transparent unit (MacDonald Fm) forming the acoustic basement (Fig. 12). This irregular acoustic basement is composed of stiff glacial diamict, as proved elsewhere on the Outer Hebrides shelf (e.g. BGS borehole 78/05; Stoker *et al.*, 1993), and forms large moraine banks (up to 30 m high) at seabed close to the continental shelfbreak (Figs. 3 and 12) where the MacIver Fm pinches out. Although thought to be Early Weichselian in age (MIS 4) or older (MIS 6-12?) (Stoker *et al.*, 1993; Stoker and Bradwell, 2005), neither the MacDonald Fm nor the overlying MacIver Fm are firmly dated, although the latter is clearly the youngest mappable glacigenic deposit on the outer shelf (Fig. 12).

On the basis of new SBP acoustic data, we subdivide the MacIver Fm into a lower acoustic facies, c. 20 ms thick, with thicker wavy sub-parallel draped reflectors with generally lower amplitude units, and occasional lensoid bodies, conformably overlying acoustic basement (MacDonald Fm). This lower, layered, facies (AF I) is separated by a subtle erosional truncation from an upper strongly layered acoustic facies (AF II) 40–45 ms thick, with thinner parallel draped reflectors but generally of higher amplitude than AF I. The whole layered sequence has been eroded, presenting a near-planar erosional unconformity at or close to seabed. This erosion surface is particularly clear in the shallower southern part of the basin where the wavy parallel beds are truncated at seabed, which is unusually flat (with < 5 m relief) over a distance of 6 km (Fig. 12).

The upper part of AF II is characterized by a distinct near-surface acoustic transparency or semi-transparency with a highly irregular undulating basal boundary. This acoustic disturbance is manifest as a chaotic distribution or 'haze' of lower amplitude intra-formational reflections from seabed to a depth of 10–15 ms (Figs. 12 and 13). This acoustic transparency is more pronounced in the shallower parts of the basin, and is absent where water depths are greatest (<195 m). Most of this acoustic 'haziness' is concentrated in relatively narrow v-shaped or u-shaped zones 5–10 ms deep and 50–300 m wide, producing a highly irregular but well-defined lower boundary (Figs. 12 and 13). In a few places a thin surficial acoustic facies (AF III) occurs at seabed, < 3 ms thick, lacking internal structure. Owing to its discontinuous nature, the stratigraphic relationship with the erosional seabed unconformity is unclear. However, AF III does not appear to have been affected by the acoustic transparency imparted on the underlying layered facies (Fig. 13).

Based on its acoustic character (Fig. 13) and 3-D expression we ascribe this near-surface acoustic semi-transparent zone to one of the following post-depositional disturbance phenomena, in order of likelihood: (i) iceberg ploughing and turbation; (ii) glaciotectonic deformation; (iii) sub-seabed gas; or (iv) cryoturbation. Of these possible processes, our preference is for iceberg ploughing. [An explanation along with proposed timeline of events is presented in the Interpretation/Discussion].

Core 039VC

Taken in a water depth of 183 m, 500 m inshore of the shelf-edge moraines, core 039VC was sited at the western margin of the Sula Sgeir Basin where the layered glaciomarine sediments of the MacIver Fm thin to only 5–8 m in thickness (Fig. 13). The core recovered 4.00 m of continuous sediment, with the lowest 0.25 m restricted to only half the core-liner diameter. Two main

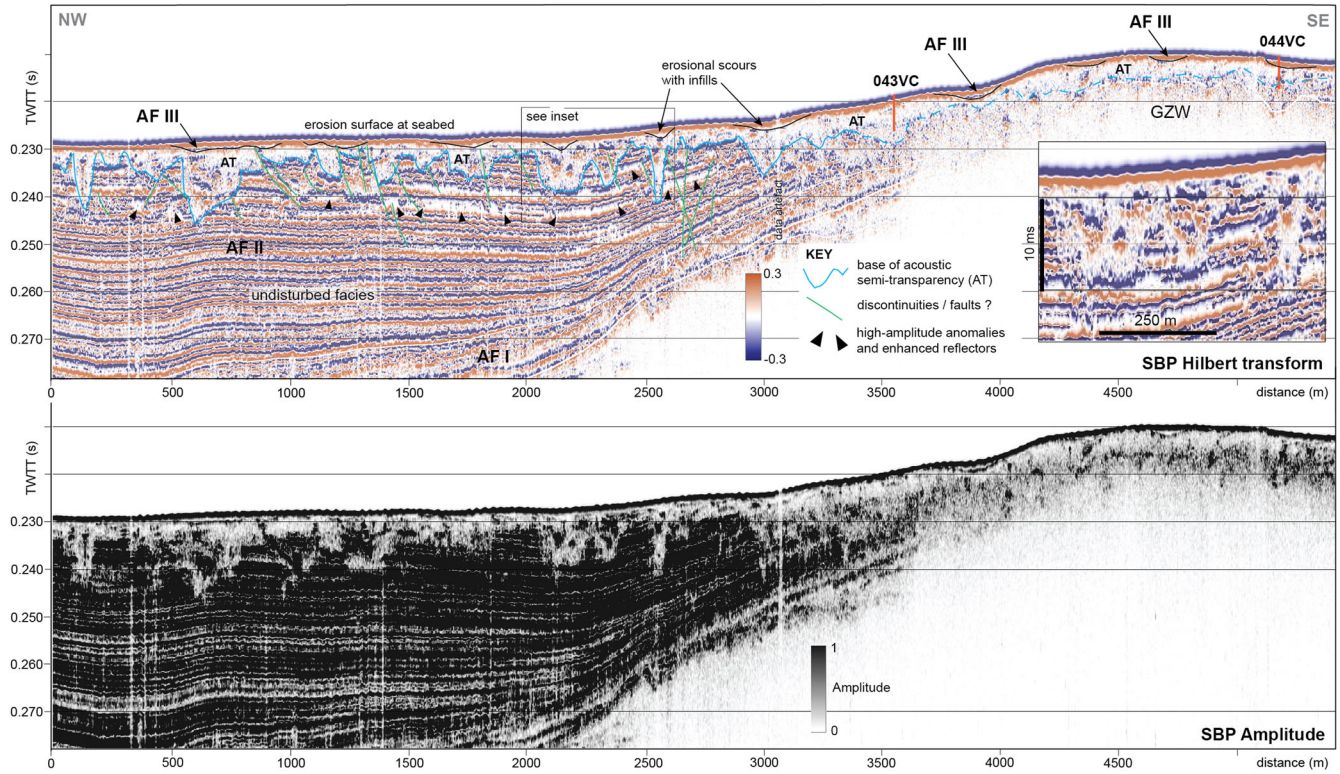

Figure 13. High-resolution image of SBP data at SE margin of Sula Sgeir Basin (see Fig. 12 for line of image). Upper panel: Hilbert transform (red = positive; blue = negative) of amplitude data highlighting strongly disturbed near-surface semi-transparent zone (<15 ms thick) cutting across otherwise regularly bedded high- to low-amplitude acoustic facies. Highly irregular base of disturbed zone is mapped (cyan line), dashed where unclear; along with dipping discontinuities or faults (green lines). White or black lines are acoustic facies boundaries. High-amplitude anomalies (enhanced reflectors) are possibly gas related. Vibrocore sites also shown; both taken within the upper semi-transparent zone. Inset shows SBP data detail of disturbed zone at 2 × magnification. Lower panel (grey scale): same acoustic SBP line showing untransformed amplitude data (dark = high; light = low). [Color figure can be viewed at wileyonlinelibrary.com].

© 2021 The Authors. *Journal of Quaternary Science* Published by John Wiley & Sons Ltd

lithofacies were identified: a lower inter-laminated stiff to firm mud- and fine-sand-dominated facies with evidence of deformation throughout (Facies I), overlain by 0.65 m of muddy fine sand with shells grading into clean sand (Facies III) with a shell-hash horizon at 0.40 m (Fig. 14). Between the two main facies is an ~0.3-m-thick unit of massive silty mud, lacking the density variability seen in Facies I, with occasional gravel clasts. This transitional unit is possibly a separate facies (Facies II). The contact between this and the overlying Facies III is abrupt, probably erosional. Shear strengths in core 039VC are highly

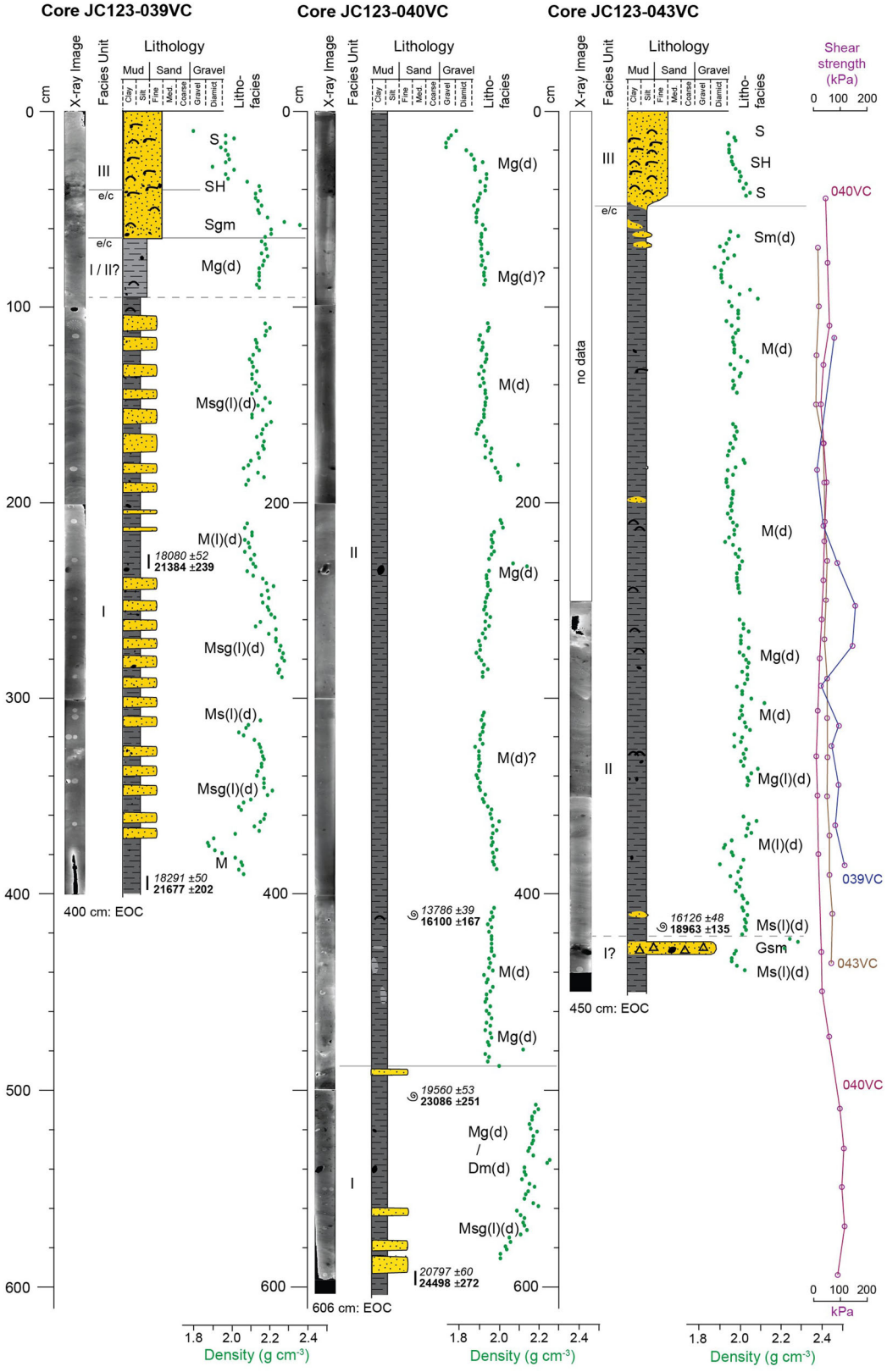

Figure 14. Sedimentology, geochronology and selected geophysical properties of seabed cores JC123-039VC, 040VC and 043VC, all within Sula Sgeir Basin. From left to right: X-radiograph, and interpreted lithofacies boundaries, lithological log, main lithofacies codes, gamma-ray attenuation (density) and undrained shear strength values all plotted on same depth scale. Ages of AMS-dated samples given in radiocarbon years (italic) and calibrated years BP (bold font) with uncertainties (see Table 8). Geophysical property data measured using a Geotek MSCL-S at 2-cm intervals. Gaps are missing data (end caps). EOC = end of core. [Color figure can be viewed at wileyonlinelibrary.com].

© 2021 The Authors. *Journal of Quaternary Science* Published by John Wiley & Sons Ltd

variable, even though grain size, p-wave and gamma-ray attenuation (bulk density) show relatively little variability (Fig. 14). Shear strengths range from 20 to 150 kPa, with the highest strengths recorded in muddy units within Facies I at 2.30–2.70 m. The fact that undrained shear strength does not increase in a predictable manner downcore indicates that the sediment has undergone post-depositional loading or stress-related deformation. This is consistent with sediment turbation by iceberg scour and/or possible glacial overriding and glaciotectonic deformation (Powell *et al.*, 1996; Ó Cofaigh *et al.*, 2005; Callard *et al.*, 2018).

Two samples of marine carbonate from Facies I were submitted for AMS radiocarbon assay: (i) cold-water not monospecific foraminifera from 2.31–2.34 m, and (ii) cold-water monospecific foraminifera (*N. labrodorica*) from 3.90–3.95 m (Fig. 16). The former returned a calibrated radiocarbon age of 21.38 ± 0.24 cal ka BP, and the latter 21.68 ± 0.20 ka cal BP (Table 8). Although in stratigraphic sequence, both calibrated ages overlap at 2-sigma despite being vertically separated by 1.6 m, suggesting sediment turbation and vertical mixing, rather than near-instantaneous deposition.

Cores 040VC and 041VC

These two cores were taken on an 18-km-long survey line perpendicular to the main cross-trough transect, to capture the glacial stratigraphy of the MacIver Fm as it pinches out at Sula Sgeir Basin's northern edge (Fig. 13). Core 040VC captured 6.06 m of continuous sediment penetrating both the upper acoustic facies (AF I) and c. 1.1 m of the underlying acoustic facies (AF II) (Fig. 14). The lowest lithofacies (I) recovered in the core is a firm (80–110 kPa) grey-brown clast-rich mud with crude cm-scale lamination/bedding and evidence of deformation seen in X-radiographs. The bedding is characterized by gravel-poor sandy units and higher density gravel-rich muddy diamictic units. Facies II has considerably lower bulk density, p-wave velocity and magnetic susceptibility than the basal unit (Facies I) (Fig. 14) and comprises 4.90 m of soft to firm (20–60 kPa) grey clay-rich mud with occasional to rare gravel clasts and numerous small intact shells (of uncertain species). Bioturbation and weak deformation structures are seen, although the latter are rare and not pervasive. Shear strength downcore is variable, although generally predictable, showing a minimum at 3.00–3.40 m in the lowest density muds and a maximum in the high-density basal diamictic facies (at 4.90–6.00 m) (Fig. 14).

Three samples of marine carbonate from core 040VC were submitted for radiocarbon analysis: (i) cold-water not monospecific foraminifera from the base of the core at 5.94–5.97 m, and (ii) a shell of uncertain species from 5.06 m, both within Facies I – interpreted as a proximal IRD-rich glaciomarine deposit or possibly a subaqueous glacigenic debris flow (Fig. 14). The basal sample returned a calibrated radiocarbon age of 24.50 ± 0.27 ka cal BP, and the shell returned an age of 23.09 ± 0.25 ka cal BP (Fig. 15). A third sample at 4.10 m, from within Facies II, interpreted as distal glaciomarine sediment, yielded a calibrated radiocarbon age of 16.10 ± 0.17 cal ka BP (Table 8). As the whole sequence in core 040VC has been pervasively deformed or turbated, probably by iceberg ploughing, we interpret these ages with caution. Rather than taking them at face value, we suggest there is a high likelihood that, as in core 039VC, the radiocarbon-dated micro- and macro-fauna are not in their original stratigraphic position and hence do *not* accurately represent the timing of sediment deposition and ice-sheet deglaciation (as encountered on the Malin Shelf; see Callard *et al.*, 2018).

Core 041VC, 100 m SW of core 040VC, recovered only 1.00 m of sediment, and was not analysed in detail. No samples were selected for radiocarbon dating. Interestingly, it captured 0.30 m of shelly sandy facies (AF III) which was not present in the adjacent core 040VC, highlighting the sporadic distribution of this thin uppermost unit and the erosional nature of the Facies II–III boundary.

Cores 042PC and 043VC

These two cores, one vibrocore and one piston core, were taken at almost identical locations on the western flank of an acoustically semi-transparent 5-km-wide ridge of glacigenic sediment – interpreted as a large buried moraine complex or GZW (Fig. 12). Core 042PC recovered only 0.47 m of sediment in total, comprising fine-grained massive to weakly bedded shelly sand with a shell hash layer at 0.25 m, part of a discontinuous surficial sand sheet seen in the SBP data (AF III; Fig. 13).

Core 043VC, taken at the same location, penetrated through the shelly sand unit to recover 4.59 m of continuous sediment. This vibrocore captured both AF II: a firm, deformed, laminated, IRD-rich grey-brown clay-rich mud facies, becoming clast-poor and more massive above ~3.0 m; and the overlying AF III: a fine-sand facies with shell-rich horizons and an erosional, possibly reworked, basal contact (Fig. 14). Shear-strength measurements show a relatively uniform increase with depth downcore (20–80 kPa). Near the base, at 4.10–4.20 m, a marked, albeit gradational, colour change to a darker grey clay occurs, interrupted by a 7-cm-thick red-brown sandy gravel layer. This ~0.40-m-thick unit may represent the uppermost part of the more diamictic Facies I (seen in core 039VC) (Fig. 14).

One broken gastropod shell sampled from just above the conspicuous gravel layer at 4.21 m returned a calibrated radiocarbon age of 18.96 ± 0.14 ka cal BP (Table 8; Fig. 14). However, as the sediments in this core (below surface Facies III) have probably been subject to an unknown degree of post-depositional deformation by iceberg ploughing (see above), this date is not considered to be a high value deglacial age constraint.

Core 044VC

This core, from the eastern flank of a large buried moraine or GZW (GZW1 in Bradwell *et al.*, 2019), yielded a 5.19-m-long complex stratigraphy (Figs. 12 and 13). Subdivided into six main lithofacies, on the basis of physical and X-radigraphic properties (Supporting Information Fig. S3), the sediments below ~3.0 m are predominantly muddy and clast-rich, probably within AF II, whilst those in the upper ~3.0 m are mainly sandy with varying proportions of shell material, part of AF III (Fig. 13).

Seventeen marine carbonate samples were submitted for AMS ^{14}C dating: four intact bivalve shells and 14 foraminifera samples at regular depth intervals from 2.20 to 4.80 m (Fig. S3). As the lower lithofacies (II, III, IV) have been deformed or turbated, probably by iceberg ploughing (see cores 039VC, 040VC, 043VC above), the stratigraphy in this core is of relatively little value for constraining deglaciation. We report the ^{14}C ages here for completeness (Table 8), ranging from 12.05 ± 0.20 to 15.88 ± 0.17 cal ka BP, whilst noting that the ages are not in stratigraphic sequence with several overlapping at 2-sigma uncertainties. It is very likely, based on all the acoustic, sedimentological and geochronological evidence, that this core was taken within a large buried iceberg ploughmark or seabed scour, perhaps one of many in the shallower parts of the Sula Sgeir Basin. We propose that this erosional scour (cut into AF I or II) was subsequently infilled, initially by slumping (Facies III–IV), and latterly by rapidly accumulating marine sands

© 2021 The Authors. *Journal of Quaternary Science* Published by John Wiley & Sons Ltd

Figure 15. A selection of marine shells from different cores chosen for AMS ^{14}C analysis. Ages quoted in radiocarbon years; scale graduated in mm and cm. See Tables 8 and 9 for full dataset. [Color figure can be viewed at wileyonlinelibrary.com].

associated with a deglacial sea-level transgression (Facies V–VI) (Fig. S3). The basal ^{14}C age of 22.15 ± 0.22 cal ka BP is harder to reconcile, being ~5.0 ka ^{14}C older than the next oldest sample, but we believe it too has been subject to post-depositional disturbance and probably lacks stratigraphic integrity.

Core 045VC

Taken at the mid- to outer shelf transition, ~45 km inshore from the shelfbreak and ~10 km SE of the Sula Sgeir Basin edge (Fig. 12), core 045VC recovered 4.93 m of continuous Quaternary sediment. Although complex at the cm-scale, the sediment can be broadly divided into two facies: an upper fine- to medium-grained, occasionally gravelly, sand unit (0.95 m thick) with an unusually high proportion of shell material (30-50%); and a lower, soft to firm, grey-brown mud-dominated, occasionally sandy facies, with an increasing proportion of gravel clasts downcore. Sedimentary laminations are seen in X-radiographs between 2.50 and 4.00 m as well as some evidence of, perhaps syn-sedimentary, deformation.

© 2021 The Authors. *Journal of Quaternary Science* Published by John Wiley & Sons Ltd

The mud-dominated facies – interpreted as moderately IRD-rich proximal to IRD-poor distal glaciomarine sediment – has a relatively uniform downcore shear strength of 20–40 kPa, somewhat lower strength than the iceberg-turbated facies seen in the Sula Sgeir Basin cores (039-044VC, see above).

Three AMS ^{14}C assays were undertaken on marine carbonate material sub-sampled from core 045VC. At a depth of 4.91–4.94 m, a sample of cold-water, not monospecific, foraminifera from the basal IRD-rich facies returned a calibrated radiocarbon age of 18.35 ± 0.17 ka cal BP. A single fragile articulated shell (of undetermined species) from a gravelly sandy silt laminae, at 4.45 m, returned a calibrated age of 16.68 ± 0.24 ka cal BP (Fig. 15). Finally, a broken shell (of undetermined species) within a non-laminated section of the dropstone-rich mud facies, at 4.24 m, returned a calibrated age of 16.95 ± 0.22 ka cal BP (Table 8). These ages are hard to interpret as this core did not penetrate the basal diamict and therefore any marine faunal ages cannot be firmly related to initial deglaciation in this setting. The oldest date (18.35 ka) is firmly within the GS-2 cold phase, but based on our developing terrestrial chronology of MnIS retreat, lags behind the timing of deglaciation on the mid-shelf by 8-10 ka (see TCN and OSL results). As such, it provides only a loose *minimum* constraint on deglaciation.

The Mid Shelf, defined here as the region approximately 45–80 km inshore of the continental shelfbreak, is a zone of more complex glacial geomorphology than the outer shelf and it is here that the cross-shelf trough, defined by the 100-m isobath, swings to the NW (Fig. 2). In several places, large low-angle asymmetric wedge-like accumulations are interpreted by Bradwell *et al*. (2019) as GZWs, or hybrid GZW/moraine banks, relating to stabilizations of the MnIS grounding zone (Fig. 3). We took seven cores on and either side of GZW3, to prove the sediments within it and recover material to constrain ice-sheet retreat on the mid shelf (Fig. 16).

The glacial stratigraphy around GZW3 (also referred to as 'North Minch Ridge') has been previously outlined on the basis of BGS seismic reflection profiles (Fyfe *et al*., 1993; Stoker *et al*., 1993; Bradwell and Stoker, 2015a). Our new acoustic SBP data capture the stratigraphy either side of GZW3 well (Fig. 16), allowing the clear demarcation of three different acoustic facies, above the acoustic basement, which we relate to the main Late Pleistocene formations (revised by Stoker *et al*., 2011). Acoustic Facies I (AF I) is a structureless semi-transparent (low-amplitude) unit with few internal reflectors and an irregular upper surface, equating to the dense diamictic Jean Fm. Acoustic Facies II, immediately overlying AF I, comprises wavy sub-parallel, rhythmically layered, conformably draped reflectors with generally alternating high-amplitude and lower amplitude laterally continuous units – equating to the glaciomarine Morag Fm (Fig. 16). This strongly layered facies (AF II) has an erosionally truncated upper boundary and is overlain by a thin (<5 ms) patchy surficial acoustic facies (AF III), with a generally transparent acoustic character or weakly developed planar horizontal reflectors. We equate AF III to the sand-dominated spatially discontinuous Catriona Fm (Fig. 16).

In places, the upper 5–10 ms of acoustic layering within AF II becomes indistinct, transparent or semi-transparent with very low-amplitude signal return (Fig. 16). A similar, but less pronounced, phenomenon to that seen in the Sula Sgeir Basin, this near-surface acoustic semi-transparency is patchy and generally restricted to the basin margins around GZW3, but cannot be discerned with confidence in AF III. As on the Outer Shelf, we ascribe these acoustically (semi-)transparent near-surface anomalies to iceberg ploughing/turbation, or possibly localized glaciotectonic deformation, and in one instance sub-seabed gas (Fig. 16).

Cores 006VC and 046VC

Core 006VC was collected in a water depth of 121 m, 4.5 km NW of GZW3. This 5.20-m-long core captured three main lithofacies corresponding well with the acoustic facies identified above (Fig. 16). From core base, Facies I is a firm (50–80 kPa) dark grey gravelly clay-rich mud, generally massive but with occasional lamination showing evidence of deformation particularly towards the base, and becoming notably less gravel-rich above 3.75 m – interpreted as proximal IRD-rich glacimarine sediment or waterlain till. Facies II is a soft (20–40 kPa) silty mud with rare isolated gravel clasts and occasional shells, showing weak wispy laminations with evidence of burrows and bioturbation throughout – interpreted as distal glacimarine sediment (Fig. 16). This is erosionally overlain by Facies III: a buff-brown medium- to fine-grained sand, with varying proportions of shell fragments, showing weak bedding structures as well as shell-rich horizons – interpreted as a marine, possibly shoreface, deposit.

One marine carbonate sample was submitted for AMS ^{14}C analysis (at 1.72 m) from within the distal glaciomarine Facies II: a gastropod shell with a barnacle-encrusted surface (Fig. 15). The shell material returned a calibrated age of 20.49 ± 0.17 ka cal BP (Table 8). Assuming that the cored sequence has good stratigraphic integrity (i.e. that sediment disturbance/deformation is not pervasive), this date indicates ice-sheet-free open-water conditions here since before 20.5 ka cal BP.

Core 046VC was taken close to the crest line or high point of GZW3 in 118 m of water (Fig. 16). Unfortunately, the core failed to penetrate the uppermost facies (AF III) recovering only 0.86 m of medium- to fine-grained shelly sand.

Cores 007VC-009VC

These three cores were taken in relatively close proximity, at c. 120 m water depth, near the base of the long ice-proximal slope of GZW3, where the Morag Fm is truncated by an extensive near-seabed erosion surface (Fig. 16). Core 007VC recovered 2.84 m of sediment split equally between: a firm, dark grey slightly gravelly mud with evidence of deformation or disturbance throughout, similar to Facies I in core 006VC (Jean Fm); unconformably overlain by 1.45 m of fine-grained sand with shell fragments and a concentrated shell-hash layer, typical of Facies III (Catriona Fm).

Core 008VC taken 250 m further SE, captured 2.82 m of sediment again split almost equally into two lithofacies (Fig. 16). The lower unit is a soft silty grey-brown generally massive silty mud with some wispy laminations, rare gravel clasts and evidence of bioturbation and possible shallow-gas disturbance, similar to the distal glaciomarine facies (II) recovered in core 006VC (=Morag Fm). The upper unit comprises well-sorted fine sand with shell fragments in a single generally structureless bed, akin to AF III seen in core 007VC (=Catriona Fm).

Core 009VC, taken 500 m further SE, again captured two main lithofacies within 4.38 m of recovered sediment: a lower muddy unit with very rare gravel clasts and abundant evidence of bioturbation and stratigraphic disturbance (Fig. 16), similar to the lower facies in Core 008VC (=Morag Fm); overlain by 1.50 m of shelly fine-grained sand with a concentrated shell bed at 1.00–1.10 m, stratigraphically within AF III (=Catriona Fm).

A sample of cold-water, not monospecific, foraminifera from near the base of core 008VC (2.71–2.76 m) yielded a calibrated radiocarbon age of 20.08 ± 0.18 ka cal BP (Table 8) indicating marine (ice-free) conditions since at least this time. However, post-depositional disturbance structures within this glaciomarine facies, seen in X-radiographs and SBP data, mean that this 'minimum' deglacial age should be viewed with caution.

© 2021 The Authors. *Journal of Quaternary Science* Published by John Wiley & Sons Ltd

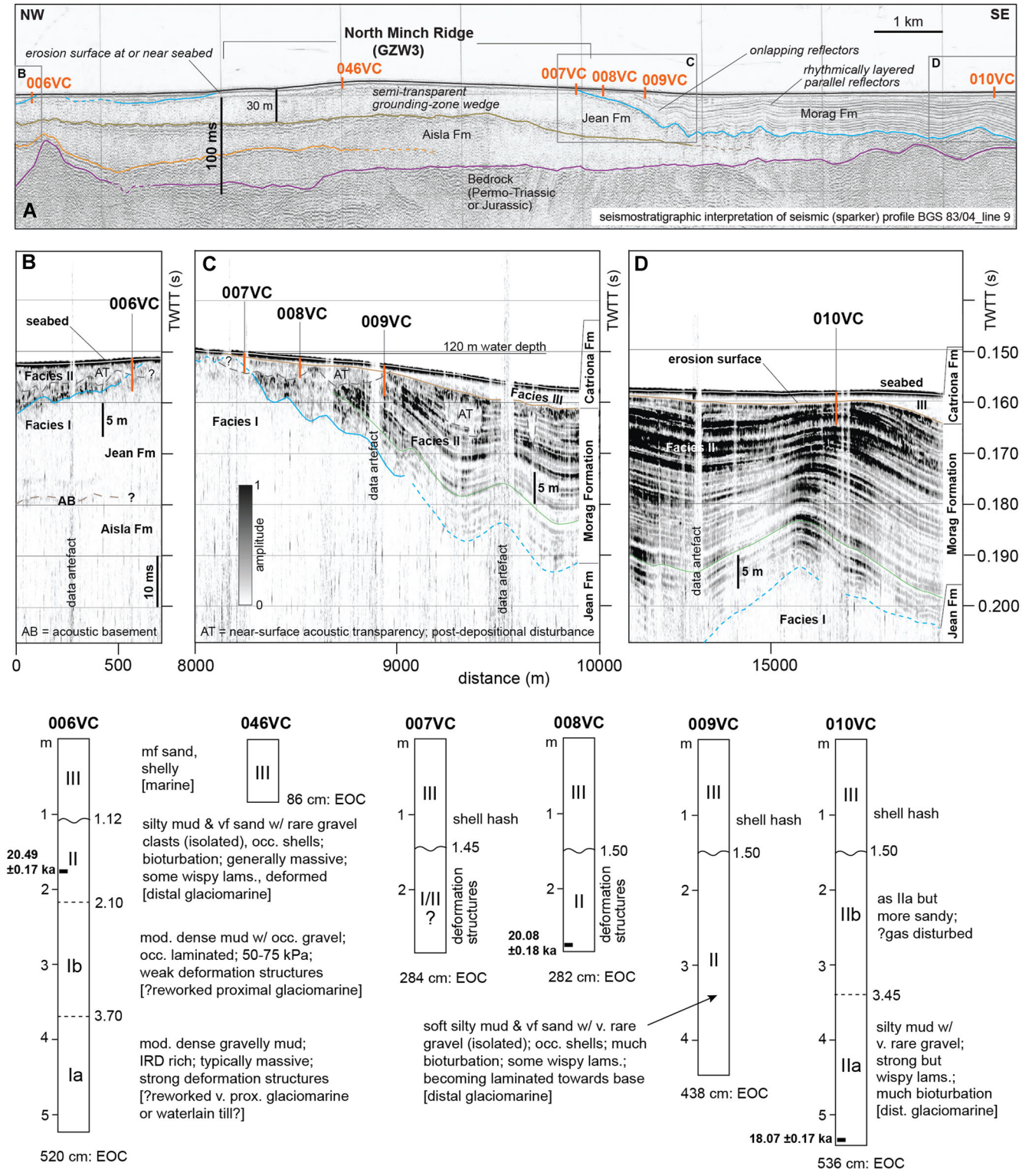

Figure 16. Mid Shelf Late Pleistocene stratigraphy. (A) BGS seismic profile over GZW3 (North Minch Ridge) showing Pleistocene geological units, seismic architecture and location of cores 006-010VC. Note onlapping relationship of strongly layered Morag Fm on Jean Fm (GZW3) and erosion surface at seabed (modified from Bradwell and Stoker, 2015a). (B) SBP data from core site 006VC showing two main acoustic facies. (C) SBP data from core sites 007, 008 and 009VC showing three main acoustic facies. Note the discontinuous zone of near-surface acoustic semi-transparency (AT) adjacent to GZW3. (D) SBP data from core site 010VC showing three main acoustic facies. Note the absence of the near-surface disturbed facies (AT). Lower panel: simplified lithologs of core 006-010VC (and 046VC) with descriptions. Ages of ^{14}C-dated samples at correct depths given in calibrated years BP with uncertainties. [Color figure can be viewed at wileyonlinelibrary.com].

Core 010VC

This vibrocore was taken 6.2 km to the SE of Core 009VC where the Morag Fm basin-fill sediments thicken considerably to c. 40 m (Fig. 16). No evidence of near-surface acoustic transparency was seen in the SBP data at this site. The core recovered 5.36 m of continuous sediment. As in Core 009VC it can be broadly classified into the same two main lithofacies – corresponding to AF II and AF III (Fig. 16). Gravel clasts are very rare in both facies. We further subdivide the lower facies into a silty mud (IIa) and coarser sandy mud unit (IIb). In this core, Facies II is highly bioturbated on a cm-scale, with larger distinct vertical disturbance structures seen in

© 2021 The Authors. *Journal of Quaternary Science* Published by John Wiley & Sons Ltd

X-radiographs – probably related to gas-escape – also pervading the sandy mud facies (ca. 2.0–3.0 m).

One sample of marine carbonate from cold-water, not monospecific, foraminifera at the base of core 010VC (5.26–5.36 m) yielded a calibrated ^{14}C age of 18.07 ± 0.17 ka cal BP (Table 8). This date is consistent with, but younger than, the date from core 008VC in the same acoustically layered package. We interpret this age (and the date from the base of core 008VC) as a 'loose' minimum constraint on the deposition of these open-water distal glaciomarine sediments. The thickness of uncored Morag Fm sediments seen in acoustic SBP data at this core site (Fig. 16) implies a considerable period of glaciomarine sedimentation and therefore ice-sheet-free conditions well before 18-20 ka cal BP.

Core 011VC was taken in 112 m water depth, 20 km further SE of GZW3 (Fig. 2); it recovered 3.14 m of continuous sediment. The core consists of soft to firm (20–50 kPa) dark brown to grey mud with varying proportions of fine sand (AF II); overlain by 0.90 m of grey-brown fine muddy sand with shells. When split lengthways the muddy lower facies showed numerous black reduction spots, surface streaks and laminae, some being highly contorted, highlighting evidence of sediment disturbance or deformation. X-radiographs identified only one or two very rare isolated gravel clasts within the whole core, as well as clear evidence of post-depositional disturbance structures in the lower mud-sand facies.

A 3-cm-thick sub-sample of facies II sediments yielded a low number of foraminifera, meaning that a larger sample than normal was needed to generate the required mass of microfauna for radiocarbon assay. One small sample of marine carbonate (36 µg), from cold-water not monospecific foraminifera (at 1.60–1.69 m), was submitted for radiocarbon analysis. It returned a calibrated age of 20.79 ± 0.20 ka cal BP (Table 8). This date corresponds well with dates from cores 006VC and 008VC within the same acoustic facies (and probably same lithofacies), indicating deglaciation here well before ~21 ka BP. However, as in other mid-shelf cores, disturbance structures mean that stratigraphic integrity cannot be presumed.

Sub-transect 2 – Inner Shelf (Cape Wrath)

The inner shelf, for the purposes of this study, includes the areas of seabed closest to shore but excludes the straits of the Minch (Fig. 2). The bathymetry of the inner shelf is generally rugged and relatively shallow (<100 m bsl) characterized by numerous bedrock highs and shallow banks (Fig. 2). The Quaternary geology on the inner shelf to the north and west of Scotland is generally thin and patchy with large areas of Pleistocene strata currently mapped only at low resolution or left lithostratigraphically undivided (Fyfe *et al.*, 1993; Stoker *et al.*, 1993). More recently, numerous, occasionally overprinted, moraine systems relating to ice-margin oscillations of a non-streaming ice-sheet sector have been mapped from extensive singlebeam and multibeam data (Fig. 3) (Bradwell and Stoker, 2015a; Bradwell *et al.*, 2019). We took eight cores on the inner shelf along a 40-km east–west transect at ~58°50′ N offshore Cape Wrath (Fig. 2) to prove the Quaternary stratigraphy between moraines and, where possible, recover material for dating purposes.

Core 002VC

Taken 28 km NW of Cape Wrath in a water depth of 89 m, vibrocore 002VC recovered a single lithofacies: 2.00 m of firm to stiff (70–150 kPa), red-brown, clast-rich, variably sandy, mud-matrix supported diamicton. The generally massive diamicitic lithofacies includes downcore variations in clast abundance giving an impression of crude bedding. Clasts are typically subrounded to subangular, with low sphericity, and predominantly of very hard Precambrian lithologies (i.e. Torridon Group sandstone, Lewisian gneisses, granitoids and grey psammites) reflecting the subjacent bedrock geology here. The highly consolidated stiff diamicton is interpreted as a terrigenous subglacial till. No shells were identified.

Cores 003PC-005VC

Taken 14.5 km to the WSW of core 002VC in water 101 m deep (Fig. 2), piston core 003PC recovered 3.24 m of generally massive, or homogeneous, coarse- to very coarse-grained sand with an unusually high abundance of marine shells throughout. P-wave velocity readings are relatively consistent in the upper 0.8 m of shelly facies (1750 m s^{-1}), whereas velocity readings below 0.80 m are sporadic with widely scattered values – possibly suggesting the presence of free gas. This massive shell-rich sand facies was probably laid down or reworked in a shallow marine environment: part of the discontinuous postglacial sand sheet locally filling hollows and forming sand waves on the inner shelf (Fyfe *et al.*, 1993; Pantin, 1991).

Core 004VC was taken at almost the same location as core 003PC. It successfully penetrated the coarse shelly sand facies (only 0.25 m thick) to recover 3.8 m of dark brown to dark grey, soft to firm, mud with black reduction spots and stains, and rare isolated gravel clasts. This mud-dominated facies is colour laminated and grain-size laminated (silt–clay–fine sand) becoming finer grained downcore. The wispy mm- to cm-scale laminations are bioturbated and highly deformed in X-radiographs with folding, faulting and mélange structures seen, especially below 2.5 m. The basal 3–4 cm of this core (and the vibrocorer 'shoe' sample) captured a very dense, stiff, red sandy gravelly clay, possibly a subglacial diamict or highly weathered Permo-Triassic bedrock.

Core 005VC recovered 1.06 m of shell-rich coarse sand, similar to core 002VC, but with a muddy gravel base (>5 cm thick) captured in the shoe sample. By contrast to core 002VC, the shelly sand facies here preserves clear stratification and a degree of size sorting. No marine carbonate samples were submitted for radiocarbon analysis from any of these three cores.

Cores 048VC and 049VC

We took two cores either side of a prominent ice-sheet retreat moraine, one of a suite mapped by Bradwell and Stoker (2015a) trending generally north–south on the seabed between Cape Wrath and the Nun Rock bathymetric high (Fig. 3). SBP data show the Quaternary succession to be thin and patchy, with discontinuous superficial facies restricted to shallow basins between acoustically structureless, low-signal-penetration (<10 ms) ridges, mapped as large seabed moraines. One small superimposed (younger) recessional moraine and fan complex has partially infilled one of these inter-morainal basins (Fig. 17).

Core 048VC, taken in water 89 m deep, recovered 3.50 m of sediment from the eastern margin of an intra-morainal seafloor basin. This relatively short core reveals a complex stratigraphy divided into six main lithofacies, of which at least three can be recognized in acoustic SBP data (Fig. 17). The lower lithofacies (I–II), > 1.38 m downcore, confirm a subaqueous ice-marginal/morainic to grounding-line depositional environment with muddy clast-rich diamicton overlain by inclined, finely bedded and, in places, size-graded sand and fine gravel. This unit is abruptly capped by a laminated, IRD-rich proximal to IRD-poor distal, glaciomarine mud sequence with rare shells (Facies III–IV). The glacial sediment sequence is unconformably overlain by a condensed, probably winnowed, gravel lag,

© 2021 The Authors. *Journal of Quaternary Science* Published by John Wiley & Sons Ltd

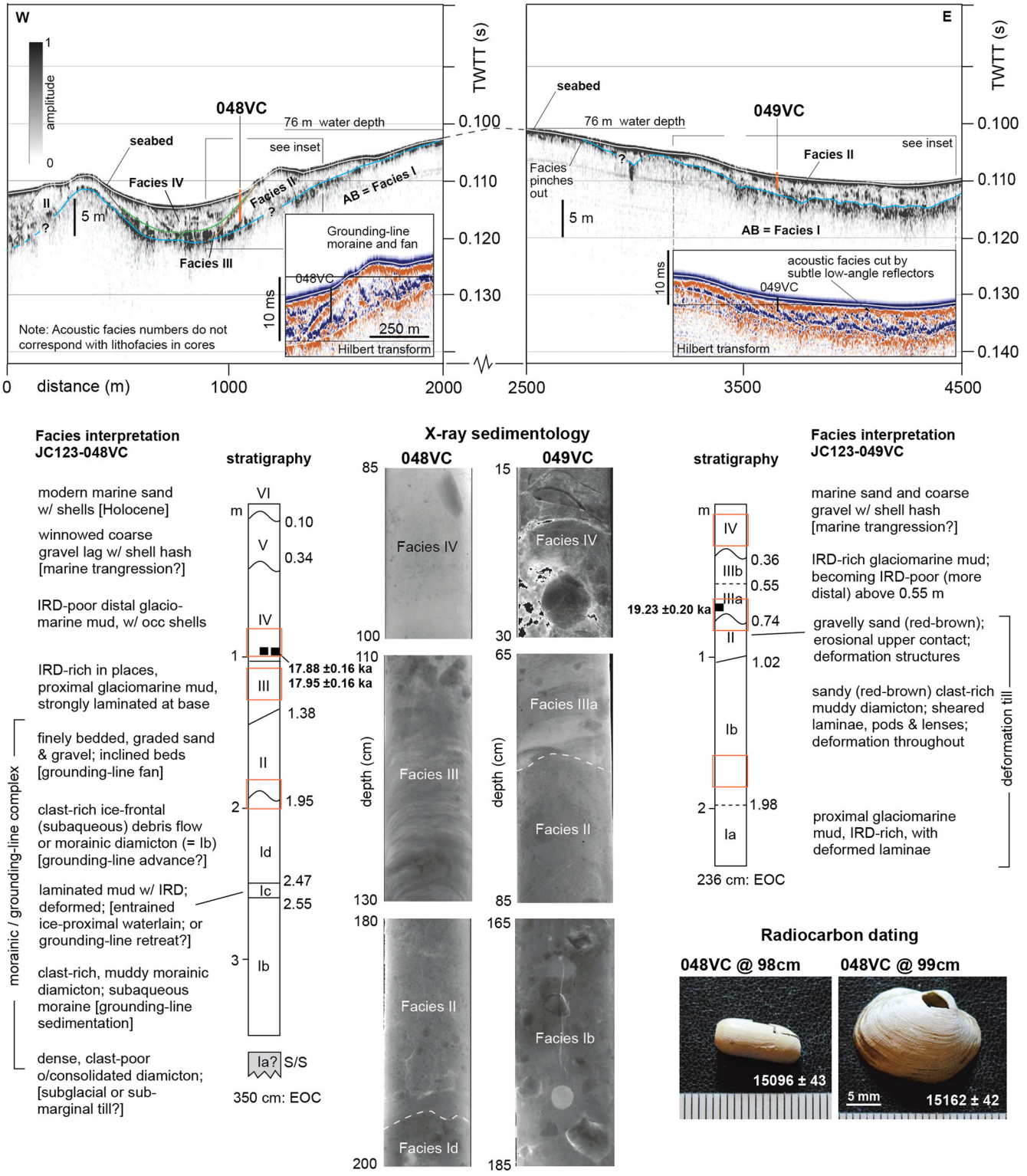

Figure 17. Acoustic stratigraphy, sedimentology and geochronology of cores 048VC and 049VC, from Inner Shelf, 20 km NE of Cape Wrath. Upper panels: SBP amplitude data (greyscale) and Hilbert transform data (insets, colour) on west and east flanks of large seabed moraine, in Nun Rock-Cape Wrath moraine sequence. Core 048VC taken on distal flank of small subaqueous moraine/grounding-line fan, superimposed on larger (older) moraine ~1.5 km wide. Core 049VC taken in acoustically disturbed facies in small inter-moraine basin. Hilbert transform highlights acoustic contrasts in SBP data allowing internal reflectors to be more clearly discerned. Lower panels: lithologs and sediment descriptions of cores 048VC and 049VC, alongside X-radiographic examples of sediment facies. ^{14}C-dated shells shown in photographs (bottom left); for calibrated ages see core log and Tables 8 and 9. [Color figure can be viewed at wileyonlinelibrary.com].

marine shell-hash and shelly sand at seabed (Facies V–VI) (Fig. 17). These uppermost facies (<0.40 m thick) cannot be resolved on SBP data.

The two stratigraphically lowest well-preserved shells from within the distal glaciomarine Facies IV (at 0.98 and 0.99 m) were submitted for radiocarbon analysis. They returned calibrated ages of 17.88 ± 0.16 and 17.95 ± 0.16 cal BP, respectively (Table 8). Even if we assume that glaciomarine sedimentation followed immediately after subaqueous fan deposition ceased, these dates provide only a 'loose' minimum constraint on the timing of moraine formation (i.e. > 18 ka BP) as we found no dateable material within lithofacies I, II or III.

© 2021 The Authors. *Journal of Quaternary Science* Published by John Wiley & Sons Ltd

Core 049VC was taken 2.3 km east of core 048VC in an ice-sheet retreat direction, based on the geomorphology of the surrounding moraines on the continental shelf (Fig. 3) (Bradwell and Stoker, 2015a). Newly acquired SBP data across these moraines show a single, semi-transparent, acoustic facies (AF I), varying in thickness from 1 to 3 m, overlying an irregular acoustic basement (Fig. 17). Low-amplitude signals dominate Facies I with sporadic spatially distributed higher amplitude reflections also seen. Applying a Hilbert transform to the SBP data (equivalent to an amplitude phase rotation of −90 degrees) highlights stratigraphic detail not visible in the processed amplitude echogram. In this case, numerous low-angle eastward-dipping reflectors can be seen cross-cutting this otherwise 'noisy' acoustic facies (Fig. 17). We interpret these as shallow thrust structures imparted by an advancing/overriding grounded ice mass. Similar glaciotectonic thrust features have been widely reported in glaciogenic sediment packages on slopes opposing the general direction of ice flow (e.g. Dogger Bank Fm; Phillips *et al.*, 2018; Emery *et al.*, 2019).

Core 049VC recovered 2.36 m, mostly from within AF I, providing clear evidence of sediment deformation. The degree of disturbance seen in high-resolution X-radiographs varies within the lower denser lithofacies (I and II), and ranges from minor reworking or disturbance of otherwise planar laminae to partial or complete disruption of laminae and shearing of sediment to form disaggregated pods, lenses or pseudo-laminations. Shear strengths within the lower 1.5 m of core 049VC also vary greatly from 40 to 140 kPa, with a complex non-uniform downcore profile. We interpret these heterogenous facies as proximal glaciomarine or ice-marginal grounding-line sediments subsequently reworked into a deformation till by an overriding ice sheet. The dense higher strength facies (I and II) are unconformably overlain by a 40-cm-thick unit of soft (<40 kPa) undeformed clast-rich to clast-poor weakly laminated mud resembling glaciomarine sediments (III). This mud is, in turn, unconformably overlain by coarse shelly sand and gravel (IV) typical of high-energy marine environments (Fig. 17).

One small sample of cold-water, not monospecific, foraminifera was submitted for AMS ^{14}C assay from the upper undeformed glaciomarine facies (III) at 0.65–0.74 m. It returned a calibrated age of 19.23 ± 0.20 ka cal BP, corresponding well with 'minimal' deglacial dates from nearby core 048VC (Table 8). We infer that oscillatory ice-sheet retreat took place here, on the inner shelf ~15 km north of the Scottish mainland, before 19.2 ka BP but after 23–24 ka BP when Cape Wrath became ice free (see Results – TCN; Table 5).

Cores 050VC and 051VC

These two cores were taken approximately 5.8 and 7.5 km east of 049VC, either side of a large seabed moraine within the same Nun Rock–Cape Wrath moraine suite (Fig. 2). Core 050VC, at 82 m water depth, proved a similar, albeit less complex, stratigraphy to core 048VC with very low-strength (<20 kPa) bioturbated, clast-poor, distal glaciomarine mud facies overlying a firm (80–100 kPa) morainic or (possibly subglacial) grounding-line diamicton. One *Hiatella arctica* shell, from near the base of the distal glaciomarine facies, yielded a calibrated radiocarbon age of 16.00 ± 0.18 ka cal BP (Fig. 15; Table 8).

Core 051VC recovered 1.18 m of very coarse shelly sand, part of the postglacial sand sheet seen on MBES imagery, unconformably overlying 0.63 m of weakly colour-laminated clast-poor soft (<40 kPa) mud. This low-strength clast-poor mud is interpreted as a distal glaciomarine facies, equivalent to the lower lithofacies seen in cores 048VC, 049VC and 050VC. No marine carbonate samples were submitted for analysis.

Sub-transect 3 – North Minch

The North Minch is defined here as the area between the Scottish mainland and the Isle of Lewis, north of 58°N, approximately the latitude of the mid-trough bedrock high (MTBH) (Fig. 2). The main bathymetric trough in the North Minch is dominated by four large, broad, low-angle asymmetric sediment prisms stretching across the full width of the trough (30–40 km) and ranging from 3 to 8 km in length (trough-axial direction) and from 5 to 20 m in vertical relief. These broad sediment accumulations are interpreted as GZWs (Bradwell *et al.*, 2019) based on their strong morphological and hydro-acoustic affinity with GZWs in cross-shelf troughs elsewhere (e.g. Batchelor and Dowdeswell, 2015; Dowdeswell *et al.*, 2016; Smith *et al.*, 2019). We collected over 100 km of SBP data across these GZWs and the intervening deposits. The acoustic architecture and main facies are summarized in Fig. 18. Unfortunately, owing to technical and operational problems only one core was collected in the central and west North Minch. This core is described below.

Core 34PC

Taken in a water depth of 100 m, on a bathymetric high 8 km offshore east Lewis, this core recovered 6.45 m of continuous sediment characterized into two lithofacies (Fig. 18). The lower 4.45 m comprises soft, grey, massive to weakly laminated mud with occasional gravel clasts (dropstones), interpreted as distal glaciomarine sediments; the upper 1.20 m is a sandy mud (silt grade) with occasional shells, interpreted as hemipelagic post-glacial sediment. The transition between the two facies is gradational over ~0.1 m. Viewed on X-radiographs, the entire core is pervasively deformed with bioturbation on a cm-scale seen in the upper 1–2 m, with larger spiral or pipe-like vertical disturbance structures seen throughout the mud facies probably related to gas-escape. The upper 0.80 m of core had an 'expansive' open texture upon recovery and a strong smell of hydrogen sulphide, indicating abundant free gas within the soft muddy sediment. The basal 30 cm of core 034PC was examined for foraminifera, but none were found.

In the eastern waters of the North Minch, 5–20 km offshore, are a number of large conspicuous arcuate seabed ridges joining the main headlands of NW Scotland and fronting the main fjords and bays (Fig. 19). These ridges range in morphology and internal acoustic architecture but collectively constitute a prominent series of connected subaqueous moraines stretching from the mouth of Loch Ewe to Greenstone Point, on to near Rubha Coigeach, north to the Point of Stoer, traversing Eddrachillis Bay and finally making landfall in NW Sutherland c. 15–20 km south of Cape Wrath (Stoker *et al.* 2006, 2009; Bradwell *et al.* 2008b; Bradwell and Stoker, 2015a, b). All of these relatively sharp-crested moraines clearly post-date the deposition of the North Minch GZWs which they overprint in places (Fig. 19). The largest feature in this moraine series is the arcuate Eddrachillis Ridge, over 25 km in length, 1000–2000 m in width and up to 35 m in height. In places, multibeam data show the large nearshore moraines are clearly superimposed by a younger generation of smaller, delicate, de Geer-type moraines (1–5 m high; < 100 m wide), especially in the vicinity of the Summer Isles (Bradwell *et al.*, 2008b; Bradwell and Stoker, 2015a, b). We took eight VCs in the eastern North Minch adjacent to the Loch Ewe – Rubha Coigeach – Eddrachillis Bay moraines (Fig. 19). In the following core descriptions, we relate the higher frequency SBP acoustic stratigraphy to the existing regional seismostratigraphic framework where possible (Fyfe *et al.*, 1993; Stoker *et al.*, 2009).

© 2021 The Authors. *Journal of Quaternary Science* Published by John Wiley & Sons Ltd

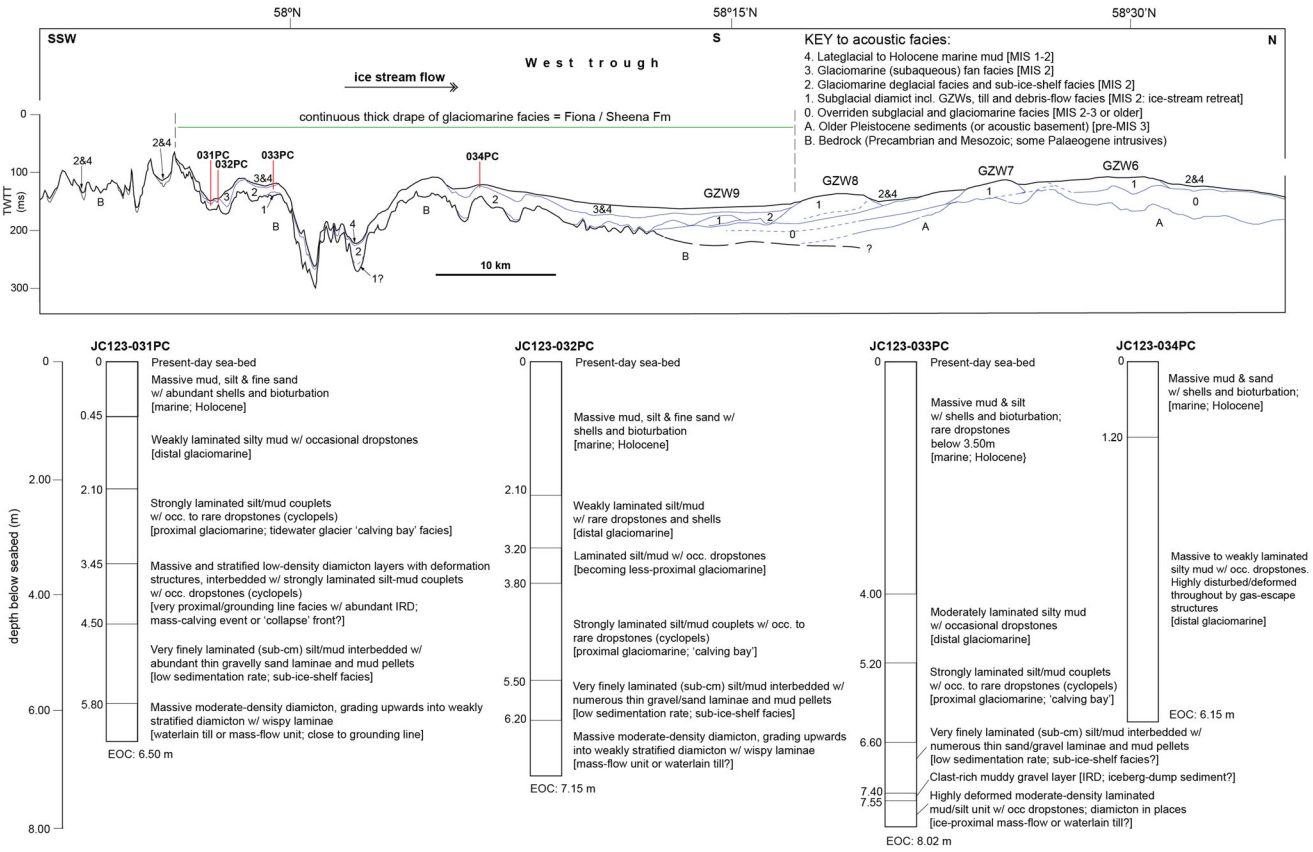

Figure 18. North Minch (west trough) Quaternary geology stratigraphic interpretation based on SBP data (upper panel), and simplified lithologs of cores 031-034PC with facies interpretations based on X-ray radiographs (lower panel). Figure modified from Bradwell *et al.* (2019).

Cores 017VC-019VC

BGS seismic sparker profiles, supplemented by new higher frequency SBP data, perpendicular to the large Eddrachillis Ridge Moraine (ERM) show a 'layer-cake' stratigraphy in the North Minch relating to ice-stream advance and decay, with bedrock overlain by deposits of the Morag, Sheena, Annie and Catriona Fm (Fyfe *et al.*, 1993; Bradwell and Stoker, 2015a, b), interrupted by a large semi-transparent prism of acoustically low-amplitude sediment comprising the ERM (Fig. 20). This unit is seen to interdigitate at its base with the acoustically higher amplitude draped sediments of the Annie Fm, indicating that the prism of morainic sediment was emplaced during the time of glaciomarine sediment (Annie Fm) deposition in the North Minch. Closer inshore the same semi-transparent acoustic facies constitutes a number of smaller recessional moraines with draped basin-fill sediments between (Fig. 20), probably of Annie Fm and/or Catriona Fm (BGS, 1990; Fyfe *et al.*, 1993).

Core 17VC was taken 1.5 km outboard of the ERM distal slope in water 118 m deep (Fig. 20). This core recovered 5.07 m of sediment in total: 1.95 m of soft (<40 kPa) slightly sandy, weakly laminated mud (within AF III = Annie Fm) with rare to occasional isolated gravel clasts and very rare shells, unconformably overlain by 3.15 m of fine generally massive shelly sand typical of the Catriona Fm (=AF IV). One articulated shell from the upper part of the glaciomarine mud unit (at 3.64 m) was submitted for AMS ^{14}C analysis; it returned a calibrated age of 12.53 ± 0.10 ka cal BP (Table 8).

Core 018VC was taken towards the base of the ERM's ice-distal slope in a water depth of 113 m (Fig. 20). This core recovered 5.02 m of continuous sediment that we broadly classify into four lithofacies on the basis of geophysical and X-ray sedimentological properties (Fig. 20; Supporting Information Fig. S4). Facies I was captured only at the base of the core (>4.95 m and shoe-sample) and consists of a firm, dense, dark red-brown, sandy clay-matrix-supported clast-rich diamicton. Overlying this, Facies II is a soft but variable density, red-brown to grey gravelly mud, crudely stratified or laminated at cm to dm scale in places with occasional sandy horizons (Fig. S4). This facies grades into the overlying Facies III at c. 3.00 m above which clasts are very rare or absent and bioturbation is marked. This clast-free mud unit is capped unconformably by Facies IV consisting of 2.22 m of medium-grained dense shelly sand with occasional shell-rich horizons, especially near the base (2.22–2.12 m). We relate Facies II and III to IRD-rich proximal to IRD-poor increasingly distal glaciomarine sediments of the Annie Fm, thought to have been deposited during the final stages of deglaciation (Fyfe *et al.*, 1993; Stoker *et al.*, 2011). One single valve of *Hiatella arctica* submitted for AMS ^{14}C analysis, from within the lower IRD-rich part of Facies II, supports this age assessment (with a calibrated age of 16.18 ± 0.17 ka cal BP) (Fig. S4; Table 8). By inference, the basal diamicton (Facies I), from within the prism of ERM sediment (Fig. 20), was deposited shortly before this time probably c. 17–18 ka BP. This timing is in good agreement with onshore dating evidence constraining ice-sheet retreat back to the adjacent Stoer peninsula by ~16.5 ka BP (see TCN Results; Table 5).

We took one further core (019VC) in a small basin at the foot of the ERM's ice-proximal slope, but outboard of the recessional moraine sequence in Eddrachillis Bay (Figs. 19 and 20). Unfortunately, this core did not penetrate the postglacial sand sheet, recovering only 1.35 m of relatively dense structureless fine sand.

Cores 015VC and 016VC

Approximately 20 km south of the previous core sites in the east North Minch, and roughly midway between the headlands of

© 2021 The Authors. *Journal of Quaternary Science* Published by John Wiley & Sons Ltd

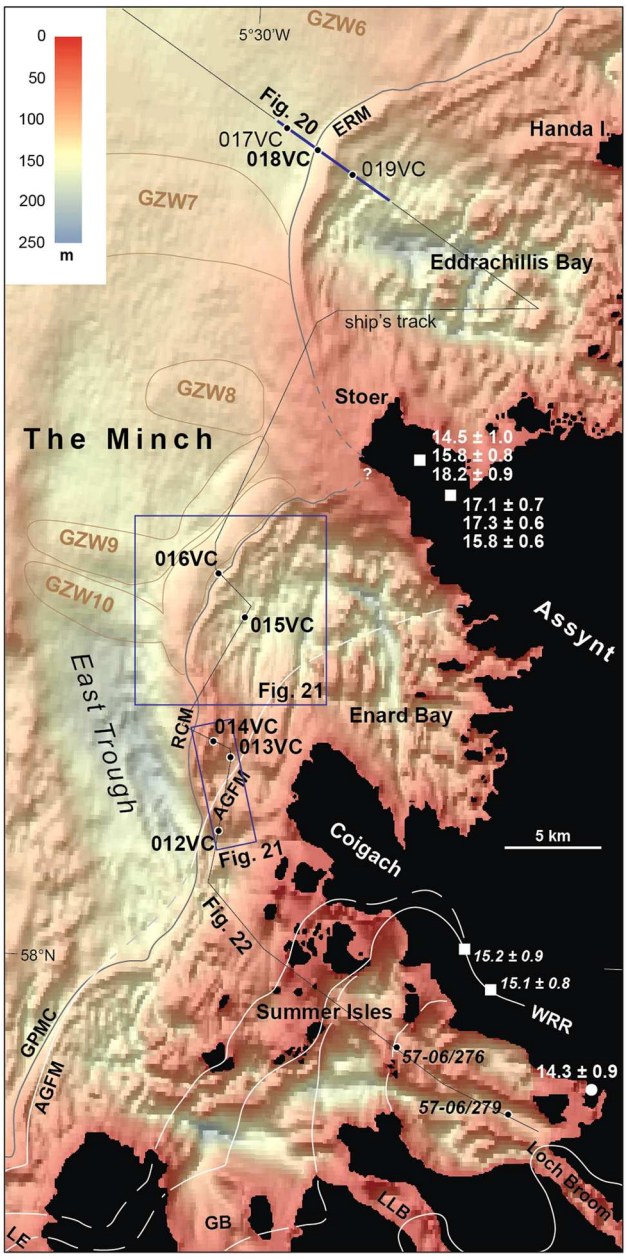

Figure 19. Bathymetry of North Minch, east of the mid-trough bedrock high. Besides the GZWs in the main trough, a number of moraine sequences are mapped 5–15 km offshore NW mainland Scotland relating to subsequent ice-sheet oscillations. Core sites 012VC-19VC are labelled. Thin grey line is geophysical data acquisition track (ship's track). Thick bue line is SBP line shown in Figure 20. Locations of Figures 21 and 22 also shown. TCN ages (squares) and OSL age (circle) from terrestrial sites are labelled (in white): roman font (this study); italic font (previously published ages; recalculated from Bradwell *et al.*, 2008; Ballantyne *et al.*, 2009). Abbreviations: ERM = Eddrachillis Ridge Moraine; GPCM = Greenstone Point Moraine Complex; RCM = Rubha Coigeach Moraines; AGFM = outer limit of Assynt Glacigenic Formation Moraines; WRR = Wester Ross Readvance; LE = Loch Ewe; GB = Gruinard Bay; LLB = Little Loch Broom; GZW= Grounding zone wedge. [Color figure can be viewed at wileyonlinelibrary.com].

Stoer and Rubha Coigeach is another prominent arcuate seafloor ridge – part of the same prominent moraine complex seen c. 5–20 km offshore NW Scotland (Fig. 20), originally mapped by Bradwell and Stoker (2015a, b). As elsewhere in the North Minch we characterize three or four main acoustic facies on the basis of high-frequency SBP data (Fig. 21). Acoustic Facies I (AF1): a high-amplitude irregular sub-bottom reflector with only limited acoustic penetration (<10 ms), forms the acoustic basement in this region. This facies is often seen at the seabed especially in regions of steep morainic topography. We map seven discrete sharp-crested ridges varying in height and width along a 3-km SE–NW transect at c. 58.17°N, 5.5°W, overprinting a larger broad GZW further offshore (Fig. 20). Between these moraine ridges are small basins containing acoustically semi-transparent sediment accumulations, locally up to 10 m thick, with both high- and low-amplitude reflection properties. The uppermost discontinuous draped unit we classify as AF IV, with AF III and AF II seen at greater depth – although separating these is not always possible (Fig. 21). Using the existing robust seismostratigraphic framework, derived from numerous seismic (sparker and boomer) profiles in the Minch and Summer Isles region (Fyfe *et al.*, 1993; Stoker *et al.*, 2009), we equate AF IV with the predominantly sandy Catriona Fm, and AF II and AF III with the predominantly muddy glaciomarine Annie Fm. AF I, forming constructional morainic topography, equates to the glacigenic Fiona Fm described by Fyfe *et al.* (1993) and Stoker *et al.* (2009). Two cores, 015VC and 016VC, were taken either side of the most prominent moraine (M1), to prove the Quaternary geology and collect material for dating (Fig. 21).

Core 016VC, taken in a small sub-basin 700 m outboard of moraine (M1) in water 102 m deep, captured 5.24 m of continuous sediment (Figs. 21 and 22). The core is dominated by a soft (<40 kPa) dark brown to grey generally massive mud with occasional isolated gravel clasts with rare shells, becoming slightly coarser (silty/sandy), laminated and bioturbation towards the top (<2.00 m). We subdivide this mud into a lower denser facies (II) and an upper less dense facies (III) largely on the basis of differing p-wave velocity, gamma-ray attenuation and magnetic susceptibility profiles (Fig. 22). We equate these soft muddy facies with the proximal-to-distal glaciomarine Annie Fm seen in other vibrocores (011VC, 018VC, 019VC, etc.; Fig. 20; Supporting Information Fig. S4) and mapped extensively in the Minch (BGS, 1990; Fyfe *et al.*, 1993). This glaciomarine mud is overlain by 0.30 m of shelly fine-grained sand with an abrupt, probably erosional, lower boundary. No samples were submitted for radiocarbon analysis as no basal diamict was recovered in this core.

Core 015VC captured 3.86 m of sediment from the margin of a small basin within the East Minch (Rubha Coigeach) late-stage recessional moraine sequence, 1.6 km inboard of moraine M1 (Figs. 21 and 22). We classify the sediments into four lithofacies, from core base: (I) a moderately soft to stiff (40–70 kPa) clast-rich, structureless, muddy matrix-supported diamict 1.00 m thick; overlain by (II) a soft (20–30 kPa) sandy mud facies with scattered gravel clasts, becoming (III) less sandy and weakly stratified above 2.25 m with rare gravel clasts and some bioturbation (Fig. 22). The uppermost facies (IV), 1.40 m thick, has an abrupt erosional lower boundary and comprises fine-grained sand with numerous intact shells and rare gravel clasts; the shells are concentrated into beds or horizons c. 20–40 cm thick. We relate this broadly four-part core stratigraphy to the existing offshore Late Pleistocene (Weichselian) lithostratigraphy in the Minch, mirrored in our own acoustic stratigraphy (Fig. 22). [Facies I = AF I = Fiona Fm; Facies II and III = AF II and III = Annie Fm; Facies IV = AF IV = Catriona Fm; see Fyfe *et al.* (1993) for detailed descriptions].

Sediment was sieved for marine carbonate microfossils at core depths of 2.75–2.85 m and 2.20–2.25 m, but foraminiferal concentrations were too low to generate sufficient material for AMS ^{14}C dating. One small broken mollusc shell (of undetermined species) at a depth of 2.00 m was submitted for radiocarbon analysis (Fig. 15). It returned a calibrated age of 15.99 ± 0.18 ka BP, supporting the Lateglacial age assessment from core 018VC, i.e. near the base of the Annie Fm (Fig. S4). We infer that the glacial diamict (Facies I) comprising

© 2021 The Authors. *Journal of Quaternary Science* Published by John Wiley & Sons Ltd

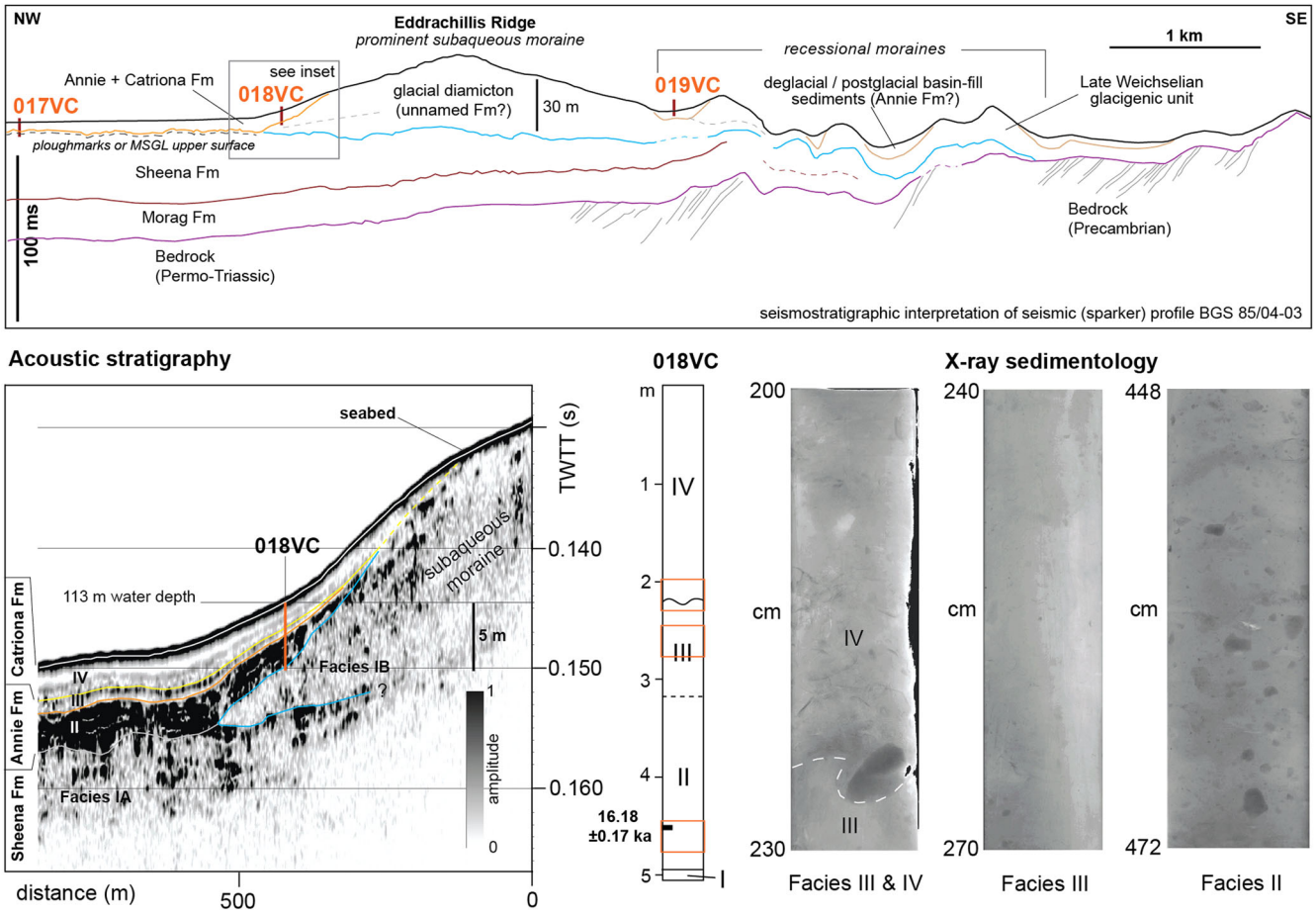

Figure 20. Seismo-stratigraphy of Eddrachillis Ridge (part of East Minch Readvance complex) and surrounding Quaternary Formations in the eastern North Minch (interpreted from BGS sparker lines), with locations of JC123 core sites (modified from Bradwell and Stoker, 2015a). Lower panels: SBP acoustic stratigraphy, showing inferred relationships with formally defined offshore Quaternary stratigraphic units (after Stoker *et al.*, 2011). Simplified lithology of core 018VC, with ^{14}C date in calibrated ka BP. X-radiographic examples of different lithofacies within core 018VC also shown. [Color figure can be viewed at wileyonlinelibrary.com].

the seabed moraines 'm2.3' and 'm2.2' was deposited by the receding ice-sheet margin before 16 ka BP, but shortly after the East Minch Readvance (see above).

Cores 012VC-014VC

Approximately 8 km further south of the previous core sites, 2–5 km off the Rubha Coigeach headland, are an excellent sequence of well-preserved superimposed seabed moraines (Fig. 21). First described by Stoker *et al.* (2006) and formally placed within a regional lithostratigraphic framework a few years later (Stoker *et al.*, 2009), these two generations of moraines represent (i) punctuated retreat of a grounded ice-sheet margin from a stable offshore position (Greenstone Point–Rubha Coigeach moraine complex) on a bathymetric high; followed by (ii) readvance and subsequent recession of a lightly grounded, partially floating tidewater glacier front. The initial retreat formed substantial subaqueous moraines (within the Fiona Fm); the latter retreat formed much smaller, more delicate, de Geer-type moraines (Fig. 21) within the Assynt Glacigenic Fm (Stoker and Bradwell, 2010) that in places overprint the larger (older) moraines.

Cores 013VC and 014VC were taken either side of a cluster of three Fiona Fm moraines in water depths of 50–70 m (Fig. 21). Core 013VC recovered 3.77 m of sediment capturing all four lithofacies seen in the regional acoustic stratigraphy (and outlined at core sites 015-016VC; see above). From core base: (I) a soft to firm, clast-rich, muddy matrix-supported diamicton; overlain by (II) a soft sandy mud with scattered gravel clasts, (III) becoming weakly laminated with fewer clasts and occasional bioturbation; overlain by 2.51 m of (IV) fine-grained shell-rich sand (Fig. 22). Barnacle plates at a depth of 3.56 m, from immediately above the basal diamict (within Facies II), were submitted for AMS ^{14}C analysis and returned a calibrated age of 16.33 ± 0.19 ka cal BP (Fig. 17; Table 8). We infer that the Fiona Fm seabed moraines (Facies I) formed shortly before this time, probably c. 17 ka BP during Heinrich Stadial 1.

Core 014VC, taken between two adjacent Fiona Fm moraines, did not penetrate the postglacial sand sheet, recovering only 1.77 m of coarse-grained shelly sand (Fig. 22).

Core 012VC was taken ~500 m inboard of the outermost Assynt Glacigenic Fm moraine, in a water depth of 70 m, c. 3 km SW of core 013VC (Figs. 21 and 22). It captured two (possibly three) main facies: (I) 0.45 m of moderately firm (50 kPa), sandy, mud-matrix-supported gravel-rich diamicton – typical of subaqueous morainic deposits; erosionally overlain by 2.10 m of slightly shelly sand, which we equate to Acoustic Facies IV (=Catriona Fm). Facies II and III (=Annie Fm) are not seen in this core (Fig. 22), probably owing to subsequent marine erosion. However, we note that Facies IV grades upwards from a muddy fine-grained sand to a 'clean' dense medium- to fine-grained sand, possibly representing more than one depositional facies.

Two marine carbonate samples, one small *Macoma* species shell (1.78 m) and one articulated *Mya truncata* shell (1.70 m), both from within the muddy basal section of the sand unit (Facies IV), returned calibrated ^{14}C ages of 12.65 ± 0.08 and 12.63 ±

© 2021 The Authors. *Journal of Quaternary Science* Published by John Wiley & Sons Ltd

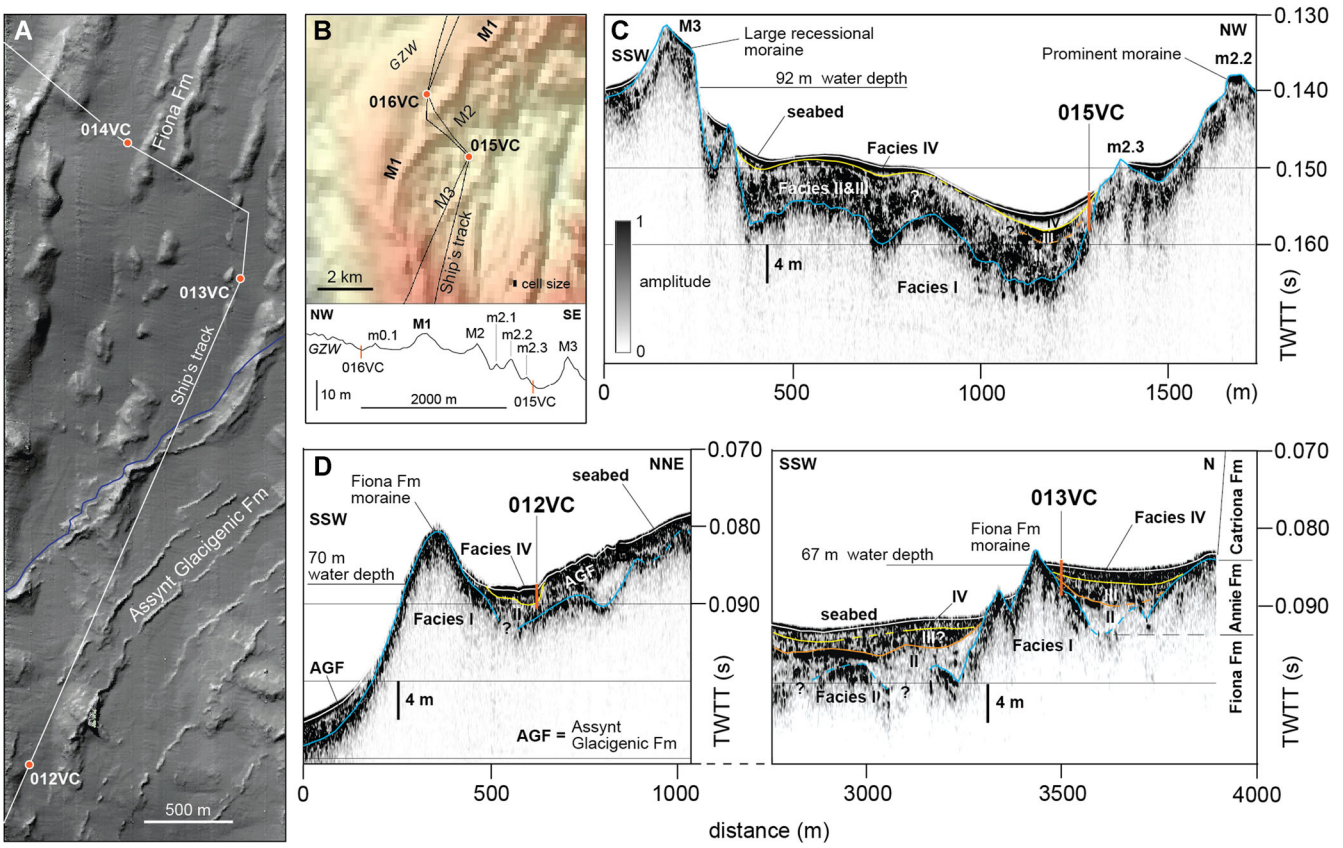

Figure 21. East Minch Readvance and younger moraines. (A) Multibeam echosounder bathymetry data (acquired by BGS in 2005) showing large Rubha Coigeach moraines (Fiona Fm) overprinted by younger de-Geer type moraines (Assynt Glacigenic Fm) (modified from Bradwell and Stoker, 2016). JC123 core locations shown. Blue line marks outer edge of Assynt Glacigenic Fm moraines. (B) Singlebeam bathymetry data showing East Minch Readvance moraines in outer Enard Bay. M1–M3 are discrete moraine ridges within the Fiona Fm. GZW also marked. (C) SBP data along ship's track line (see panel B) showing acoustic stratigraphy, core 015VC site and facies sub-divisions across small inter-moraine basin. (D) SBP data (see panel A) in vicinity of core 012VC and (E) core 013V. Note: SBP acoustic stratigraphy is related to formal/regional lithostratigraphy (see Stoker *et al.*, 2011) wherever possible. [Color figure can be viewed at wileyonlinelibrary.com].

0.08 cal ka BP (Figs. 17 and 26; Table 8). These near-identical ages imply that the base of this unit was deposited during GS-1 – a return to cold-climate stadial conditions in Scotland with a rejuvenation of glaciers, some reaching the marine limit in NW Scotland (Golledge, 2010; Small *et al.*, 2012).

Sub-transect 4 – Inner Minch

The Inner Minch is defined here as the area south of 58°N, at approximately the latitude of the MTBH, stretching from the Summer Isles in Wester Ross to Loch Sealg in eastern Lewis south to the Kyle of Lochalsh and the Isle of Skye (Fig. 2). The area includes a highly varied bathymetry which generally deepens inshore from north to south, and includes pronounced nearshore deeps (>300 m) east of Raasay at 57°30'N, as well as submerged banks and rugged bedrock highs. Eroded into the NW seaboard of Scotland are numerous deep-water fjords (sea lochs), and narrow 'sounds' which we distinguish separately from the waters of the Inner Minch (Fig. 2), for the purposes of our reconstruction (see Discussion/Interpretation). Unlike the North Minch, the Inner Minch exhibits only three relatively small GZWs stretching across the partial width of the trough. Mapped as GZW15, 16 and 17 by Bradwell *et al.* (2019), these glacigenic sediment accumulations represent stabilizations of the ice-sheet grounding zone in the vicinity of the MTBH during the final stages of ice-stream retreat. One VC and seven PCs were taken in key deposits and basins along our SBP survey lines (Fig. 2) to prove the sub-bottom sediments and potentially constrain the timing of deglaciation.

Cores 020PC, 021PC and 022VC

SBP data acquisitions across GZW15 show an asymmetric wedge 1000–2000 m wide with a shorter steeper east-facing ice-distal slope, a longer gentler up-ice slope and a strongly iceberg-furrowed surface (Fig. 23; Supporting Information Fig. S5). The wedge has a complex acoustic architecture comprising four main acoustic facies. Overlying the undulating acoustic basement (AB), presumed to be bedrock, we define a low-amplitude semi-transparent structureless unit typically 5–8 ms thick. This acoustic facies thickens in an eastward direction towards the GZW margin and into the adjacent basin where it comprises an upper higher amplitude unit with some evidence of layering and a lower semi-transparent structureless unit (Fig. 23). Although the boundary between them is gradational and indistinct, we define two separate sub-facies in places: AF I (upper) and AF I (lower). Overlying this, comprising the distal section of GZW15, is a 15–20-ms-thick package of wavy, parallel draped, generally high-amplitude reflectors, interbedded with thin low-amplitude layers. This thick acoustically layered facies (AF II) interdigitates with a low-amplitude structureless unit with lenticular geometry to the west (Fig. 23). This internal architecture change takes place approximately at the crestline or high point of GZW15, with no discrete planar reflectors traceable any further west within a generally acoustically structureless facies (AF IIw on Fig. 23).

The upper part of AF II is characterized by a distinct near-surface acoustic transparency (AT) or semi-transparency with a highly irregular undulating basal boundary but a strong surface reflector. This acoustically incoherent or 'disturbed' unit is

© 2021 The Authors. *Journal of Quaternary Science* Published by John Wiley & Sons Ltd

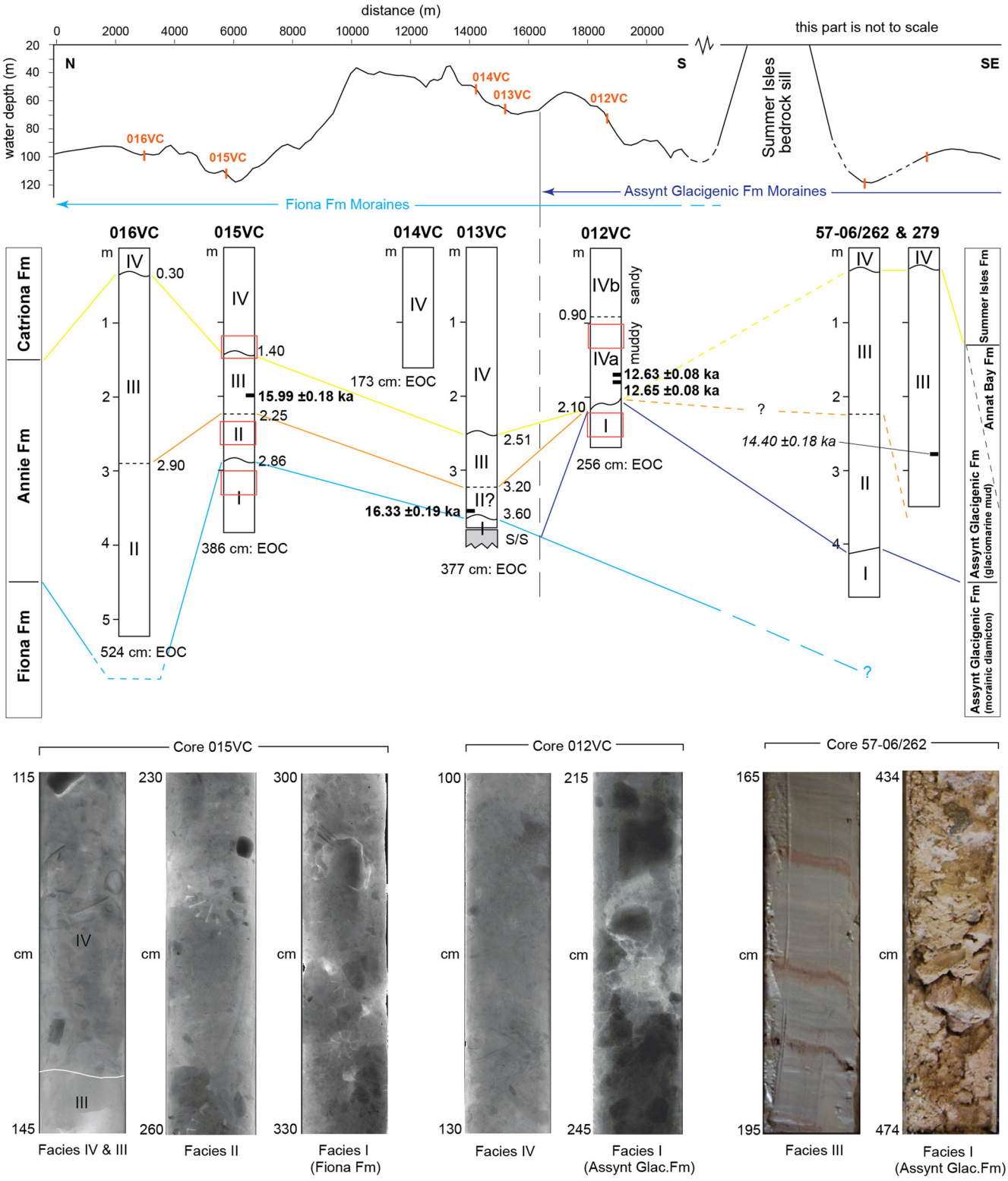

Figure 22. East Minch and Summer Isles offshore stratigraphy. Upper panel: bathymetric profile showing generalized elevation along line in Fig. 19, and sites of vibrocores. Middle panel: simplified lithologs showing facies relationships between cores and correlations to formal offshore lithostratigraphy in the east Minch (Fyfe *et al.*, 1993) and in the Summer Isles region (Stoker *et al.*, 2009). BGS vibrocores 57-06/262 and 57-06/279, east of the Summer Isles Sill, are from Stoker *et al.* (2009). Lower panel: positive X-radiographic imagery of lithofacies within cores 015VC and 012VC. Photographs of facies within BGS core 57-06/262 (modified from Stoker *et al.*, 2009). [Color figure can be viewed at wileyonlinelibrary.com].

manifest as a haze of low-amplitude intra-formational reflections from seabed to a depth of 10–15 ms (Fig. 23). This acoustic transparency is most pronounced around the crestline of GZW15, where the largest iceberg scours are seen (in MBES data and SBP data; Supporting Information Fig. S5; Fig. 23). The acoustic incoherence is concentrated in relatively narrow v- or u-shaped zones < 10 ms deep and 50–200 m wide, but is pervasive at seabed masking the 'true' acoustic stratigraphy in the upper 5–10 ms. This near-surface acoustic transparency does not continue into the adjacent basins, where a thin uppermost acoustic facies can be seen at seabed (AF III) (Fig. 23). Based on its acoustic character, 3-D expression and association with clearly developed iceberg scours at seabed we ascribe this acoustically (semi-) transparent 'disturbed' zone to strong post-depositional sediment

© 2021 The Authors. *Journal of Quaternary Science* Published by John Wiley & Sons Ltd

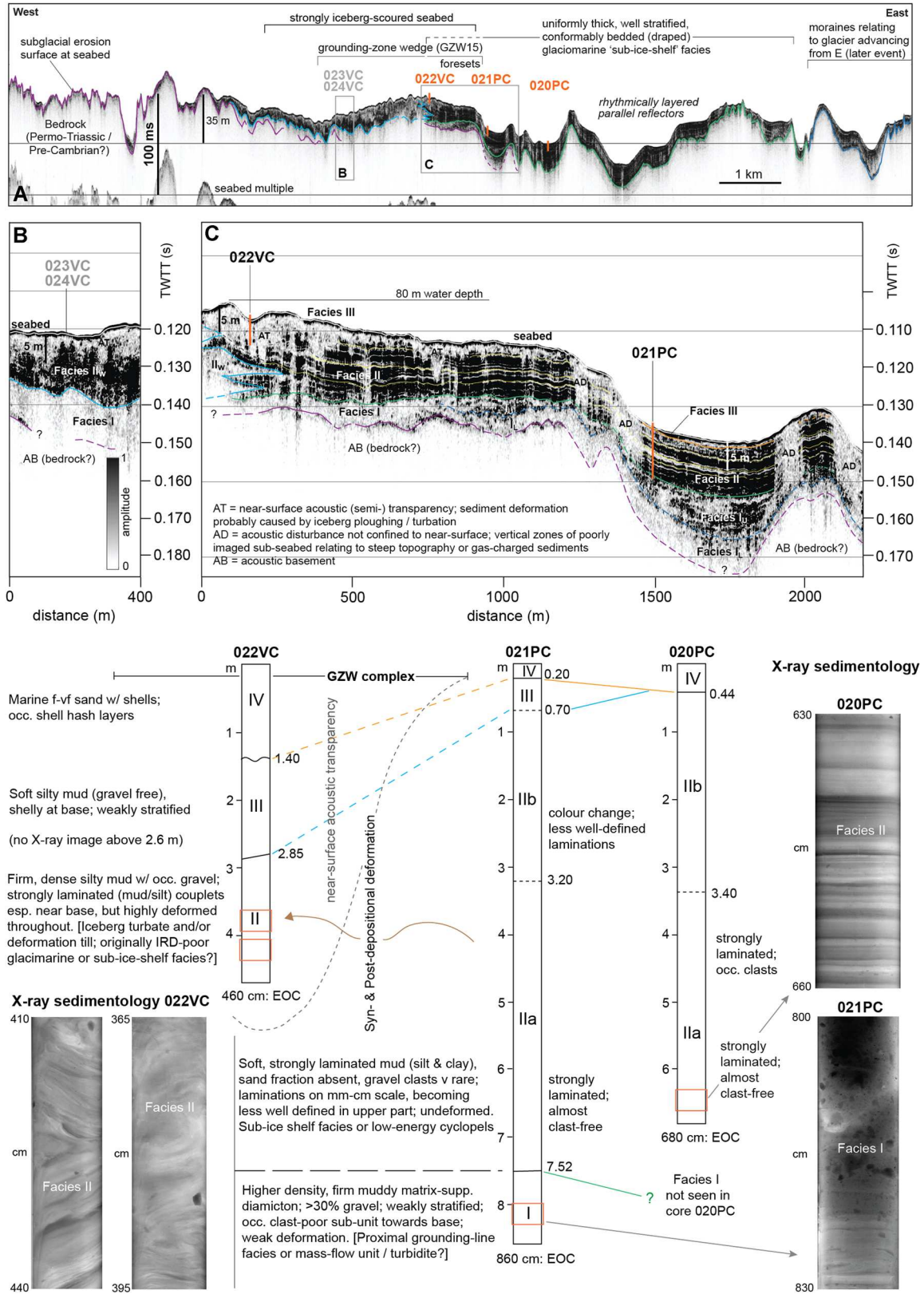

Figure 23. Acoustic stratigraphy and sedimentology of GZW15 and associated cores, Inner Minch. (A) SBP amplitude data (greyscale) of W–E transect across GZW and adjacent deposits with interpretations. Cores sites labelled. (B) SBP data at site of unsuccessful vibrocoring attempts '023VC' and '024VC'. (C) High-resolution image of SBP data across crestline and distal flank of GZW15 and adjacent basin. Note the complex interdigitating relationship between acoustic facies II and IIw beneath core site 022VC, within an iceberg ploughmark. Also note the near-surface acoustic semi-transparency (<15 ms thick) on GZW15 – probably relating to sediment disturbance by iceberg ploughing. Lower panel: simplified lithologs of cores 020PC, 021PC and 022VC with sediment descriptions and facies correlations. Positive X-radiographic images of selected sediment facies. [Color figure can be viewed at wileyonlinelibrary.com].

© 2021 The Authors. *Journal of Quaternary Science* Published by John Wiley & Sons Ltd

turbation by iceberg ploughing. Similar acoustic phenomena have been reported by others from strongly iceberg-ploughed seabed elsewhere (e.g. Jakobsson and O'Regan, 2016).

A second type of acoustic phenomena is also seen in the SBP data adjacent to GZW15. Several relatively narrow, vertical, sheet-like zones of acoustic disturbance (AD) blank out the acoustic stratigraphy below (Fig. 23). They are only seen beneath steeper slopes and typically result in a weak or absent seabed reflector. We relate these structures to acoustic signal loss possibly associated with gas-charged or micro-fractured fine-grained sediments causing signal dispersal (e.g. Judd and Hovland, 2009).

Two PCs were taken in sediment basins immediately adjacent to GZW15. Core 021PC was taken at the foot of the distal slope of GZW15. Core 020PC was taken 1200 m further west, in a separate sub-basin (Fig. 23). Both piston cores had 100% recovery and captured similar sediment sequences. Although neither yielded suitable material for radiocarbon dating. Core 021PC, the longer of the two, recovered 8.60 m of sediment, and is described below.

The lowest lithofacies (I) comprises a mixed unit of firm (>50–80 kPa) moderate-density (>2.0 g cm^{-3}) massive to weakly stratified diamicton and gravelly muds with weak lamination and evidence of deformation structures in places (Fig. 23). This unit is indicative of a rapidly changing depositional environment, switching from a low-sedimentation, possibly sub-ice-shelf environment to proximal grounding-line facies, with high-sediment-load turbid meltwater and/or debris flows delivering sediment downslope from the subglacial grounding line. We equate this lithofacies with Acoustic Facies I (upper) seen in the SBP data. This unit is conformably overlain by Facies II: 6.80 m of soft (<30 kPa), low-density (1.6–1.75 g cm^{-3}) rhythmically laminated dark grey-brown mud facies with well-defined silt–clay couplets and rare isolated gravel clasts (dropstones). Above 3.20 m these couplets become less well defined (Fig. 23). This entire facies is indicative of either a quiescent sub-ice-shelf setting with relatively low sedimentation rates and rare clastic (gravel-grade) input, or meltwater-deposited cyclopels, typical of semi-enclosed tidewater-glacier 'calving bays' with seasonal sea-ice cover (Hogan *et al.*, 2016; Jennings *et al.*, 2018; Smith *et al.*, 2019). Evidence from SBP acoustic stratigraphy (Fig. 23) shows that the iceberg scouring post-dates the deposition of this sediment (AF II), and hence we favour the former 'sub-ice-shelf' interpretation. Overlying Facies II, close to the seabed, are thin units of more recently deposited sediments: (III) 0.2 m of soft, grey, massive gravel-free mud with shells; and (IV) 0.15 m of fine- to very fine-grained shelly sand. Core 020PC, 6.80 m long, captured almost an identical stratigraphy to core 021PC (up to 7.50 m) but did not penetrate the lowermost unit (Facies I) (Fig. 23).

Core 022VC was taken in a large, 160-m-wide, 2-m-deep, u-shaped iceberg scour near the crestline of GZW15 (Fig. 23; Supporting Information Fig. S5). This VC was the only one to recover sediment from within the GZW itself. Core 022VC captured 4.60 m of sediment from within the disturbed near-surface acoustic transparent (AT) unit seen in SBP data (Fig. 23). The core contains three main facies, from the base upwards: a firm, dense, strongly laminated silty mud with occasional gravel clasts showing evidence of strong and pervasive deformation throughout. The deformation cannot be confused with core-recovery-related deformation. It is manifest in X-radiographic images as steeply dipping laminae with multi-directional dip angles; blended sediment units with mixed grain-size characteristics; tight folds and augen-like shear lenses; wisps, pods and inclusions of different density sediment intermixed with one another (Fig. 23). All laminae show signs of deformation: from weak disturbance (3.30–3.50 m), through disruption and strong disturbance (4.10–4.20 m), to complete homogenization of the original horizontal planar structures (3.60–3.90 m). We ascribe this highly disturbed sediment Facies II, within the zone of near-surface acoustic transparency (Fig. 23), to (syn- and) post-depositional turbation by icebergs to depths of a least 4.6 m below seabed. Undisturbed sediments of the same facies can be traced to the east within GZW15; we deem these to be acousto-stratigraphically equivalent to those fine-grained interlaminated sediments captured in cores 020PC and 021PC (Facies II). Unconformably overlying this complex unit in core 022VC are two other facies: (III) a soft silty mud with a well-developed shell hash at its base (0.80 m); and (IV) a fine-grained shelly sand with occasional shell-hash layers (0.32 m); both deposited after the formation of the iceberg scour mark. These thin uppermost units are not resolved in the SBP data (Fig. 23). No suitable material was found in this core for radiocarbon dating.

Cores 031-033PC

The western trough of the Minch deepens southwards from around 125 m at 58.5°N to water depths exceeding 200 m at around 58°N (Fig. 2). The trough is interrupted by the Shiant Isles Sill, an arc of bedrock exposed at seabed stretching from Harris to the MTBH, where water depths shallow to around 20–60 m. Our new SBP acoustic data clearly show a Quaternary sediment package thickening northwards from the Shiant Isles Sill (where they are absent) to the deepest parts of the West trough (where they reach 20 ms in thickness) (Fig. 24). The Quaternary stratigraphy in this part of the Minch can be subdivided into three main acoustic facies (Fig. 24): lowermost, AF I is a high-amplitude but generally structureless facies; overlain by AF II, also moderate to high amplitude but with a more stratified, weakly bedded, character; and uppermost, AF III is a low-amplitude, almost transparent, drape of variable thickness with a well-defined base. At the eastern margin of the trough a large (1 km wide), thick (~30 ms) package of alternating high-/low-amplitude sigmoidal reflectors with prograding geometry is captured on the SBP data. This sediment wedge has fan- or delta-like geometry on closely spaced 2D SBP lines and MBES data, with an apparent source in the east (Fig. 24). The whole fan-like acoustic package (AF IIIw) gives the impression of progradation into restricted accommodation space. Furthermore, the acoustic package can be subdivided into seven units based on strong internal reflectors, all of which pinch out or have onlapping relationships upslope and down-lapping or truncated relationships at their western extremity (Fig. 24). The acousto-stratigraphic relationship between Facies III (upper drape) and Facies IIIw (wedge-like fill) is unclear as these units do not interrelate on the SBP data, but are 'cut out' at seabed over a small bedrock high. However, we assume that these facies are broadly synchronous based on their stratigraphic setting and clearly both must post-date AF I and II. We interpret the large sigmoidal-reflection package to represent a large subaqueous fan fed directly from the former ice-stream/ice-sheet margin grounded on the western flank of the MTBH.

Three 7- to 9-m-long piston cores were taken in the deeper waters of the West Minch trough at varying distances from the Shiant Isles Sill where the Quaternary sediment thickness exceeds 20 m and the key acoustic facies are closest to seabed (Fig. 24). These three valuable cores record similar overall stratigraphies but with subtle differences (Figs. 18 and 24; Supporting Information Fig. S6).

Sediment facies within cores 031PC are subdivided and interpreted on the basis of physical sedimentological,

© 2021 The Authors. *Journal of Quaternary Science* Published by John Wiley & Sons Ltd

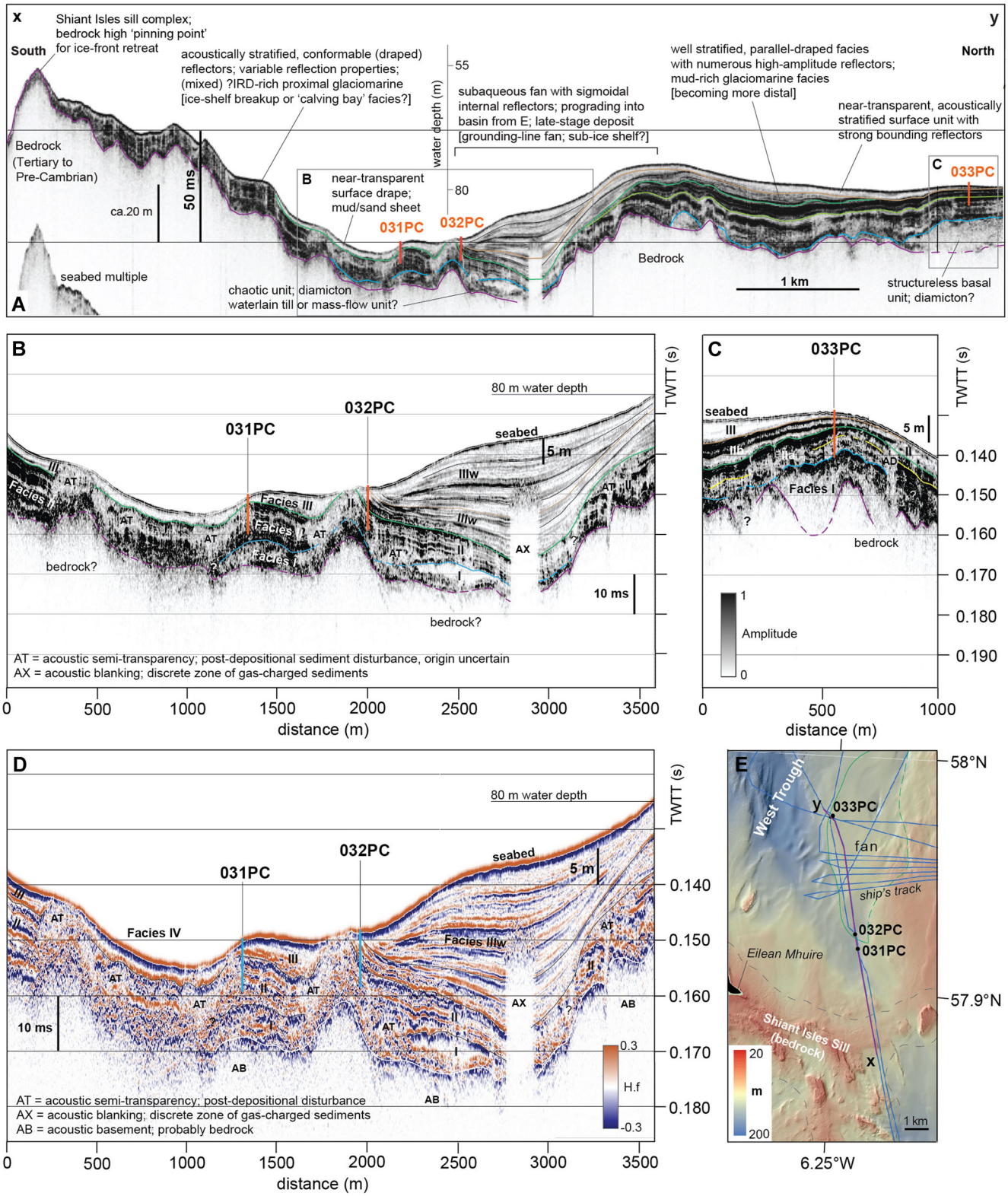

Figure 24. Inner Minch (west trough) acoustic stratigraphy. (A) SBP amplitude data (greyscale) of S–N transect across Shiant Isles Sill into West Trough, with descriptions and interpretations. (B) High-resolution image of SBP amplitude data (greyscale) on floor of West Trough including foot of late-stage subaqueous fan on west flank of MTBH, and core sites 031PC and 032PC. (C) Hilbert transform of data in panel B (red = positive; blue = negative), highlighting internal (sigmoidal) reflectors in subaqueous fan package and complexity of basin-floor acoustic facies. (D) Detail of SBP amplitude data at core site 033PC, where Quaternary stratigraphy thins on submarine high. (E) Hillshaded high-resolution bathymetric DTM model (MBES data from MCA/UKHO) showing seabed geomorphology, location of geophysical lines (in panels A–D) and core sites. Subaqueous fan margin shown by thin green line. [Color figure can be viewed at wileyonlinelibrary.com].

geophysical analyses, and X-radiographic measurements (Fig. S6). From core-base, Facies I is a 0.70-m-thick weakly stratified gravel-rich diamicton, with weak deformation structures, exhibiting high p-wave velocity and magnetic susceptibility values. We interpret this as a waterlain till or mass-flow unit deposited at or close to the grounding line of a large tidewater glacier in the vicinity of the MTBH or the Shiant Isles Sill. Facies II is very finely (mm- to cm-scale) laminated mud (silt and clay) with intercalated terrigenous sand and fine-gravel laminae and very rare outsized gravel

© 2021 The Authors. *Journal of Quaternary Science* Published by John Wiley & Sons Ltd

clasts (Fig. S6). We ascribe these fine rhythmites to low sedimentation rates in a former ice-shelf or ice-tongue cavity proximal to the grounding line, interrupted by occasional pulses of meltwater-derived sediment. Facies III is a mixed unit containing massive and stratified thin diamicton layers, mud-rich sandy gravels and gravelly muds, with weak lamination and deformation structures in places. We relate this to a rapidly changing higher energy environment, probably associated with rapid grounding-line migration and brief but high volumes of iceberg-rafted detritus and/or turbid meltwater outflows into the basin – typical of glacier 'calving bay' development (e.g. Leventer *et al.*, 2006; Mackintosh *et al.*, 2014; Hogan *et al.*, 2016). This unit is overlain by Facies IV: a rhythmically laminated (cm-scale) low-density mud facies with well-defined silt–clay couplets and rare isolated gravel clasts (dropstones) (Fig. S6). These low-energy meltwater-fed cyclopels are found in seasonally sea-ice-covered glaciomarine settings. The relative absence of IRD in this facies suggests either a more distal environment within a large 'calving bay' (e.g. Jennings *et al.*, 2018), or perhaps that the shallow bathymetric sill blocked iceberg influx to the basin (see Fig. 24). This sediment unit grades upwards into a weakly laminated low-density gravel-free mud facies (V) with laminations becoming poorly defined and wispy in the upper ~1.0 m, indicating distal glaciomarine to non-glacial hemipelagic sedimentation in relatively deep water. The sequence is capped by 0.45 m of muddy shell-rich fine sand (Facies VI) at seabed (Fig. S6). We relate the lower lithofacies (I–III) to the higher amplitude AF II, and the upper facies (IV–V) to the near-transparent AF III (Fig. 24) seen close to seabed across the West Minch trough.

Cores 032C (7.15 m long) and 033PC (8.02 m) penetrate the same acoustic facies (AF II and III) and display similar downcore stratigraphies to core 031PC (Fig. S6), but with differing unit thicknesses (Fig. 18). No suitable material was found for radiocarbon assay in cores 031PC, 032PC or 033PC.

Core 029PC

The southernmost core in the T8 coring campaign, taken 2.6 km east of Skye in the Sound of Raasay, this piston core recovered 8.89 m of continuous sediment in a water depth of 84 m (Supporting Information Fig. S7). Core 029PC consists of two main facies, from the base upwards: (I) 7.9 m of soft, grey-brown mud with varying proportions of silt and clay, showing bioturbation and faint wispy laminations, occasional shells and very rare lithic clasts (1–5 m^{-1}); capped by (II) 1.0 m of very fine muddy sand grading upwards into medium-grained sand at seabed. The soft muddy facies is relatively homogeneous in visible light and X-radiographs with only faint density laminations, few internal structures and no evidence of pervasive deformation. The mud shows unusually low downcore variation in p-wave velocity and resistivity, and only a slight increase in gamma-ray attenuation values (bulk density) with depth, from 1.60 to 1.80 g cm^{-3} (Fig. S7) Facies I can be subdivided on the basis of magnetic susceptibility (MS) trends into four sub-facies (a–d): relatively high MS values showing a stepped decline from core base (from ~600 to 400 SI units) (Ia); followed by a further gradual fall (to ~300 SI units) between ~7.40 and 6.00 m (Ib); a marked low-value MS unit (<250 SI units) between 5.80 and 5.00 m (Ic), followed by a relatively abrupt rise into a fluctuating MS-value unit (300–400 SI units) thereafter (Id) (Fig. S7). The lowest sub-facies (Ia) can also be distinguished from the upper sub-facies (Ib-d) based on a number of other subtle properties, for example: the visible colour change between 7.0 and 8.0 m (from 7.5YR 5/0 to 2.5YR 5/0); the decrease in the number of clasts, interpreted to be dropstones, above 7.25 m; the relative abundance of macrofaunal shells above 7.40 m; the absence of bioturbation below 8.0 m; the (near-) absence of foraminifera microfossils below 8.0 m; and the strengthening of sediment laminations below 8.50 m.

Three marine shells were sampled for AMS ^{14}C analysis from within the muddy facies (Ib) at depths of 7.03, 7.21 and 7.34 m (Fig. 15). No shells were seen at core depths > 7.50 m in X-radiographic imagery, and foraminiferal abundances below ~8.0 m downcore were insufficient for dating purposes. All three radiocarbon ages were in stratigraphic order (Table 8) and when calibrated yield ages of 14.47 ± 0.32, 14.03 ± 0.13 and 13.98 ± 0.14 cal ka BP – falling within the early part of GI-1 (Sub-stages 1d–1e; Lateglacial Interstadial). These dates on marine shells provide only a minimal age for the timing of deglaciation in the Inner Minch (Sound of Raasay). However, these three stratigraphically concordant ages are from within the sedimentological transition from distal IRD-poor glaciomarine (Ia) to predominantly non-glacial hemipelagic marine facies (Ib), indicating that tidewater glaciers perhaps transiently existed within the Inner Minch, or had only recently retreated, by this time.

Chronological synthesis, interpretation and palaeoglaciological reconstruction

So far this article has presented new geomorphological (pattern), geological (stratigraphic) and chronological information, from NW Scotland and the surrounding continental shelf, regarding ice-sheet extent and ice-margin positions during the last glacial cycle. In the following section we provide a chronological synthesis of the major glaciological events based on new and existing information underpinned by probabilistic Bayesian-chronosequence modelling.

Two Bayesian chronosequence models have been developed: one for the mainland-sourced ice sheet and one for Lewis. Both models were developed independently of the age information reasoned from the geomorphology, but with some iteration using age information where readvances or dynamic behaviour were implied. The motivation for the Bayesian modelling was to test hypotheses about the relative order of events (e.g. ice-sheet retreat) and explore spatio-temporal correlations of former ice-margin positions in NW Scotland. The final prior model (Fig. 25) included all the geochronological measurements, judged to provide meaningful deglacial constraints, and comprised a uniform phase-sequence model punctuated by boundaries coded using OxCal 4.3 (Bronk Ramsey, 2013). Note that ages relating to ice-sheet fluctuations before ~35 ka BP were not included in the Bayesian modelling for reasons of computational complexity. The approach is described in detail by previous workers (e.g. Chiverrell *et al.*, 2018; Bradwell *et al.*, this issue; and see the Supporting Information). Our Bayesian analysis produced a conformable age model with an overall agreement index of 158% for the MnIS and 138% for Lewis, exceeding the 60% threshold advocated by Bronk Ramsey (2009a, 2013).

One of the main strengths of using an ice-mass-wide or transect/sectoral approach is that even though not all stages or 'isochrons' can be robustly constrained, all sites sit within a wider (geo-) morphostratigraphic framework – i.e. a coherent spatial pattern – giving them a sense of chronological 'place'. A similar approach has been successfully used by others seeking to reconstruct the pattern and timing of ice-sheet-wide retreat elsewhere (e.g. Hughes *et al.*, 2016; Stroeven *et al.*, 2016).

The main palaeo-glaciological events in NW Scotland over the last ~45 000 years are briefly described below. These descriptions should be viewed alongside the accompanying overview map (Fig. 26), Bayesian modelling output (Fig. 25) and timeline

© 2021 The Authors. *Journal of Quaternary Science* Published by John Wiley & Sons Ltd

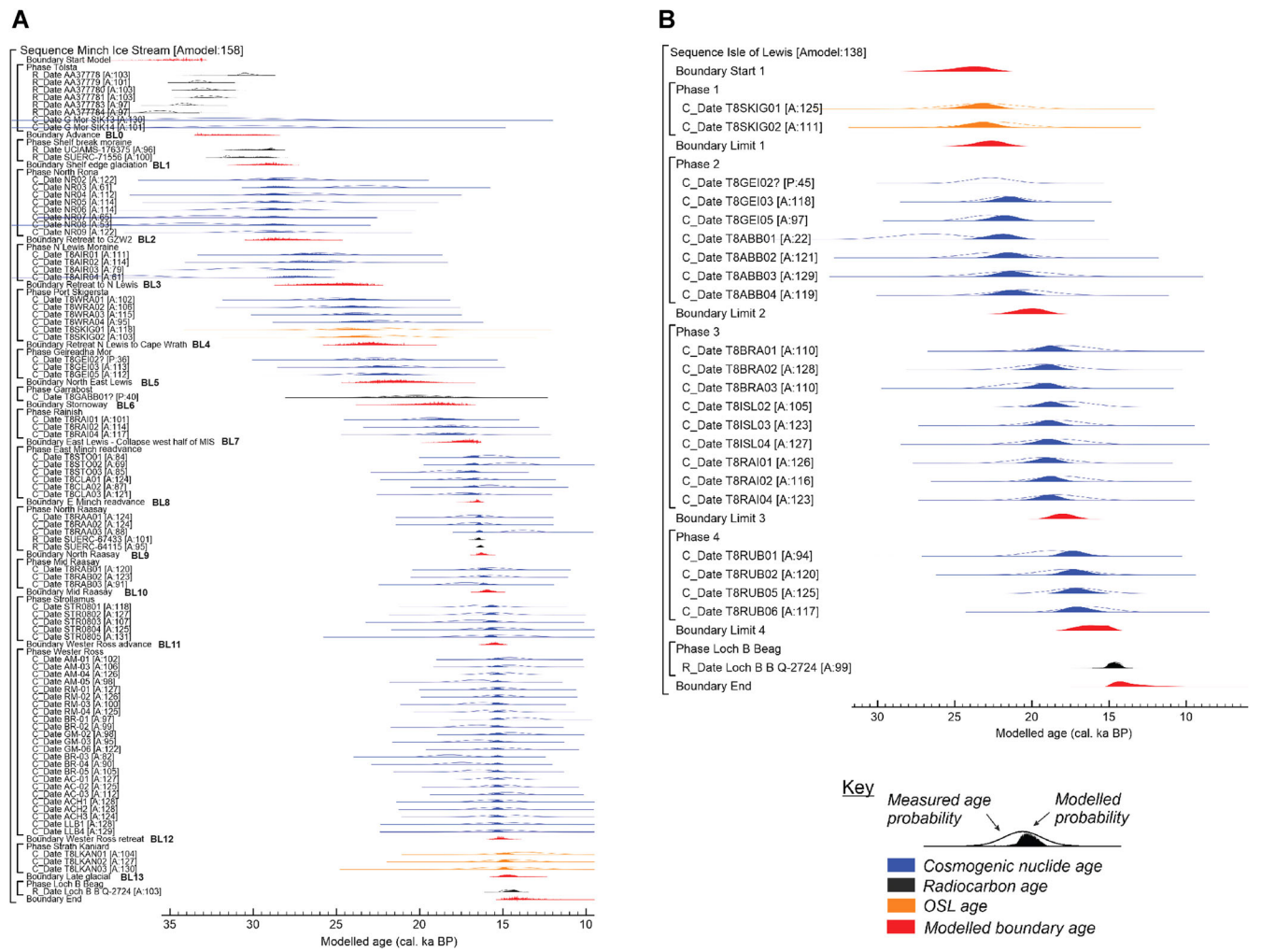

Figure 25. Bayesian chronosequence age-model output of dating constraints using Oxcal 4.3. (A) Minch ice stream/main ice sheet (BIIS); (B) Lewis ice cap, Outer Hebrides. Agreement index shown alongside chronosequence conformability. Modelled age (cal ka BP) on *x*-axis. Key shows different age assessments used (colour coded). [Color figure can be viewed at wileyonlinelibrary.com].

synthesis figure (Fig. 27). The following sections develop, extend and update the recently presented chronology (Bradwell *et al.*, 2019), using new and revised exposure-age calculations (Table 5), a new offshore radiocarbon chronology (Table 8) and a revised Bayesian chronosequence model (Fig. 25). [Note: all ages in the following sections refer to calendar years before present, i.e. the median of the calibrated 2-sigma result for ^{14}C dates; and the site-average UWM for TCN exposure ages and OSL ages. See Results for uncertainties. Bayesian boundary limits refer to those in Supporting Information Tables S2 and S3].

Mid-Weichselian (MIS 3): c. 45 – c. 38 ka cal BP

Evidence of a Mid-Weichselian, pre-LGM, ice-sheet advance followed by ice-sheet withdrawal is preserved within the thick sedimentary sequences along the NW Lewis coast. The sandy glaciotectonized sediments (LFA 2) at Suainebost clearly post-date the deposition of the lower grey shelly till (LFA 1), and pre-date the deposition of the upper grey-brown diamicton (LFA 3), identified at numerous localities in northernmost Lewis, known as the Port Beag Till (Merritt *et al.*, 2019). Based on its sedimentological properties and geomorphic context, we concur with others that the Port Beag Till (LFA 3) was deposited subglacially, beneath the lateral margin of the MnIS (Merritt *et al.*, 2019), pervasively deforming the underlying sandy sediments (and lower till) now exposed in coastal sections (Fig. 9). Our OSL ages from these glaciotectonically deformed deltaic-outwash sands, at Suainebost Sands and Traigh Chumail, attest to sedimentation in an ice-dammed (or ice-marginal) lake or shallow marine/lagoonal setting between ~44 and 38 ka BP, possibly on more than one occasion (Fig. 9). This places MIS 3 ice-sheet glaciation of NW Lewis within GS-9, 10, 11 or 12. However, calibrated radiocarbon dates from reworked shells in the underlying till (Sutherland, 1986) suggest glaciation after ~40–41 ka cal BP (i.e. in GS-9). GS-9 (39.8–38.2 ka BP) is also the longest stadial between 45 and 38 ka BP, and would represent the optimum 'window' for ice-sheet advance on to the Hebrides Shelf (Fig. 27).

The wider configuration of this MIS 3 ice sheet is not known, as offshore geomorphological evidence for pre-MIS 2 glaciations is still poorly defined. However, we surmise that this ice mass was sourced in the Western Scottish Highlands, as with subsequent ice sheets, and advanced along a similar flow path as the LGM ice sheet, depositing shelly till and Torridonian sandstone clasts at least as far as the present-day NW Lewis coast, before retreating. Ice-sheet retreat must have been well underway by 38 ka BP (Whittington and Hall, 2002; see below). Supporting evidence for an extensive MIS 3 glaciation in Scotland comes from BIIS-sourced IRD peaks at 39–41 ka BP in deep-water marine cores MD04-2822, MD01-2461 and MD04-2829 (Peck *et al.*, 2007; Scourse *et al.*, 2009; Hibbert *et al.*, 2010), around the time of Heinrich Event 4 (H-4) (Fig. 27). Furthermore, OSL dates from a glacigenic gravel fan at Howe of Byth in Buchan, NE Scotland, also suggest

© 2021 The Authors. *Journal of Quaternary Science* Published by John Wiley & Sons Ltd

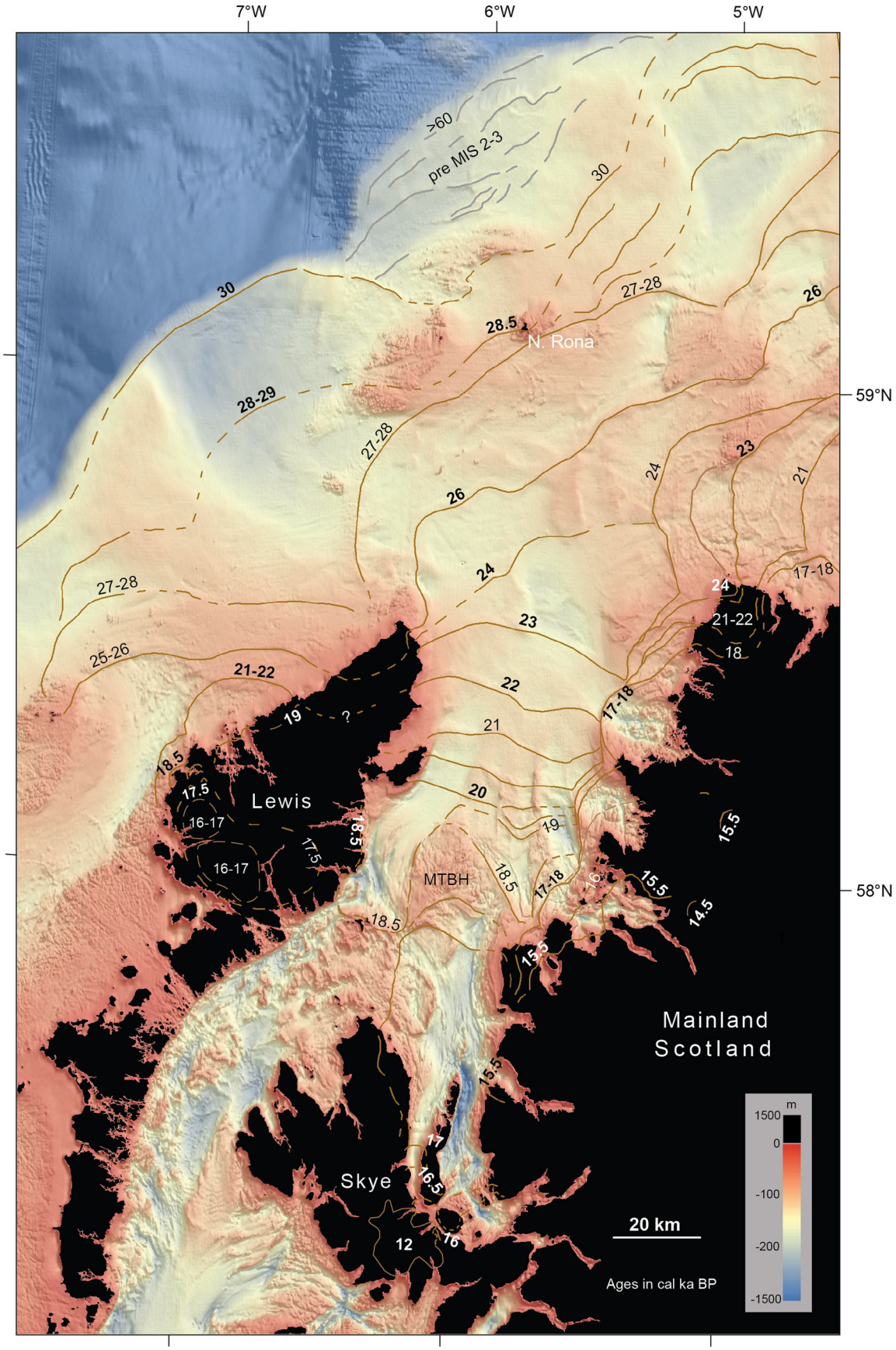

Figure 26. Summary palaeoglaciological reconstruction of ice sheet and ice cap deglaciation in the NW sector of BIIS, centred on 58°30′W, 59°N. Palaeo ice margins (brown lines) based on all available geomorphological/geological evidence and Bayesian-age-modelled chronology. Solid lines where glacio-geomorphological evidence is strong; dashed where connections are uncertain. Grey lines indicate pre-MIS 2–3 palaeo ice margins on outer continental shelf, north of North Rona. Numbered ice-sheet margins denote ages in calendar ka BP. Bold font, firmly dated; roman font, less firmly dated but 'in sequence'. Map area to the NE is extended beyond study area to show optimal connectivity with adjacent Britice-Chrono Transect (i.e. Shetland sector, T1; Bradwell *et al.*, this issue). Base map is EMODnet 2018 data (present-day bathymetry, not GIA corrected). DTM lit from NE/045. MTBH = mid-trough bedrock high. Note: linear features in NW of base-map image are survey artefacts. [Color figure can be viewed at wileyonlinelibrary.com].

© 2021 The Authors. *Journal of Quaternary Science* Published by John Wiley & Sons Ltd

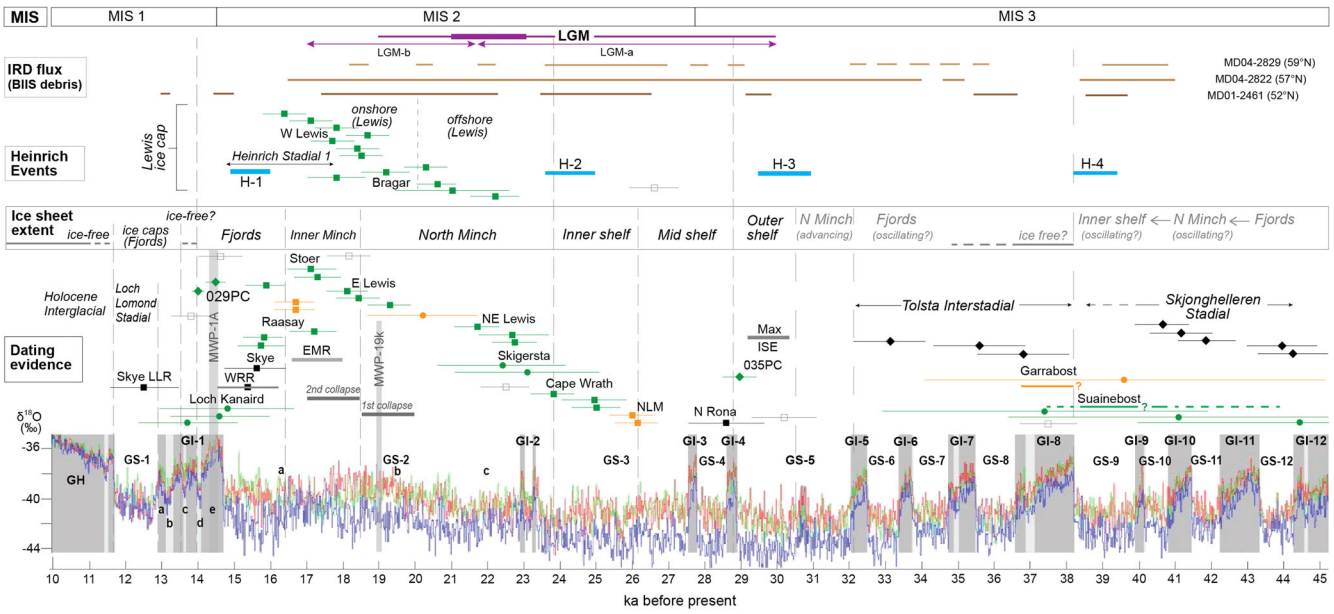

Figure 27. Geochronological overview of palaeoglaciological events in NW sector of BIIS spanning last 45 ka. From base: (i) GRIP (red), GISP2 (green) and NGRIP (blue) oxygen-isotope data from separate Greenland ice-core projects harmonized on common timescale (GICC05) in ka before present (2000 CE) (from Lowe *et al.*, 2008; Rasmussen *et al.*, 2014). Formal Greenland Stadial (GS) and Interstadial (GI; grey shading) names shown, with subdivisions where appropriate. Meltwater pulses 1A at 19 ka also shown (tall grey columns). (ii) Dating evidence from this study, all on same timescale: ^{10}Be TCN ages (squares); OSL ages (circles); calibrated ^{14}C ages (diamonds); symbol colours denote quality assurance (green = robust; amber = acceptable); black symbols are previously published dates (see text for details and references); hollow squares are TCN outliers. Horizontal bars are full (external) uncertainties at ± 1σ. (iii) Ice-sheet extent indicates position of ice-sheet (ice stream) margin at various time intervals determined in this study; those in grey font (i.e. > 30 ka BP) are based on fewer dates and lack geomorphological constraints, and hence are less reliable. (See Fig. 2 for definitions of seabed areas). Grey bars relate to discrete ice sheet events: e.g collapses or readvances. Max ISE = maximum ice-sheet extent in NW sector; NLM = North Lewis moraine; EMR = East Minch Readvance; WRR = Wester Ross Readvance. (iv) Heinrich Events (blue bars); ages defined by various workers (e.g. Scourse *et al.*, 2009). (v) IRD flux (brown bars) with BIIS-sourced debris, recorded in deep-water cores in NE Atlantic: MD01-2461 (Peck *et al.*, 2007), MD04-2822 (Hibbert *et al.*, 2010), MD04-2829 (Scourse *et al.*, 2009). (vi) Timing of global LGM (magenta line) based on widely accepted definition (e.g. Clark *et al.*, 2009; Carlson and Clark, 2012); definition of LGM in Europe (thick magenta bar) from Hughes *et al.* (2016); global LGM based on sea-level evidence (labelled LGM-a and LGM-b) after Yokoyama *et al.* (2018). Internationally defined Marine Isotope Stages (MIS) from Anderson *et al.* (2006) and Svensson *et al.* (2006). [Color figure can be viewed at wileyonlinelibrary.com].

ice-sheet advance as far as the Scottish coast between c. 45 and 38 ka BP (Duller *et al.*, 1995; Merritt *et al.*, 2017, 2019). To our knowledge, these OSL ages from Suainebost Sands are the first to record terrestrial ice-sheet fluctuations (probably associated with ice streaming) in western Scotland during MIS 3. We equate this early phase of BIIS advance to the 'Skjonghelleren Stadial', spanning GS-12 to GS-9 (Fig. 27), according well with fragmentary evidence of MIS 3 glaciation in Norway and around the margins of the North Sea Basin (Sejrup *et al.*, 2000, 2009; Lambeck *et al.*, 2010; Merritt *et al.*, 2003, 2017, 2019).

Ice-free conditions and build-up to advance: 38.6 ± 4.4 – 31.4 ± 2.6 ka cal BP [Base to Bayesian Boundary Limit 0]

Organic sediments overlain by till at Tolsta Head in NE Lewis (Whittington and Hall, 2002) provide maximum bracketing ages for the onset of glaciation in NW Scotland shortly before the start of the Late Weichselian stage (=MIS 2) (Fig. 27). Radiocarbon dates on sub-fossil peat, with temperate and arboreal pollen, attest to a relatively mild ice-free interval between ~38 and ~32 ka BP. These dates are used to define the base of our Bayesian chronosequence model (Fig. 25). Defined as the 'Tolsta Interstadial' in Scotland, this warm (or less cold) period corresponds in time with other dated interstadial sites preserving flora and fauna around NW Europe (Whittington and Hall, 2002). Eight published AMS ^{14}C dates from the Tolsta Head organic unit span several millennia, not permitting a precise correlation with the Greenland ice-core oxygen-isotope record. However, the spread of ages indicates that interstadial conditions at Tolsta Head started in GI-8 and probably terminated in GI-5 (Whittington and Hall, 2002). This important site strongly indicates that northern Lewis and the North Minch remained ice-free until ~32 ka cal BP, although we suggest that ice masses probably existed in mainland Scotland during the latter part of this period (GS-6, and perhaps GS-7) with the most likely Scotland-wide ice-free period being in GI-8 (c. 38–37 ka BP; Fig. 27).

One new OSL date from till-capped wind-blown sands at Garrabost (east Lewis) could also support ice-free conditions in the North Minch c. 37–38 ka BP (Fig. 27). This single age assessment, with rather large uncertainties (±5.5 ka), could equate to a number of interstadial phases from GI-12 to GI-7. We place probable aeolian dune development at Garrabost in GI-8 – the longest and warmest Dansgaard–Oeschger event within the 5- to 6-ka-long 'Tolsta Interstadial' (Whittington and Hall, 2002); with the lower grey over-consolidated till at Garrabost therefore dating from before this time, perhaps to the 'Skjonghelleren Stadial' (40–44 ka BP; see above). However, we accept that dune development in east Lewis could have taken place in any of the shorter MIS 3 Greenland Interstadials between 45 and 35 ka BP (Fig. 27).

Maximum ice-sheet extent: 31.4 ± 2.6 – 29.7 ± 1.9 ka cal BP [Bayesian Boundary 0 to 1]

Bayesian modelling of the available dates (Fig. 25; Supporting Information Tables S2 and S3) constrains the main phase of 'Late Weichselian' ice-sheet build-up in NW Scotland to GS-5

(<32.0 ka cal BP) (Fig. 27). During this pronounced Northern Hemisphere (NH) cold phase large ice-masses must have developed rapidly, in < 1000 years, evolving from mountain ice fields to a coalescent ice sheet complex with marine-terminating ice streams. This rate and magnitude of ice-sheet growth is consistent with modelling experiments by Hubbard *et al.* (2009), who simulate a period of uninterrupted, climatically driven, ice-sheet growth lasting from 31.5 to 30.4 ka BP.

In GS-5, with the MnIS fully developed, the ice sheet was able to transport large volumes of ice from its interior to the periphery regulating balance flux and maintaining equilibrium. Stratigraphic and dating evidence from cores 035PC and 036PC on the upper part of the ice stream depocentre (Sula Sgeir Fan) point to early shelf-edge glaciation c. 30 ka BP, with (initial) recession from these shelf-edge moraines by 29.0 ± 0.4 ka cal BP (Figs. 26 and 27). In its broadest sense, our age modelling brackets the timing of maximum ice-sheet extent on the continental shelf off NW Scotland to between 31.4 and 29.7 ka BP coeval with Heinrich Stadial 3. It is tempting to equate the maximal ice-sheet extent with the strong NH climatic nadir recorded in all Greenland ice cores between 30.4 and 29.5 ka BP (Rasmussen *et al.*, 2014).

Although the geomorphology clearly indicates ice-sheet termination near the shelfbreak to the west of the Sula Sgeir High, uncertainty still remains regarding the age of the Sula Sgeir basin-fill sediments and the grounding status of the ice sheet on the outer shelf, with several different palaeoglaciological scenarios presented by previous studies (cf. Stoker *et al.*, 1993; Sejrup *et al.*, 2005; Bradwell *et al.*, 2007, 2008a; Clark *et al.*, 2012; Bradwell and Stoker, 2015a, 2015b). Morphologically, the shelf-edge moraines do not resemble GZWs, as exemplified elsewhere on mid- to high-latitude continental shelves (Batchelor and Dowdeswell, 2015; Dowdeswell *et al.*, 2016), but are smaller features with well-defined crestlines which we consider to be subaqueous moraines superimposed on larger relict morainal banks (McDonald Fm). Acoustic stratigraphy in the Sula Sgeir Basin is complex (Fig. 12), but the unusual thickness of layered glaciomarine MacIver Fm facies (>80 m) and their onlapping architecture has been taken to indicate a prolonged period of sedimentation (or high sedimentation rates) *after* the deposition of the shelf-edge McDonald Fm. Stoker *et al.* (1993) equate the thick basin-fill MacIver Fm to pre-LGM glaciation(s) on the basis of seismo-stratigraphic relationships, borehole stratigraphy and amino acid racemizations. We present a revised multi-stage model (below) which reconciles the old (pre-MIS 3) sediment stratigraphy in the Sula Sgeir Basin with our young (MIS 2–3) chronology and geomorphological evidence for more recent shelf-edge glaciation.

First, large McDonald Fm morainal banks were deposited at the continental shelfbreak during a grounded Mid-Pleistocene ice-sheet glaciation (MIS 6–12) (Stoker and Holmes, 1991; Stoker and Bradwell, 2005). These deposits interdigitate with those of the Upper MacLeod Fm on the Sula Sgeir Fan (Fig. 12). Second, during a phase of substantial ice-sheet retreat (in MIS 6–12) MacIver Fm basin-fill sediments were deposited on the outer shelf in the Sula Sgeir Basin (Fig. 13). Third, at some point between 35 and 31 ka BP (MIS 3), an ice-sheet overrode the Sula Sgeir Basin – probably in the form of a low basal-shear-stress ice-stream advance – depositing relatively small moraines at the shelfbreak, superimposed on the larger relict (MacDonald Fm) morainal banks, and feeding glacigenic debris to the upper Sula Sgeir Fan slope (Macauley Fm) (Fig. 11). We propose that this rapid advance left little stratigraphic evidence in the Sula Sgeir Basin, perhaps only deforming the uppermost MacIver Fm sediments to a depth of < 10 m (Figs. 12 and 13). Fourth, during ice-stream retreat, icebergs released en-masse from the ice-sheet margin ploughed and scoured the seabed in this region. It is this iceberg-keel turbation which we genetically link to the near-surface acoustic disturbance seen in SBP data across much of the Sula Sgeir Basin (Figs. 12 and 13). We cannot precisely date this event but we believe it took place soon after maximum ice-sheet extent c. 29–27 ka BP. Fifth, marine sediment deposition occurred in shallow seabed depressions and iceberg scours, possibly in response to sea-level fall (Facies III; Figs. 12 and 13). And finally, sixth, extensive marine transgression occurred across the wider continental shelf forming a prominent erosion surface and resulting in the loss or truncation of surface stratigraphy (Fig. 12). This widespread erosion event would explain the horizontal nature of the seabed in the eastern Sula Sgeir Basin, the general lack of iceberg scour marks seen at seabed here, and the 'missing' MIS 2–3 stratigraphy. We cannot date this erosional event, but a marked marine regression–transgression episode during early MIS 2 (c. 27–22 ka BP) would accord well with marked eustatic sea-level fluctuations around the time of global LGM (e.g. Peltier and Fairbanks, 2007; Lambeck *et al.*, 2010).

Uncertainty surrounds the limit of the maximum ice-sheet advance on the outer continental shelf to the north of North Rona. Moraine evidence is largely lacking in this crystalline bedrock-dominated region of seabed (Fig. 26), making palaeoglaciological reconstruction difficult. However, projection of a prominent east-trending shelf-edge moraine places the ice margin in the vicinity of the Sula Sgeir High at the time of maximal ice-sheet extent on the outer continental shelf (c. 30 ka BP; GS-5). This revised ice-sheet margin pattern is consistent with recalculated TCN ages from North Rona (Everest *et al.*, 2013; Ballantyne and Small, 2019) indicating ice-sheet coverage in GS-5 followed by retreat c. 28.5 ka BP (Fig. 26). By implication, this ice-margin pattern also necessitates an ice-free area of continental shelf, potentially exposed as land (assuming 100–130 m lowered sea levels) throughout the last glacial cycle, to the north of the North Rona/Sula Sgeir High (Fig. 26). This is entirely consistent with the occurrence of pre-Weichselian sediments in boreholes and Mid-Pleistocene sediment sequences (MIS 8–12?) at seabed on the outer shelf c. 59.5°N, 6°W (Stoker *et al.*, 1993; Bradwell and Stoker, 2015b).

Local ice-sheet maximum to GZW2: 29.7 ± 1.9 – 27.7 ± 1.0 ka cal BP [Bayesian Boundary Limit 1 to 2]

Ice-sheet retreat from the continental shelfbreak maximum was underway by ~29 ka with the MnIS terminus on the mid-shelf inboard of the Sula Sgeir Basin by ~28 ka (Fig. 26). This is well before the timing of maximum ice-sheet extent for the rest of the BIIS complex, c. 23–27 ka cal BP, as defined by others (e.g. Peck *et al.*, 2007; Scourse *et al.*, 2009; Chiverrell and Thomas, 2010; Clark *et al.*, 2012; Peters *et al.*, 2015; Praeg *et al.*, 2015; Callard *et al.*, 2018; Bradwell *et al.*, this issue). We are confident that the marked asynchrony between the NW sector and other BIIS sectors is not a dating artefact but is real. We suggest that this distinct temporal asynchrony stems from: (i) the rapid evolution and sensitivity of the Scottish (proto British–Irish) Ice Sheet to climate cooling in GS-5; (ii) the proximity of the Hebrides Shelf to the main ice-sheet accumulation areas in NW Scotland (<150 km); and (iii) the dynamic response of the fast-flowing, low driving stress, MnIS to (internally driven) glaciological changes in mass flux.

Although an unexpected result, the concept of early rapid ice-stream advance to the shelfbreak in the NW sector is supported by numerical modelling experiments. Ice-sheet growth simulations by Hubbard *et al.* (2009) place the MnIS

© 2021 The Authors. *Journal of Quaternary Science* Published by John Wiley & Sons Ltd

terminus close to the continental shelf edge at 30.4 ka, < 1000 model years after a terrestrial ice sheet was confined to the Scottish mainland (at 31.5 ka model years). Similarly, more recent modelling experiments by Gandy *et al.* (2019) simulate a fast-flowing (300–1000 m a^{-1}) MnIS reaching the outer continental shelf in < 2500 years.

Our interpretation of SBP data from the outer shelf suggests extensive iceberg turbation and seabed disturbance, with ploughmarks largely removed by a widespread marine erosion event. If correct, this hypothesis points towards sustained iceberg calving of a floating ice-sheet terminus or ice-shelf c. 29-28 ka BP – around the time of the brief interstadial events (GI-4 and GI-3; Fig. 27). We propose that GZW1 may have been re-occupied at this time, but find no other evidence for significant ice-front or grounding-line stabilizations on the outer to mid-shelf until GZW2, c. 50 km inboard of the shelfbreak (Fig. 26).

Strong morphological connectivity between seabed moraines immediately adjacent to (inboard of) North Rona and the large GZW2 complex place a well-defined ice-sheet grounding-line stabilization on the mid-shelf (Fig. 26). The mean exposure age of recalculated TCN samples ($n = 5$) from North Rona places deglaciation of this island and hence the deeper-water mid-shelf by 28.5 ka BP. Our Bayesian modelling brackets ice-sheet recession followed by stabilization at GZW2 by ~27.7 ka BP (Fig. 26). Dating resolution is currently insufficient to refine this further or establish the duration of this stabilization event, with ^{14}C ages from overlying glaciomarine sediments providing only a loose minimum constraint (>20.5 ka BP).

GZW2 to GZW3: 27.7 ± 1.0 – 25.2 ± 2.1 ka cal BP [Bayesian Boundary Limit 2 to 3]

From this significant grounding-line stabilization (GZW2) ice-sheet retreat was re-instigated, possibly forced by the brief warming event GI-3 (27.8–27.6 ka BP), before another significant ice-stream stabilization occurred at GZW3. This broad mid-shelf ridge can be traced to the northern tip of Lewis, where TCN exposure ages from glacially transported boulders on the North Lewis moraine provide a deglaciation age of 26.0 ka BP (Figs. 26 and 27). This period is important because it represents the first significant exposure of present-day land (rather than present-day seabed) from beneath the BIIS in NW Scotland. Although mapped ice-sheet limits are lacking in NW Lewis, there is abundant evidence of long-lived subaerial exposure in a very cold climate. The coastal sediment exposures between Borve and the Butt of Lewis show extensively developed cryoturbation to a depth of 1.5 m (Peacock, 1984; Gordon, 1993) – evidence of intense periglacial conditions – strongly supporting the notion of very early ice-sheet deglaciation of NW Lewis and the adjacent continental shelf. We place the ice-sheet margin in NW Lewis at ~26 ka BP, though its precise location remains uncertain – owing to the probable presence of frozen-bed conditions and a general absence of glacial deposition (Fig. 26). Compare this scenario with the hypothesis proposed in the 1980s of a small (<20 km^2) ice-free enclave in NW Lewis (Sutherland and Walker, 1984) that escaped glaciation entirely during the Late Weichselian glaciation. As others have done (e.g. Hall, 1995; Hall *et al.*, 2003), we strongly refute this 'ice-free enclave' hypothesis based on our ice sheet sector-wide chronology. However, we note curiously that in our reconstruction NW Lewis would have been ice-free at the nadir of the global LGM (c. 26–22 ka BP) (Fig. 27). This may go some way to reconciling the original 'ice-free enclave' hypothesis (Sutherland and Walker, 1984) with the current, generally accepted, view of extensive shelf-edge glaciation in the same glacial stage [i.e. MIS 2 (e.g. Bradwell *et al.*, 2008a; Clark *et al.*, 2012), or MIS 2-3 (this study)].

GZW3 to Cape Wrath: 25.2 ± 2.1 – 22.9 ± 1.3 ka cal BP [Bayesian Boundary Limit 3 to 4]

Ice stream retreat from GZW3 across the inner shelf to the North Minch was interrupted by at least two periods of grounding-line stabilization and/or ice margin stillstand. We relate these ice-stream terminus stillstands to ice-marginal sediment-landform assemblages on the coast of NE Lewis where OSL ages indicate retreat of the MnIS margin at c. 23–24 ka BP, around the same time or shortly before the deglaciation of Cape Wrath, NW mainland Scotland, ~50 km to the east (Fig. 26). Numerous seabed moraines converge on the Cape Wrath headland indicating that it acted as a significant 'pinning point' during ice-sheet deglaciation. Moraine patterns suggest that as the ice stream thinned and retreated into the Minch straits, the high-elevation headland emerged, forcing the ice-sheet to diverge around it (Fig. 26). This is supported by our TCN exposure ages from Cape Wrath ($n = 4$) ranging from 22.5 to 25.0 ka BP, indicating early, possibly prolonged, deglaciation. Modelling experiments by Hubbard *et al.* (2009) clearly illustrate this pattern of headland emergence, although the timing is not correctly simulated. Our Bayesian modelling places deglaciation of the Cape Wrath headland at c. 23–24 ka BP with no evidence for subsequent ice-cover since. We believe this to be the earliest deglaciation date for any site in mainland Scotland – some 2–3 ka after the NW seaboard of Lewis became ice free (Fig. 26) (see above).

Cape Wrath to GZW7: 22.9 ± 1.7 – 21.4 ± 1.3 ka cal BP [Bayesian Boundary Limit 4 to 5]

During this period the MnIS remained relatively stable (static) with the grounding line located at the mouth of the Minch straits, between north Lewis and NW Sutherland. The largest two MnIS grounding-zone wedges by volume (GZW6 and GZW7) are located here, representing significant ice-stream stabilizations. We link their formation to ice stream 'pinning' or lateral confinement by the topography of the Minch straits and the resulting adjustment/reduction in ice flux. Notably, this period of palaeo-ice stream stability is well simulated in high-resolution modelling experiments (Gandy *et al.*, 2018). These recent model ensembles consistently predict a period of grounding-line stability, termed the 'stagnation phase', with a confined ice-stream configuration, and an 'unconfined' ice shelf extending 20–30 km across the inner continental shelf (Gandy *et al.*, 2018: fig 4d). Our chronology places the formation (or occupation) of the large GZW6 c. 23 ka BP, and GZW7 slightly later around 22 ka BP, with uncertainties of around ± 1 ka (Figs. 25 and 26). This phase of GZW formation equates to a period of relatively stable cold climate (GS-2c), immediately following two very brief, though muted, less cold intervals (GI-2), reflected in Greenland ice-core data (Fig. 27). This combination of topographic confinement and a stable NH glacial climate probably led to a period of unusual ice-stream and ice-shelf stability in the North Minch (lasting c. 1–2 ka), even against a backdrop of rising global sea levels (Lambeck *et al.*, 2010).

GZW7 to GZW15: 21.4 ± 1.7 – 17.3 ± 0.9 ka cal BP [Bayesian Boundary Limit 5 to 7]

Overall ice-steam recession continued in the North Minch during the next ~2 ka, punctuated by oscillations and

© 2021 The Authors. *Journal of Quaternary Science* Published by John Wiley & Sons Ltd

stabilizations of the grounding line in the topographic/bathymetric narrows between the projecting Eye and Stoer peninsulas on either side of the Minch. Several seafloor GZWs occur in this part of the North Minch, mapped and described previously (Bradwell *et al.*, 2019). It is also in this region where the main ice-stream trough splits around the large MTBH. These separate troughs have different width and depth profiles and, notably, host different glacial landform assemblages – with the east trough possessing numerous small GZWs, whilst the west trough is devoid of GZWs (south of the Eye peninsula; c. 58.1°N). GZW9 represents the last time that the MnIS filled the full width of the trough and behaved as a single coherent ice-stream/ice-shelf system, with a simple E–W-trending grounding line. We place the formation of GZW9 at ~20 ka BP (Fig. 27) (and see Bradwell *et al.*, 2019). Shortly after this time, but certainly before ~18.5 ka BP, the ice stream grounding-line in the west trough retreated c. 20 km without interruption, resulting in the rapid removal and breakup of the ice-shelf portion adjacent to eastern Lewis (ca. 500 km^2 in area). This ice-stream mass loss in the west trough appears to have affected the dynamics of the east trough ice stream, with a number of quasi-stationary grounding-line oscillations mapped at seabed (GZW11-14) (Bradwell *et al.*, 2019). These closely spaced GZWs indicate that a largely unconfined ice shelf or ice tongue remained in the east trough, as the grounding line underwent a series of readjustments, for some time, after the breakup (of the west trough ice stream/ice shelf; Fig. 27). By inference, and with reference to our Bayesian modelling, we place this '1st collapse' phase and dynamically driven ice-stream readjustment to c. 20.0–18.5 ka BP.

Several grounding-zone landforms in the east trough of the North Minch probably date from the second half of this time period as the ice stream underwent 'threshold behaviour' in response to the permanent loss of ice-shelf buttressing in the adjacent west trough. By c. 18.5 ka BP, the ice-stream grounding line was stably situated at GZW15 – the last of the major GZWs – approximately at the boundary between the North Minch and Inner Minch (Fig. 27). At this time an ice shelf, or ice tongue, was partially confined or supported by the shallow MTBH to the west and the projecting headland of Coigach, in NW mainland Scotland, to the east. We expect that the ice-sheet terminus was also grounded in shallow water on the MTBH, with a N–S-oriented ice margin depositing conspicuous subaqueous sediment fans on the flanks of the west trough around this time (Figs. 24 and 27). This ice-stream/ice-shelf configuration is closely simulated by the modelling of Gandy *et al.* (2018) in their retreat-phase experiments (their fig. 4e; i.e. 6300 model years), with fast ice-flow velocities (>400 m a^{-1}) and high calving rates maintained at ice-shelf termini. The bathymetry and Quaternary geology indicate that the ice-stream terminus remained quasi-stable in the Inner Minch c. 58°N for a relatively long period of time. Unlike the smaller GZWs (11–14), the large size (1.5–2.5 km wide, 20–30 m thick) and complex acoustic stratigraphy of GZW15 indicate (i) a sustained grounding-line stabilization, and/or (ii) high subglacial sediment flux and deposition at the grounding line here. Previously published estimates of GZW formation at ice-stream grounding lines offshore Antarctica and Greenland indicate formation of features this size on decadal timescales (<100 years) rather than longer (Batchelor and Dowdeswell, 2015; Hogan *et al.*, 2016).

Regardless of the precise formation time of GZW15, ice-stream recession inshore of this point was almost certainly rapid – with the shoreward deepening bathymetry promoting ice-front collapse probably via marine ice-sheet instability (Gandy *et al.*, 2018; Bradwell *et al.*, 2019). Bradwell *et al.* (2019) proposed that grounding-line destabilization and rapid ice-stream recession in the Inner Minch occurred as a series of dynamically linked events: (i) the retreating calving front reached the grounding line (at GZW15) causing (ii) collapse or abrupt loss of the partially confined ice shelf/ice tongue; (iii) formation of a deep 'calving bay' upstream of GZW15 with brief transient stabilizations (at GWZ16 and 17); followed by (iv) rapid uninterrupted ice-front retreat and breakup; until (v) stabilization and grounding of tidewater margins at fjord mouths close to the marine–terrestrial transition (Figs. 26 and 27). The total collapsed ice-front area in the Inner Minch, from GZW17 to the Sound of Raasay, was c. 800 km^2 (±10%) and took place sometime between 18.5 and 16.7 ka BP, perhaps focused within a few decades (Bradwell *et al.*, 2019). This final rapid ('2nd collapse') phase of recession from the MTBH marked a major behavioural shift, from a coherent buttressed ice-stream/ice-shelf system, at GZW15, to a number of separate unsupported tidewater glaciers responding to different glaciological drivers in the Inner Minch (Bradwell *et al.*, 2019). This dynamic sequence of ice-shelf disintegration, increased ice-flow velocities and rapid ice-mass loss is captured in recent ice-sheet modelling simulations of the NW BIIS sector (Gandy *et al.*, 2018).

East Minch Readvance and retreat: 17.3 ± 0.9 – 15.4 ± 1.5 ka BP [Bayesian Boundary Limit 7 to 8]

By 17.5–18.0 ka BP, with the collapse of the remaining ice shelf/ice tongue, the east trough of the Minch was a large deep marine embayment receiving icebergs from calving ice-sheet margins to the south and east. Submarine landform evidence strongly indicates a substantial late-stage readvance of glaciers, possibly by 1–10 km, from the catchments of Wester Ross, Assynt and West Sutherland into waters previously occupied by the MnIS around this time (Fig. 27). We cannot date the advance phase precisely; however, it must have taken place *after* the deposition of GZWs 7–10 (i.e. < 21.4–19.0 ka BP) as these are clearly overprinted or truncated by the readvance moraines in Eddrachillis Bay and NW of Rubha Coigeach (Fig. 25). Our new dating evidence and Bayesian modelling place *retreat* from this *East Minch Readvance* in the time window from 17.3 to 15.4 ka BP, with a relatively large uncertainty term. This temporal uncertainty stems from the spread in TCN ages ($n = 6$) from boulders on moraines and bedrock recording retreat across the Stoer headland (Assynt). Assuming that the mean of the six TCN ages most accurately represents the timing of deglaciation (=16.5 ka), regional ice-sheet advance must have culminated shortly *before* this time at ~16.5–17.0 ka BP. However, if the older three TCN ages are a better constraint on ice-sheet retreat (=17.4 ka) then the East Minch Readvance could have occurred somewhat earlier c. 17.5–18.0 ka BP (Figs. 26 and 27). Both these timings fit within the overall Bayesian model sequence and place the readvance in the first half of Heinrich Stadial 1. The earlier date suggests a substantial ice-sheet readvance into the East Minch in the immediate aftermath of ice-shelf collapse; the later date suggests a delay between ice-shelf loss and subsequent ice-sheet readvance. Irrespective of the precise timing, this significant ice-sheet oscillation – the East Minch Readvance – took place *before* ~16.5 ka BP, c. 1–2 ka earlier than the regional WRR (see below), based on clear overprinting geomorphological relationships and the age assessments reported here (Fig. 27). Indeed, by the time of the WRR, ice-sheet margins in Assynt and West Sutherland had receded from the coastal plain to the mountain belt 20–25 km inland (Bradwell *et al.*, 2008b), indicating a strong physiographic asymmetry between tidewater glaciers in Wester Ross and

© 2021 The Authors. *Journal of Quaternary Science* Published by John Wiley & Sons Ltd

land-terminating glaciers in West Sutherland at this time (Fig. 27).

GZW17 to Raasay and the fjords: 17.3 ± 0.9 – 15.6 ± 0.8 cal ka BP [Bayesian Boundary Limit 7 to 10 (excl. BL 8)]

Following rapid, instability triggered, ice-front collapse from the MTBH (GZWs 15–17) (see above), the ice-sheet margin stabilized where the Inner Minch trough narrows and divides between Skye, Rona–Raasay and the Applecross Peninsula (Scottish Mainland). Here the confining topography, shallower water depths and numerous islands offered lateral and basal support for large tidewater glaciers able to ground and maintain equilibrium (with ice flow typically balanced by calving). This restricted ice-sheet configuration is well simulated by the high-resolution modelling of Gandy *et al.* (2018; their fig. 4f). Our dating evidence places the end of the Inner Minch rapid retreat (or '2nd collapse') phase before 16.7 ka BP, with calving fluxes and grounding-line retreat decreasing considerably in the much narrower trough geometry closer to shore (Fig. 27). Further ice-front recession at the head of the Inner Minch (Inner Sound and Sound of Raasay) was slow, with net retreat of only 10–12 km in the next ~500 yrs (c. 20 m a^{-1}), implying a linear response to external forcing in a stable bathymetric/topographic setting. Modest rates of tidewater glacier retreat probably continued over the next ~500 years as receding glaciers approached the marine–terrestrial transition – with most glaciers in fjord-mouth settings in Skye (Loch Ainort, Loch Sligachan), and the adjacent mainland (e.g. Loch Alsh, Loch Carron, Loch Torridon in Wester Ross), by 16.0–15.6 ka BP (Fig. 27) (Small *et al.*, 2012; Bradwell *et al.*, 2019). Considerable paraglacial landscape adjustment probably took place in this period as steep unstable slopes on land and underwater were exposed from beneath the ice-sheet for the first time in many millennia. Large deep-seated landslips and block slides in southeast Raasay, such as the Beinn na Leac block (Smith *et al.*, 2009), may have foundered in the wake of ice-sheet retreat and fluctuating stress conditions shortly after ~16.0 ka BP.

WRR and retreat: 15.6 ± 1.0 – 14.6 ± 0.6 ka BP [Bayesian Boundary Limit 10 to 13]

The WRR is a well-documented regional ice-sheet oscillation in NW mainland Scotland with moraine fragments stretching from Loch Torridon (57°N) in the south to Achiltibuie (58°N) and beyond (Robinson and Ballantyne 1979; Everest *et al.*, 2006; Bradwell *et al.*, 2008b; Ballantyne *et al.*, 2009) (Fig. 27). The most recent recalculation of existing TCN ages ($n = 16$) indicate the WRR culminated around 15.3 ± 0.7 ka (Ballantyne and Small, 2019), several centuries before the rapid warming at the onset of the Lateglacial Interstadial in NW Europe (GI-1). Our Bayesian modelling places this significant ice-sheet margin oscillation between 15.6 and 14.6 ka BP, with advance in the early part of this time window (>15.0 ka BP) followed by stepped retreat. The 1.0 ka time range reflects the large number of TCN analyses and best-fit modelling in the Bayesian chronosequence computation.

What caused the WRR is still unclear. Greenland ice-core oxygen-isotope data point towards a relatively stable climate during this period, with cold-climate conditions dominating the final phase of Heinrich Stadial 1 (15.6–14.8 ka BP) (Fig. 27). Sea-level reconstructions and models all indicate relative sea-level fall in NW mainland Scotland during this time. Given the sensitivity of this ice-sheet sector to instability-driven ice-front oscillations, highlighted recently (Gandy *et al.*, 2018; Bradwell *et al.*, 2019) and reinforced in this work (e.g. the East Minch Readvance), we cannot rule out the possibility that the WRR may simply represent another such event at a later stage.

Final deglaciation (G1-1 and GS-1): 14.6 ± 0.6 – 12.8 ± 2.2 ka BP [Bayesian Boundary Limit 13 to End of Sequence]

Abrupt warming defined the end of Heinrich Stadial 1 (GS-2) and the start of GI-1 at 14.7 ka BP (Rasmussen *et al.*, 2008, 2014). By this time, the surviving remnants of the former ice sheet in mainland NW Scotland had separated into small ice fields and upland ice caps with atmospheric warming driving glacier mass losses at all elevations (Fig. 3). The pattern and timing of this final ice-mass-decay phase is still much debated (e.g. Bradwell *et al.*, 2008b; Finlayson *et al.*, 2011; cf. Stone and Ballantyne, 2010; Ballantyne and Small, 2019) and we can add little to the existing reconstructions. However, our new OSL dates from the shore of Loch Kanaird indicate that an extensive glaciofluvial outwash fan formed during this time c. 14.3 ka BP (Fig. 7), one of a number of abandoned coastal terraces or raised glacio-deltaic deposits in northern Wester Ross and West Sutherland, currently at 10–15 m asl. This places a conspicuous sea-level highstand here early in GI-1 and by inference also puts the ice-mass margin inland of Loch Kanaird by ~14.3 ka – though glaciers almost certainly still existed in the catchment supplying large volumes of sand and gravel to outwash terraces here and in Loch Broom (Stoker *et al.*, 2009). We equate this marine highstand evidence with Meltwater Pulse 1A (MWP-1A) – an abrupt +15-m eustatic event recorded globally and well dated at 14.65–14.31 ka BP (Deschamps *et al.*, 2012; Liu *et al.*, 2016). Other workers have recently postulated the likely presence of an MWP-1A signature along the seaboard of west Scotland (Shennan *et al.*, 2018; Smith *et al.*, 2019); our new dating evidence makes the case much stronger (Fig. 27). We expect that rapid build-up of these glaciofluvial deltas and terraces took place between 14.7 and 14.3 ka BP in response to MWP-1A, followed by gradual incision and abandonment as relative sea level fell over the remainder of GI-1 and into GS-1.

Lewis: ice sheet maximum and aftermath: 31.4 ± 2.6 – 22.7 ± 0.9 ka BP [Bayesian Boundary Limit 0 to 1]

Relatively little is known about the timing of deglaciation on Lewis, especially on low ground. Our new dating evidence establishes a much-needed framework chronology in key areas. We constrain ice-sheet retreat from the Sula Sgeir Fan shelfbreak moraines (at 7°W) by 29.5 ka BP, with the ice-stream grounding-line on the mid-shelf (at GZW2) inshore of North Rona by 27–28 ka BP (Figs. 26 and 27). Morphostratigraphic correlations between ice-sheet limits mapped on the outer shelf NW of Lewis are less clear across the ice-stream trough owing to the lack of clear grounding-line features and a widespread marine erosion event (Bradwell *et al.*, 2019) (Fig. 26). Based on moraine patterns and no dating evidence to the contrary, we assume that the MIS 2–3 BIIS reached the continental shelfbreak, at least as far west as 7°30'W, at broadly the same time (~30 ka BP). South and west of here, on the outer Hebrides Shelf, ice-sheet moraines trend south and south-west towards shallower waters. It should also be noted that submarine landforms (Hiemstra *et al.*, 2015) and terrestrial dating evidence (Ballantyne *et al.*, 2017) from the island of St Kilda (57.8°N, 8.75°W) indicate that the Mid- to Late Weichselian BIIS did not over-top the highest points on the island (>270 m asl).

© 2021 The Authors. *Journal of Quaternary Science* Published by John Wiley & Sons Ltd

We place the ice-sheet limit on the mid-Hebrides Shelf, in early GS-3 (26–27.5 ka BP) at a time of falling global sea-levels (Figs. 26 and 27). Soon after, by the time of the LGM eustatic minimum 26–25 ka BP (~130 m below present; Peltier and Fairbanks, 2007; Lambeck *et al.*, 2014), the BIIS in this sector had receded landward to present-day NW Lewis, exposing a large area of the Hebrides shelf to full-glacial cold-climate subaerial conditions (see above). This ice-sheet configuration allowed the widespread development of periglacial features in sediments now exposed along the coastline of NW Lewis, between Borve and the Butt of Lewis (Fig. 33); these include highly frost-shattered bedrock, mature solifluction lobes, bedded gelifractate gravels and cryoturbation structures within older (MIS 5) raised beach gravels (Peacock, 1984; Hall, 1995; Merritt *et al.*, 2019). Collectively, the evidence indicates that during the extremely cold eustatic LGM lowstand (~26–22 ka BP) much of the continental shelf west of Lewis as well as parts of NW Lewis itself were exposed as a barren periglacial, or permanently frozen, coastal plain (Figs. 26 and 27).

Lewis: ice sheet retreat: 22.7 ± 0.9 – 20.1 ± 0.9 ka BP [Bayesian Boundary Limit 1 to 2]

By the start of this time interval the MnIS terminus had retreated across the inner shelf to a stable position at the mouth of the Minch straits (see above) (Fig. 26). The ice-stream trunk was probably still being fed by an ice-stream tributary draining much of central and east Lewis, whilst a significant portion of NW Lewis, c. 25–100 km^2, was now ice free. Approximately 10 km SW of the relict periglacial features in NW Lewis, exposure ages from Ard Bheag Bhragar headland coupled with offshore moraine evidence indicate that an ice lobe probably extended ~10 km beyond the mouth of Loch Roag at, or shortly before, 21–22 ka BP. We tentatively connect this limit with geomorphological evidence and exposure ages from NE Lewis (near Tolsta Bay) indicating ice-sheet retreat here at broadly the same time (Fig. 26). However, we admit that any glaciological linkage between ice stream (and ice shelf?) retreat in the Minch and ice-lobe recession on Lewis's west coast is still speculative and requires further investigation.

Lewis: Ice sheet retreat: 20.1 ± 0.9 – 18.0 ± 0.7 ka BP [Bayesian Boundary Limit 2 to 3]

After reaching the present-day coastline at Ard Bheag Bhragar, ice-mass retreat appears to have slowed considerably with net ice-margin recession of only ~3 km over the next ~2 ka. During this time prominent moraines formed at Bragar. However, we cannot determine how far the ice-margin receded inland of these moraines before readvancing, or whether the moraines simply mark a minor oscillation (<100 m) of the ice-front. If a significant readvance of the ice margin (>1 km) did occur at Bragar, as we suspect based on geomorphological similarities with readvance moraines elsewhere (e.g. WRR), we place it between 19.3 and 20.3 ka BP, and certainly no earlier than 21.0 ka, based on the available dating evidence. Interestingly, there is no obvious climate forcing recorded during this interval – Heinrich Stadial 1 (14.7–17.8 ka BP; Scourse *et al.*, 2009) and the so-called Extra-polar Climate Reversal (17.5–18.6 ka BP; Asmerom *et al.*, 2017) both occur > 1–2 ka later (Fig. 27). Instead, we propose that the *Bragar Readvance* on Lewis may relate to glaciological events occurring in the Minch at this time, with rapid ice-front losses causing dynamic readjustment (i.e. readvance) of the Lewis-centred ice mass in the wake of ice-shelf debuttressing c. 20–19 ka BP. Similar dynamically driven ice-sheet fluctuations are hinted at in the OSL-dated glacial stratigraphy from east Lewis/Eye Peninsula (at Garrabost) around the same time (~20 ka BP), and more extensively in the East Minch Readvance following a second ice-shelf collapse at ~18.5 ka BP (see above) (Figs. 26 and 27). Although strongly suggestive, further work is needed to substantiate these potentially important glaciological connections and refine this chronology further.

Lewis: Ice cap stage: 18.0 ± 0.7 – 16.1 ± 1.0 ka BP [Bayesian Boundary Limit 3 to 4]

The ice mass in Lewis started to act independently of the main Scottish Ice Sheet once connection was lost with the MnIS c. 20–19 ka BP, with ice firmly onshore in east Lewis by ~18.5 ka BP. We note very little geomorphological pattern information from east or central Lewis relating to this transition to an independent ice-cap. However, moraine morphologies on-shore in west Lewis at Islibhig, Carnish and Uig Sands indicate lobate, terrestrial, ice-cap-style deglaciation undergoing minor oscillations at c. 18.0–17.5 ka BP. Associated sediment-landform assemblages demonstrate the impounding of glacial lakes in west Lewis, possibly with rapid drainage events, during this punctuated retreat phase. We equate the youngest set of dated west Lewis ice-cap moraines (Rubha Linish; ~17.6 ka BP), just NW of Loch Suainaval, to general cooling experienced at the onset of Heinrich Stadial 1 (18.0–17.5 ka BP) (Figs. 26 and 27).

Lewis: final deglaciation: 16.1 ± 1.0 – 13.8 ± 1.1 ka BP [Bayesian Boundary Limit 4 to End of Sequence]

Subsequent West Lewis ice-cap losses took place predominantly on low ground in GS-2 forcing the ice-mass margins back towards the Uig Hills (>500 m asl) (Fig. 26). Final GS-2 disappearance of glaciers in Lewis is not well constrained; however, we envisage final ice-cap remnants melted during the latter stages of Heinrich Stadial 1 (16–15 ka BP), prior to the marked GI-1e warming at 14.7 ka BP (Fig. 27). Ballantyne (2006) reconstructed small glaciers, or an ice-field complex, in the Uig Hills during the Loch Lomond Stadial (GS-1) based on established morpho-stratigraphic grounds. However, caution is advised as similar-looking supposed 'GS-1' landform assemblages elsewhere in Scotland have, when dated, proven to be considerably older (e.g. Everest and Kubik, 2006; Bradwell *et al.*, 2008b; Small *et al.*, 2012, Bradwell *et al.*, this issue).

Summary and conclusions

Understanding the response of ice sheets to internal and external drivers is fundamental to refining predictions of future sea-level rise and reducing uncertainties in global change forecasts. Marine ice sheets, from the Pleistocene, grounded largely below sea level with ice streams and extensive marine margins are the best analogues for the most vulnerable ice sheet sectors on Earth in present-day West Antarctica. This work forms part of a larger project to explore the deglaciation of one such former ice sheet – the BIIS – aiming to generate a benchmark or test bed against which to calibrate and refine future numerical ice-sheet models.

This article has presented new geomorphological (pattern), geological (stratigraphic) and chronological information regarding former ice-margin positions and ice-sheet fluctuations, in streaming and non-streaming sectors, of the former BIIS in NW Scotland and on the adjacent continental shelf. We build on and extend previous work but present, for the first time, a

© 2021 The Authors. *Journal of Quaternary Science* Published by John Wiley & Sons Ltd

synoptic assessment of ice-sheet pattern information and glaciological connections between different areas within this BIIS sector at different times over the last 45 000 years.

We have generated 104 new absolute-age assessments for the NW sector of the BIIS from onshore and offshore. This collection of new dates greatly increases the existing number of robustly dated sites for this important and dynamic sector of the BIIS, part of the wider Eurasian ice-sheet complex. This multi-proxy integrated study, combining numerous lines of empirical evidence, draws several key conclusions relating specifically to the NW sector of the BIIS. Some of these findings have wider implications for ice-sheet dynamics more generally, and marine ice-sheet instability in particular. The main conclusions in geochronological order are summarized:

1. Our new evidence indicates extensive marine-terminating ice-sheet glaciation in the BIIS NW sector between ~44 and 38 ka cal BP (between GS-12 and GS-9). Ice-sheet advance at least as far as NW Lewis, and possibly further on to the continental shelf, probably occurred in GS-9 and GS-10 – prior to the main 'Late Weichselian' ice-sheet glaciation. We equate this Mid-Weichselian glaciation with the 'Skjonghelleren Stadial' glaciation in Norway. As this MIS 3 BIIS waned, its margin fluctuated in the vicinity of NW Lewis, depositing ice-marginal sediments in ice-dammed lakes or lagoons at the present-day coastline c. 44–38 ka BP, possibly on more than one occasion. Mid-Weichselian ice-sheet glaciation of Scotland is supported by BIIS-derived IRD peaks c. 39–41 ka BP (identified by others) in deep-water marine cores. We presume that the Minch ice stream operated during this Mid-Weichselian glaciation, as in later periods. But we note that our onshore dating constraints come with relatively large uncertainties.
2. There was a period of restricted ice-cap glaciation or no glaciation in NW Scotland during GI-8 to GI-5 – the 'Tolsta Interstadial' – with Lewis and at least the North Minch ice-free for some of this period (probably from ~38 to 35 ka BP). The size reduction of Scottish-sourced ice masses during the mildest phases of this variably temperate–cool interstadial is not known. Fragmentary evidence from other sites in Scotland indicates that any surviving ice-masses were probably restricted to the Scottish Highlands during the early Tolsta Interstadial (GI-8); but, we suggest, tidewater (fjordic) glaciation may have existed in NW Scotland soon after ~35 ka BP (i.e. in GS-7 and GS-6), supported by IRD evidence from marine cores.
3. Build-up and advance of the 'Late Weichselian' BIIS actually started in the latter part of MIS 3. Soon after the onset of GS-5 (c. 32 ka BP), the largely terrestrial Scottish Ice Sheet centred over Western Scotland must have undergone a significant and sustained increase in volume and areal extent with the re-establishment of a major ice stream in the Minch. We place the advancing ice-sheet margin in the North Minch c. 32–31 ka BP. By c. 30 ka BP the BIIS extended to the outer shelf in the NW sector, reaching the continental shelfbreak at 7°W, adjacent to the Sula Sgeir Fan, but not at 6°W (see below). This GS-5 advance represents the maximal extent of the BIIS in the NW sector during the whole of MIS 3 and MIS 2 (i.e. in the last ~55 ka BP) – and probably since the Mid-Pleistocene ice-sheet glaciations of MIS 6, MIS 8 and MIS 12. The timing of maximal BIIS extent in the NW sector corresponds with a sustained very cold period (>800 years) in the Greenland ice-core oxygen-isotope records (30.4–29.5 ka BP), and with the timing of the widespread North Atlantic iceberg-rafting event H-3. However, this maximal shelf-edge ice-sheet configuration did not leave a strong geomorphological imprint and may not have lasted long – indeed, we cannot rule out a dynamic ice-stream surge as the cause. By ~29.0 ka BP the ice stream was already in retreat and by ~28.5 ka BP its margin was situated adjacent to the island of North Rona on the mid-shelf.
4. The limit of the Mid–Late Weichselian maximum ice-sheet advance to the north of North Rona is still unclear owing to the general lack of moraine evidence. We place the GS-5 maximal BIIS limit on the outer continental shelf ~10–15 km beyond North Rona but topographically 'pinned' by the Sula Sgeir High. Our reconstructed BIIS outline differs from previous depictions in not extending across the outer shelf to the north of the Sula Sgeir High, and implies an ice-free area of continental shelf existed here throughout the last glacial cycle.
5. Our collective evidence indicates that maximal Mid–Late Weichselian BIIS extent in the NW sector occurred significantly earlier (at least 3–5 ka) than in adjacent BIIS sectors: Malin Sea/Barra Fan (~27 ka BP); West of Shetland/Northern North Sea (~25–26 ka BP); and in southern BIIS sectors: Celtic Sea/Irish Sea (~25–26 ka BP) and Southern North Sea (~21–24 ka BP) (see other papers in this issue). We propose that this very early, possibly short-lived, maximal extent in the NW BIIS reflects (i) proximity to the ice-sheet accumulation areas in NW Highland Scotland, (ii) a relatively narrow continental shelf NW of Lewis (<100 km), and (iii) the dynamic behaviour and high discharge flux of the Minch palaeo ice stream. We stress, however, that maximum ice-sheet areal *extent* may not necessarily correspond with maximum ice-sheet *volume*, especially in streaming sectors.
6. Deglaciation of the NW BIIS sector took place in numerous stages. Several large GZWs, and their continuations as moraines on the surrounding shelf, mark significant stabilizations of the ice-sheet grounding line and/or ice margin during overall retreat, with or without the development of ice shelves. We have constrained a timeline of ice-sheet retreat spanning MIS 2 (~28–15 ka BP). Major stillstands of the grounding line, and presumably the wider ice-sheet margin, took place at c. 28–27, c. 26 and 24 ka BP, within the bathymetric trough between the Sula Sgeir High and the Outer Hebrides. Equivalent ice-marginal positions c. 28–25 ka BP are mapped on the Hebrides Shelf to the west of Lewis although palaeo-glaciological connections with the Minch ice-stream corridor remain equivocal. It was also during this period, in early MIS 2, that parts of NW Lewis became ice-free; with the ice-sheet margin > 80 km inshore of the continental shelfbreak and demonstrably onshore in north Lewis by 26–25 ka BP. Our chronology places deglaciation here during the global sea-level minimum defining the LGM.
7. Ice-sheet retreat slowed at the entrance to the Minch c. 24–23 ka BP. Large seafloor GZWs here indicate a cluster of ice stream grounding-line stabilizations in this more restricted, trough-narrowing setting. It was during this phase, in the Minch straits between the headlands of North Lewis and Cape Wrath, that the ice-stream/ice-shelf terminus transitioned from being unconfined to topographically confined – receiving both lateral and longitudinal buttressing support. This process is well captured in modelling simulations (of others) as the 'stagnation phase' of Minch ice-stream retreat. We note that this phase of relative ice-stream stability occurred during a ~1000-year period of relatively uniform full-glacial climate, centred c. 24 ka BP, seen in Greenland ice-core records, and coincident with the timing of Heinrich Event 2.

© 2021 The Authors. *Journal of Quaternary Science* Published by John Wiley & Sons Ltd

8. Once fully confined by the landmasses on either side of the North Minch, after ~23 ka BP, ice stream retreat was episodic and more predictable with large GZWs deposited during grounding-line stabilizations across the full trough width. In this phase, we suggest intermittent ice-stream stability across a relatively uniform bed profile was aided by ice-shelf buttressing – with peaks in lateral drag retarding flow and promoting GZW formation at trough narrowings (c. 22, 21 and 20 ka BP).
9. Around ~20–19 ka BP the style and tempo of ice-sheet retreat in the NW sector changed significantly, heralded by a phase of rapid uninterrupted ice-stream retreat or ice-shelf collapse totalling ~500 km^2 in area. Soon after, and no later than ~18.5 ka BP, the western Minch became ice free with a large marine embayment opening between the mid-trough bedrock high and eastern Lewis. By inference, the ice-mass on Lewis would have become glaciologically independent from the mainland Scotland-centred ice sheet at this time, following the collapse of the connecting ice stream/ice shelf. According to our dating evidence, the independent Lewis ice cap fluctuated in size c. 18.5–19.5 ka BP, forming conspicuous moraines close to the Atlantic coast – possibly a re-equilibration response to the dynamic events in the Minch.
10. The ice-stream probably remained quasi-stable in the east Minch trough for a further ~1 ka, forming relatively small GZWs (10–15) and hosting a partially confined ice shelf. En-masse retreat occurred abruptly, perhaps catastrophically, sometime between c. 18.5 and 17 ka BP, caused when the calving front reached the grounding line (at GZW15) prompting a second ice-shelf (or ice-tongue) collapse. This led to the formation of a deep 'calving bay' with a wide calving front that accelerated ice loss to the ocean. The deepening and widening trough bathymetry in the Inner Minch, inshore of GZW 15, provided optimal conditions for rapid 'runaway' grounding-line destabilization via marine ice-sheet instability. This finding is well supported by modelling simulations (of others). We propose that, once underway, grounding-line retreat proceeded in an uninterrupted fashion until stabilization occurred in the fjords between Skye, Raasay and the mainland c. 17 ka BP. We estimate the collapsed ice-front area in the Inner Minch was c. 800 km^2, with the majority of this loss probably occurring within a few decades.
11. Ice sheet lobes readvanced substantially offshore NW mainland Scotland sometime between ~19 and ~17 ka BP, leaving a clear geomorphological imprint at the seabed. This coherent 'East Minch Readvance' affected an area from near Cape Wrath (58.5°N) to the Gairloch (Rubha Reidh) peninsula (57.8°N) – a distance of over 150 km. Based on strong morphostratigraphic relationships and TCN dates on retreat, this readvance is constrained to around the time, or shortly after, the collapse of the ice-front/ice shelf in the east Minch trough (at ~18.5–17 ka BP). We see striking parallels between this event and the glacier surges seen in the immediate aftermath of the Larsen A and B ice-shelf collapses, Antarctic Peninsula – a direct response to altered stress fields and new boundary conditions in the wake of widespread ice-front collapse.
12. The period of instability-driven rapid ice-front retreat in the Inner Minch had ended by ~17 ka BP. The confining topography and shallower water depths allowed large tidewater glaciers to maintain equilibrium and remain relatively stable close to the terrestrial transition – with most glaciers occupying fjord-mouth settings in Skye and Wester Ross by 16.0–15.6 ka BP.
13. A separate ice cap in the northern Outer Hebrides continued to retreat across low ground towards the mountainous areas of west Lewis and Harris. The moraine record is relatively sparse here but we constrain oscillations of the ice cap margin c. 18.5–17.5 ka BP, associated with the impounding of glacial lakes in west Lewis. The youngest dated moraines suggest glacier reinvigoration at the onset of Heinrich Stadial 1. We propose final glacier retreat and disappearance on Lewis by ~15–16 ka BP, although firm dating constraints are lacking.
14. Between 16 and 15 ka BP the much-reduced BIIS underwent a regional ice-sheet oscillation in NW mainland Scotland, depositing a prominent series of partly terrestrial, partly subaqueous moraines during the WRR. Collective dating evidence indicates that post-readvance retreat had initiated by ~15.5 ka, several centuries before the rapid warming at the onset of GI-1.
15. By 14.7 ka BP, at the termination of GS-2, the surviving remnants of the ice sheet in mainland NW Scotland had separated into small ice fields and mountain ice caps. The pattern and timing of this final ice-mass-decay phase in Highland Scotland is much debated. Our new dating evidence places glaciers in NW coast catchments delivering outwash sediment to coastal deltas c. 14.3 ka BP during a marine highstand which we equate with the global eustatic event Meltwater Pulse 1A, securely dated (by others) at 14.31–14.65 ka BP.

Stepping back from the geographically framed findings, our work on the NW sector of the former BIIS shows the role of ice streams in ice-sheet evolution to be complex but mechanistically important. During phases of ice-sheet build up and advance, the Minch Ice Stream initially acted as a major ice-sheet artery – transferring mass, regulating flow and promoting extension of the ice sheet on to the outermost continental shelf. By contrast, once deglaciation was underway – perhaps triggered by external climatic or sea-level drivers – the ice stream acted, at times, as a major weakness within the ice sheet, something of an *Achilles' Heel*. Unsupported ice shelves, grounding-line fluctuations and high-flux tidewater margins coupled with shoreward-deepening bathymetry, variable trough geometry and bed strength characteristics all made the Minch ice stream prone to marine ice-sheet instability and collapse as it waned, even without additional external forcing factors. We find that these events irrevocably altered the flow pattern, configuration and flux regulation of the ice sheet during the latter stages of deglaciation ultimately hastening its demise.

Although commonly referred to by the community as the '*Late Weichselian*' British-Irish Ice Sheet, the early advance of the ice sheet's NW sector, determined in this work, places its maximal extent firmly in MIS 3 (=Mid-Weichselian) at ~30 ka BP. This fact, coupled with the consensus view that *most,* if not all, BIIS sectors reached their maximal extents early in MIS 2 (~23–27 ka BP), leads us to recommend adoption of the term '*Mid to Late Weichselian (Ice Sheet) Glaciation*' in the UK, or simply 'MIS 2–3 glaciation', to avoid chrono-stratigraphical ambiguity.

Finally, regarding the BIIS, we propose moving away from the traditional concept of a simple 'Late Weichselian' ice-sheet glaciation with emphasis on the LGM, towards a semi-continuous but pulsed glaciation waxing and waning dynamically throughout the last glacial cycle with periods of expansive ice-sheet glaciation in Scotland interspersed with more restricted ice-cap or tidewater/fjordic glaciation. In support of selected previous work, we find that the general rhythm of BIIS growth and decay was governed by sub-millennial-scale climatic cycles,

© 2021 The Authors. *Journal of Quaternary Science* Published by John Wiley & Sons Ltd

global Dansgaard–Oeschger events, over the last ~45 000 years. But importantly, in addition, we find that internal instabilities in this marine ice-stream-dominated sector – conditioned by local topographic factors, tidewater dynamics and glaciological feedbacks – drove the tempo of higher frequency events probably on decadal to centennial timescales.

Supporting information

Additional supporting information can be found in the online version of this article.

Figure S1: Sedimentology, geochronology and geophysical properties of seabed core JC123-035VC. From left to right: X-radiograph, interpreted lithofacies boundaries, lithological log, main lithofacies codes, P-wave velocity, gamma-ray attenuation (density), magnetic susceptibility and undrained shear strength values all plotted on same depth scale. Ages of AMS-dated samples given in radiocarbon years (italic) and calibrated yrs BP (bold font) (see Table 8). Geophysical properties data measured using a Geotek MSCL-S at 2 cm intervals. Gaps are missing data (end caps).

Figure S2: Sedimentology, geochronology and geophysical properties of seabed core JC123-036VC. From left to right: X-radiograph, interpreted lithofacies boundaries, lithological log, main lithofacies codes, P-wave velocity, electrical resistivity, gamma-ray attenuation (density) and magnetic susceptibility values all plotted on same depth scale. Ages of AMS-dated samples given in radiocarbon years (italic) and calibrated yrs BP (bold font) (see Table 8). Geophysical properties data measuredusing a Geotek MSCL-S at 2 cm intervals. Gaps are missing data (end caps).

Figure S3: Sedimentology, geochronology and geophysical properties of seabed core JC123-044VC. From left to right: positive X-radiograph, interpreted lithofacies boundaries, lithological log, main lithofacies codes, P-wave velocity, electrical resistivity, gamma-ray attenuation (density) and magnetic susceptibility values all plotted on same depth scale. Ages of AMS-dated samples given in radiocarbon years (italic) and calibrated years BP (bold font) with uncertainties (see Table 8). Geophysical properties data measured using a Geotek MSCL-S at 2 cm intervals. Gaps are missing data (end caps). Note: see text for explanation and relevance of chronology.

Figure S4: Sedimentology, geochronology and geophysical properties of seabed cores JC123-018VC. From left to right: positive X-radiograph, interpreted lithofacies boundaries, lithological log, main lithofacies codes, P-wave velocity, gamma-ray attenuation (density) and magnetic susceptibility values all plotted on same depth scale. Age of AMS-dated sample in radiocarbon years (italic) and calibrated years BP (bold font) with uncertainties (see Table 8). Geophysical properties data measured using a Geotek MSCL-S at 2 cm intervals. Gaps are missing data (end caps).

Figure S5: GZW15 – evidence of iceberg scouring and former ice-shelf breakup. A: Hillshaded surface model of MBES data (collected by MCA/UKHO), showing GZW15 and its association with the large submarine bedrock high – the East Shiant Bank. B: Close-up of MBES data, highlighting strongly iceberg-scoured GZW surface. SBP line and core site also shown (see Fig. 27). C: Bathymetric profile across GZW15 (perpendicular to crestline) showing typical geomorphology; red = Q3 profile; green =median; Blue = Q1 profile. D: Scatter plot of ploughmark width vs ploughmark depth (incision into seabed). Note the different width : depth profiles predominantly relating to two different ploughmark types: u- and v-shaped. E: Typical cross profiles of u- and v-shaped iceberg ploughmarks on GZW15. F: Rose diagram showing preferred NNE-NE orientation of iceberg scours on GZW15.

Figure S6: Sedimentology and geophysical properties of seabed core JC123-031PC. From left to right: positive X-radiograph, interpreted lithofacies boundaries, lithological log, main lithofacies codes, P-wave velocity, gamma-ray attenuation (density) and magnetic susceptibility values all plotted on same depth scale. Geophysical properties data measured using a Geotek MSCL-S at 2 cm intervals. Gaps are missing data (end caps).

Figure S7: (above) sedimentology, geophysical properties and acoustic stratigraphy of seabed core JC123-029PC, Sound of Raasay, Inner Minch. From left to right: positive X-radiograph, interpreted lithofacies boundaries, lithological log, main lithofacies codes, magnetic susceptibility and P-wave velocity values all plotted on same depth scale. Ages of AMS-dated sample in radiocarbon years (italic) and calibrated years BP (bold font) with uncertainties (see Table 8). Geophysical properties data measured using a Geotek MSCL-S at 2 cm intervals. Gaps are missing data (end caps). Note the break between 80-300 cm to allow for Figure to be scaled appropriately on printed page.

Supplementary Data Table S1. Table S2:
Bayesian age-modelled boundaries: Minch Ice Stream (main BIIS).

Table S3: Bayesian age-modelled boundaries: Lewis (Outer Hebrides)- ice mass.

Acknowledgements. This work was supported by the UK Natural Environment Research Council (NERC) consortium grant NE/J009768/1, the NERC Cosmogenic Isotope Analysis Facility, and NERC Radiocarbon Facility. We thank staff at the SUERC AMS Laboratory, East Kilbride, for carbon, beryllium and chlorine isotope measurements. We thank the BGS Marine Operations team (vibrocorer) and NOC/NMEP team (piston corer) for their help during NERC Science Cruise JC123. We thank the master and crew of the *RRS James Cook* (JC123). We also thank the landowners and communities of Assynt, NW Sutherland, Raasay and Lewis for providing access to land for the purposes of this research. James Shreeve and Briony Shreeve (Geotek) are thanked for assistance with X-radiography data acquisition. Use of EMODnet Bathymetry Consortium (2018) data is acknowledged. Figure 21 contains MBES data collected by BGS as part of the MAREMAP project. Figure 24 contains Maritime and Coastguard Agency MBES data (Crown Copyright), collected as part of the UKHO Civil Hydrography Programme; its use is gratefully acknowledged. IHS Kingdom Suite was provided under the University Grant Programme 2018-19. D.D. publishes with the permission of the Executive Director, British Geological Survey. Martyn Stoker is thanked for advice and assistance during the early stages of this project. We thank the JQS Special Editor Arjen Stroeven and Chief Editor Neil Roberts for their patience and generosity with this extended contribution. We also thank Martin Margold and an anonymous reviewer for their extremely helpful and thorough comments on an earlier version of the manuscript.

Data availability statement

All marine geological data will be available via the British Geological Survey online data repository: https://www.bgs.ac.uk/geological-data/national-geoscience-data-centre/. All other data will be made available upon reasonable request (to the lead author).

References

Andersen K, Svensson A, Johnsen SJ, *et al.* 2006. The Greenland Ice Core Chronology 2005, 15-42 ka. Part 1: constructing the time scale. *Quaternary Science Reviews* **25**: 3246–3257.

Applegate PJ, Urban NM, Keller K, *et al.* 2012. Improved moraine age interpretations through explicit matching of geomorphic process models to cosmogenic nuclide measurements from single landforms. *Quaternary Research* **77**: 293-304.

Asmerom Y, Polyak VJ, Lachniet, MS. 2017. Extrapolar climate reversal during the last glaciation. *Scientific Reports* **7**: 7157.

© 2021 The Authors. *Journal of Quaternary Science* Published by John Wiley & Sons Ltd

Baden-Powell DEW. 1938. On the glacial and interglacial marine beds of northern Lewis. *Geological Magazine* **75**: 395-409.

Balco G, Stone JO, Lifton NA, *et al*. 2008. A complete and easily accessible means of calculating surface exposure ages or erosion rates from 10-Be and 26-Al measurements. *Quaternary Geochronology* **3**: 174-195.

Balco G, Briner J, Finkel RC, *et al*. 2009. Regional beryllium-10 production rate calibration for late-glacial northeastern North America. *Quaternary Geochronology* **4**: 93-107.

Ballantyne CK. 2006. Loch Lomond Stadial glaciers in the Uig Hills, western Lewis, Scotland. *Scottish Geographical Journal* **122**: 256–273.

Ballantyne CK. 2010. Extent and deglacial chronology of the last British–Irish Ice Sheet: implications of exposure dating using cosmogenic isotopes. *Journal of Quaternary Science* **25**: 515-534.

Ballantyne CK. 2012. Chronology of glaciation and deglaciation during the Loch Lomond (Younger Dryas) Stade in the Scottish Highlands: implications of recalibrated ^{10}Be exposure ages. *Boreas* **41**: 513-526.

Ballantyne CK, Hall AM. 2008. The altitude of the last ice sheet in Caithness and east Sutherland, Northern Scotland. *Scottish Journal of Geology* **44**: 169-181.

Ballantyne CK, Small D. 2019. The last Scottish ice sheet. *Earth and Environmental Science Transactions of the Royal Society of Edinburgh* **110**: 93-131.

Ballantyne CK, Schnabel C, Xu S. 2009. Readvance of the last British-Irish Ice Sheet during Greenland Interstade 1 (GI-1): the Wester Ross Readvance, NW Scotland. *Quaternary Science Reviews* **28**: 783-789.

Ballantyne CK, Fabel D, Gheorghiu D, *et al*. 2017. Late Quaternary glaciation in the Hebrides sector of the continental shelf: cosmogenic nuclide dating of glacial events on the St Kilda archipelago. *Boreas* **46**: 605-621.

Batchelor C, Dowdeswell J. 2015. Ice-sheet grounding-zone wedges (GZWs) on high-latitude continental margins. *Marine Geology* **363**: 65-92.

Bickerdike HL, Evans DJA, Stokes CR, *et al*. 2018. The glacial geomorphology of the Loch Lomond (Younger Dryas) Stadial in Britain: a review. *Journal of Quaternary Science* **33**: 1-54.

Boomer I, von Grafenstein U, Moss A. 2012. Lateglacial to early Holocene multiproxy record from Loch Assynt, NW Scotland. *Proceedings of the Geologists' Association* **123**: 109-116.

Bowen DQ, Phillips FM, McCabe AM, *et al*. 2002. New data for the Last Glacial Maximum in Great Britain and Ireland. *Quaternary Science Reviews* **21**: 89–101.

Bradwell T. 2010. Strath Kanaird: Glaciofluvial terraces and Lateglacial sea levels. In *The Quaternary of Western Sutherland and Adjacent Areas: Field Guide*, Lukas S, Bradwell T, eds. Quaternary Research Association: London; 123-128.

Bradwell T. 2013. Identifying palaeo-ice-stream tributaries on hard beds: mapping glacial bedforms and erosion zones in NW Scotland. *Geomorphology* **201**: 397–414.

Bradwell T, Stoker M, Larter R. 2007. Geomorphological signature and flow dynamics of the Minch palaeo-ice stream, NW Scotland. *Journal of Quaternary Science* **22**: 609–617,

Bradwell T, Stoker MS, Golledge NR, *et al*. 2008a. The northern sector of the last British Ice Sheet: maximum extent and demise. *Earth-Science Reviews* **88**: 207-226.

Bradwell T, Fabel D, Stoker M, *et al*. 2008b. Ice caps existed throughout the Lateglacial Interstadial in northern Scotland. *Journal of Quaternary Science*, **23**: 401-407.

Bradwell T, Stoker MS. 2015a. Submarine sediment and landform record of a palaeo-ice stream within the British–Irish Ice Sheet. *Boreas*, **44**: 255-276.

Bradwell T, Stoker M. 2015b. Asymmetric ice-sheet retreat pattern around northern Scotland revealed by marine geophysical surveys. *Earth and Environmental Science Transactions of the Royal Society of Edinburgh* **105**: 1-26.

Bradwell T, Stoker MS. 2016. Glacial sediment and landform record offshore NW Scotland: a fjord–shelf–slope transect through a Late Quaternary mid-latitude ice-stream system. *Geological Society of London* **46**: 421-428.

Bradwell T, Small D, Fabel D, *et al*. 2019. Ice-stream demise dynamically conditioned by trough shape and bed strength. *Science Advances* **5**: eaau1380.

Bradwell T, Small D, Fabel D, *et al*. this issue. Pattern, style and timing of British–Irish Ice Sheet retreat: Shetland and northern North Sea sector. *Journal Quaternary Science*. in press.

British Geological Survey (BGS). 1990. *Sutherland. Sea-Bed Sediments and Quaternary Geology. 1:250 000 Offshore Map Series*. British Geological Survey: Keyworth.

Bromley GR, Putnam AE, Rademaker KM, *et al*. 2014. Younger Dryas deglaciation of Scotland driven by warming summers. *Proceedings of the National Academy of Sciences, USA* **111**: 6215-6219.

Bromley G, Putnam A, Borns HW, *et al*. 2018. Interstadial rise and Younger Dryas demise of Scotland's last ice fields. *Paleoceanography and Paleoclimatology* **33**: 412-429.

Bronk Ramsey C. 2009a. Dealing with outliers and offsets in radiocarbon dating. *Radiocarbon* **51**: 1023-1045.

Bronk Ramsey C. 2009b. Bayesian analysis of radiocarbon dates. *Radiocarbon* **51**: 337-360.

Bronk Ramsey C. 2013. OxCal 4.3. Manual [online] available at: https://c14.arch.ox.ac.uk/oxcalhelp/hlp_contents.html

Borchers B, Marrero S, Balco G, *et al*. 2016. Geological calibration of spallation production rates in the CRONUS-Earth project. *Quaternary Geochronology* **31**: 188–198.

Boulton GS, Dongelmans PW, Punkari M, *et al*. 2001. Paleoglaciology of an ice sheet through the Weichselian. *Quaternary Science Reviews* **20**: 591-625.

Boulton GS, Hagdorn M. 2006. Glaciology of the British Isles Ice Sheet during the last glacial cycle: form, flow, streams and lobes. *Quaternary Science Reviews* **25**: 3359-3390.

Callard SL, Ó Cofaigh C, Benetti S, *et al*. 2018. Extent and retreat history of the Barra Fan Ice Stream offshore western Scotland and NORTHERN IRELAND during the last glaciation. *Quaternary Science Reviews* **201**: 280-302.

Carlson A, Clark PU. 2012. Ice sheet sources of sea level rise and freshwater discharge during the last deglaciation. *Reviews of Geophysics* **50**: RG4007.

Child D, Elliott G, Mifsud C, *et al*. 2000. Sample processing for earth science studies at ANTARES. *Nuclear Instruments and Methods in Physics Research Section B: Beam Interactions with Materials and Atoms* **172**: 856-860.

Chiverrell RC, Thomas GSP. 2010. Extent and timing of the Last Glacial Maximum (LGM) in Britain and Ireland: a review. *Journal of Quaternary Science* **25**: 535-549.

Chiverrell RC, Smedley RK, Small D, *et al*. 2018. Ice margin oscillations during deglaciation of the northern Irish Sea Basin. *Journal of Quaternary Science* **33**: 739-762.

Clark CD, Hughes ALC, Greenwood SL, *et al*. 2012. Pattern and timing of retreat of the last British–Irish Ice Sheet. *Quaternary Science Reviews*, **44**: 112-146.

Clark CD, Ely JC, Greenwood SL, *et al*. 2018. BRITICE Glacial Map, Version 2: a map and GIS database of glacial landforms of the last British–Irish Ice Sheet. *Boreas* **47**: 11-27.

Clark PU, Dyke AS, Shakun JD, *et al*. 2009. The Last Glacial Maximum. *Science* **325**: 710-714.

Croudace IW, Rothwell RG. 2015. *Micro-XRF Studies of Sediment Cores: Applications of a non-destructive tool for the environmental sciences*. Springer Science: London.

De Conto RM, Pollard D. 2016. Contribution of Antarctica to past and future sea-level rise. *Nature* **531**: 591–597.

Deschamps P, Durand N, Bard E, *et al*. 2012. Ice-sheet collapse and sea-level rise at the Bølling warming 14,600 years ago. *Nature* **483**: 559-64.

Dowdeswell JA, Bamber JL. 2007. Keel depths of modern Antarctic icebergs and implications for sea-floor scouring in the geological record. *Marine Geology* **243**: 120-131.

Dowdeswell JA, Canals M, Jakobsson M, *et al*. (eds). 2016. *Atlas of submarine glacial landforms: Modern, Quaternary and Ancient*. Geological Society: London.

Dowdeswell JA, Ottesen D, Forwick M. 2016. Grounding-zone wedges on the western Svalbard shelf. In Dowdeswell JA *et al*. (eds) *Atlas of Submarine Glacial Landforms: Modern, Quaternary and Ancient*. Geological Society: London; 233-234.

Duller GAT, Wintle AF, Hall AM. 1995. Luminescence dating and its application to key pre-Late Devensian sites in Scotland. *Quaternary Science Reviews* **14**, 495-519.

© 2021 The Authors. *Journal of Quaternary Science* Published by John Wiley & Sons Ltd

Emery AR, Hodgson DM, Barlow NLM, *et al*. 2019. Topographic and hydrodynamic controls on barrier retreat and preservation: An example from Dogger Bank, North Sea, *Marine Geology* **416**: 105981.

EMODnet Bathymetry Consortium. 2018. EMODnet Digital Bathymetry (DTM). https://doi.org/10.12770/c7b53704-999d-4721-b1a3-04ec60c87238

Everest JD, Bradwell T, Fogwill CJ, *et al*. 2006. Cosmogenic Be-10 age constraints from the Wester Ross Readvance Moraine: insights into British Ice Sheet behaviour. *Geografiska Annaler* **88A**: 9-18.

Everest J, Kubik P. 2006. The deglaciation of eastern Scotland: cosmogenic ^{10}Be evidence for a Lateglacial stillstand. *Journal of Quaternary Science* **21**: 95-104.

Everest JD, Bradwell T, Stoker M, *et al*. 2013. New age constraints for the maximum extent of the last British–Irish Ice Sheet (NW sector). *Journal of Quaternary Science* **28**: 2-7.

Fabel D, Ballantyne CK, Xu S. 2012. Trimlines, blockfields, mountain-top erratics and the vertical dimensions of the last British–Irish Ice Sheet in NW Scotland. *Quaternary Science Reviews*, **55**: 91-102.

Finlayson A, Golledge NR, Bradwell T, *et al*. 2011. Evolution of a Lateglacial mountain ice cap in northern Scotland. *Boreas* **40**: 536-554.

Fyfe JA, Long D, Evans D. 1993. *United Kingdom Offshore Regional Report: Geology of the Malin-Hebrides Sea Area*. HMSO for the British Geological Survey: London.

Gale A, Dalton CA, Langmuir CH, *et al*. 2013. The mean composition of ocean ridge basalts. *Geochemistry, Geophysics, Geosystems* **14**: 489–518.

Gandy N, Gregoire LJ, Ely JC, *et al*. 2018. Marine ice-sheet instability and ice-shelf buttressing of the Minch Ice Stream, northwest Scotland. *The Cryosphere* **12**: 3635-3651.

Gandy N, Gregoire LJ, Ely JC, *et al*. 2019. Exploring the ingredients required to successfully model the placement, generation and evolution of ice streams in the British-Irish Ice Sheet. *Quaternary Science Reviews* **223**: 105915.

Gordon JE. 1993. North West Coast of Lewis. In *The Quaternary of Scotland*, Gordon JE, Sutherland DG, eds. Chapman and Hall: London; 414-421.

Gordon JE, Sutherland DG. 1993. *The Quaternary of Scotland*. Geological Conservation Review Series. Chapman and Hall: London.

Golledge NR, Hubbard AL, Sugden DE. 2008. High-resolution numerical simulation of Younger Dryas glaciation in Scotland. *Quaternary Science Reviews* **27**: 888-904.

Golledge N. 2010. Glaciation of Scotland during the Younger Dryas Stadial: a review. *Journal of Quaternary Science* **25**: 550-566.

Golledge NR, Kowalewski, DE, Naish TR, *et al*. 2015. The multi-millennial Antarctic commitment to future sea level rise. *Nature* **526**: 421-425.

Hall AM. 1995. Was all of Lewis glaciated in the Late Devensian? *Quaternary Newsletter*, **76**: 1-7.

Hall AM, Peacock JD, Connell ER. 2003. New data for the Last Glacial Maximum in Great Britain and Ireland: a Scottish perspective on the paper by Bowen *et al*. (2002). *Quaternary Science Reviews* **22**: 1551-1554.

Hedges REM, Housley RA, Law IA, *et al*. 1989 Radiocarbon dates from the Oxford AMS system: archaeometry datelist 9. *Archaeometry* **31**: 207-234.

Hemming SR. 2004. Heinrich events: Massive late Pleistocene detritus layers of the North Atlantic and their global climate imprint. *Reviews of Geophysics* **42**: RG1005.

Heyman J, Applegate PJ, Blomdin R, *et al*. 2016. Boulder height - exposure age relationships from a global glacial ^{10}Be compilation. *Quaternary Geochronology* **34**: 1-11.

Hibbert FD, Austin WEN, Leng MJ, *et al*. 2010. British Ice Sheet dynamics inferred from North Atlantic ice-rafted debris records spanning the last 175 000 years. *Journal of Quaternary Science* **25**: 461-482.

Hiemstra JF, Shakesby RA. Vieli A. 2015. Late Quaternary glaciation in the Hebrides sector of the continental shelf. *Boreas* **44**: 178-196.

Hogan KA, Ó Cofaigh C, Jennings AE, *et al*. 2016. Deglaciation of a major palaeo-ice stream in Disko Trough, West Greenland. *Quaternary Science Reviews*, **147**: 5-26.

Hubbard AL, Bradwell T, Golledge NR, *et al*. 2009. Dynamic cycles, ice streams and their impact on the extent, chronology and deglaciation of the British-Irish ice sheet. *Quaternary Science Reviews* **28**: 758-776.

Hughes ALC, Greenwood SL, Clark CD. 2011. Dating constraints on the last British-Irish Ice Sheet: a map and database. *Journal of Maps* **7**: 156-184.

Hughes ALC, Clark CD, Jordan CJ. 2014. Flow pattern evolution of the last British Ice Sheet. *Quaternary Science Reviews* **89**: 148-68.

Hughes ALC, Gyllencreutz R, Lohne ØS, *et al*. 2016. The last Eurasian ice sheets – a chronological database and time-slice reconstruction, DATED-1. *Boreas* **45**: 1-45.

IPCC. 2018. *Global Warming of 1.5°C. An IPCC Special Report et al*. Masson-Delmotte V., eds. IPCC: New York.

Jakobsson M, O'Regan MO. 2016. Deep iceberg ploughmarks in the Central Arctic Ocean. *In Atlas of Submarine Glacial Landforms: Modern, Quaternary and Ancient*, Dowdeswell JA *et al*., eds. Geological Society: London; 287-288.

Jennings AE, Andrews JT, Ó Cofaigh C, *et al*. 2018. Baffin Bay paleoenvironments in the LGM and HS1: Resolving the ice-shelf question. *Marine Geology* **402**: 5-16.

Jones RS, Small D, Cahill N, *et al*. 2019. iceTEA: Tools for plotting and analysing cosmogenic-nuclide surface-exposure data from former ice margins. *Quaternary Geochronology* **51**: 72-86.

Judd A, Hovland M. 2009. *Seabed Fluid Flow: the impact on geology, biology and the marine environment*. Cambridge University Press: Cambridge.

Kaplan MR, Strelin JA, Schaefer JM, *et al*. 2011. In-situ cosmogenic 10-Be production rate at Lago Argentino, Patagonia: Implications for late-glacial climate chronology. *Earth and Planetary Science Letters* **309**: 21–32.

Kirk W, Godwin H. 1963. A Late-glacial site at Loch Droma, *Ross and Cromarty. Transaction of the Royal Society of Edinburgh* **65**: 225-248.

Kleman J, Borgström I. 1996. Reconstruction of palaeo-ice sheets: the use of geomorphological data. *Earth Surface Processes and Landforms* **21**: 893-909.

Kleman J, Glasser N. 2007. The subglacial thermal organization (STO) of ice sheets. *Quaternary Science Reviews* **26**: 585–597.

Knutz PC, Austin WEN, Jones EWJ. 2001. Millennial-scale depositional cycles related to British Ice Sheet variability and North Atlantic palaeo-circulation since 45 kyr BP, Barra Fan, UK margin. *Paleoceanography* **16**: 53-64.

Knutz PC, Hall IR, Zahn R, *et al*. 2002. Multidecadal ocean variability and NW European ice sheet surges during the last deglaciation. *Geochemistry Geophysics Geosystems* **3**: 1-9.

Kohl CP, Nishiizumi K. 1992. Chemical isolation of quartz for measurement of *in situ* -produced cosmogenic nuclides. *Geochimica et Cosmochimica Acta*, **56**: 3583-3587.

Krabbendam M, Bradwell T. 2014. Quaternary evolution of glaciated gneiss terrains: pre-glacial weathering vs. glacial erosion. *Quaternary Science Reviews* **95**: 20-42.

Lambeck K, Purcell A, Zhao J, *et al*. 2010. The Scandinavian Ice Sheet: from MIS 4 to the end of the Last Glacial Maximum. *Boreas* **39**: 410-435.

Lambeck K, Rouby H, Purcell A, *et al*. 2014. Sea level and global ice volumes from the Last Glacial Maximum to the Holocene. *Proceedings of the National Academy of Sciences, USA* **111**: 15296–15303.

Larsen ES, Gottfried D. 1960. Uranium and thorium in selected suites of igneous rocks. *American Journal of Science* **258A**: 151–169.

Larsen E, Sejrup HP, Janocko J, *et al*. 2000. Recurrent interaction between the Norwegian Channel Ice Stream and terrestrial-based ice across southwest Norway. *Boreas* **29**: 185-203.

Lawson TJ. 1995. An analysis of sediments in caves in the Assynt area, NW Scotland. *Cave and Karst Science* **22**: 3-30.

Lawson TJ. 2010. The Allt nan Uamh valley and its caves: their significance for the chronology of glaciation and deglaciation of northern Scotland. In *The Quaternary of Western Sutherland and adjacent areas: Field Guide*, Lukas S, Bradwell T, eds. Quaternary Research Association: London; 165-168.

Lawson TJ, Young IR, Kitchener AC, *et al*. 2014. Middle and Late Devensian radiocarbon dates from the Uamh an Claonaite cave system in Assynt, Scotland. *Quaternary Newsletter* **133**: 4-10.

Leventer A, Domack E, Pike J, *et al*. 2006. Marine sediment record from the East Antarctic margin reveals dynamics of ice sheet recession. *GSA Today* **16**: 4-10.

© 2021 The Authors. *Journal of Quaternary Science* Published by John Wiley & Sons Ltd

Liu J, Milne GA, Kopp RE, *et al*. 2016. Sea-level constraints on the amplitude and source distribution of Meltwater Pule 1A. *Nature Geoscience* **9**: 130-134.

Lowe JJ, Rasmussen, SO, Bjorck S, *et al*. 2008. Synchronisation of palaeo-environmental events in the North Atlantic region during the Last Termination: a revised protocol recommended by the INTIMATE group. *Quaternary Science Reviews* **27**: 6-17.

Lowe J, Matthews I, Mayfield R, *et al*. 2019. On the timing of retreat of the Loch Lomond ('Younger Dryas') Readvance icefield in the SW Scottish Highlands and its wider significance. *Quaternary Science Reviews* **219**: 171-186.

Mackintosh AN, Verleyen E, O'Brien PE, *et al*. 2014. Retreat history of the East Antarctic Ice Sheet since the Last Glacial Maximum. *Quaternary Science Reviews*, **100**: 10-30.

MacLeod A, Palmer AP, Lowe JJ, *et al*. 2011. Timing of glacier response to Younger Dryas climatic cooling in Scotland. *Global and Planetary Change* **79**: 264-274.

Marrero SM. 2012. *Calibration of Cosmogenic Chlorine-36*. PhD thesis, New Mexico Institute of Mining and Technology.

Marrero SM, Phillips FM, Borchers B, *et al*. 2016. Cosmogenic nuclide systematics and the CRONUScalc program. *Quaternary Geochronology* **31**: 160-187.

McMillan, AA, Hamblin RJO, Merritt JW. 2011. *A lithostratigraphical framework for onshore Quaternary and Tertiary superficial deposits of Great Britain and the Isle of Man*. British Geological Survey Research Report, RR/10/03.

Merritt JW, Auton CA, Connell ER, *et al*. 2003. *Cainozoic Geology and Landscape Evolution of NE Scotland*. Memoir of the British Geological Survey. Sheets 66E, 67, 76E, 77, 86E, 87W 87E, 95, 96W, 96E and 97 (Scotland). British Geological Survey: Keyworth.

Merritt JW, Connell ER, Hall AM. 2017. Middle to Late Devensian glaciation of north-east Scotland: implications for the north-eastern quadrant of the last British–Irish Ice Sheet. *Journal of Quaternary Science* **32**: 276–294.

Merritt JW, Hall AM, Gordon JE, *et al*. 2019. Late Pleistocene sediments, landforms and events in Scotland: a review of the terrestrial statigraphic record. *Earth and Environmental Science Transactions of the Royal Society of Edinburgh* **110**: 39-91.

Ó Cofaigh C, Dowdeswell JA, Allen *et al*. 2005. Flow dynamics and till genesis associated with a marine-based Antarctic palaeo-ice stream. Quaternary Science Reviews **24**: 709-740.

Pantin, HM. 1991. *The sea-bed sediments around the United Kingdom*. British Geological Survey Research Report SB/90/1: London.

Pattyn F, Ritz C, Hanna E, *et al*. 2018. The Greenland and Antarctic ice sheets under 1.5C global warming. *Nature Climate Change* **8**: 1053-1061.

Peacock JD. 1984. *Quaternary Geology of the Outer Hebrides*. Report of the British Geological Survey: London.

Peck VL, Hall IR, Zahn R, *et al*. 2007. The relationship of Heinrich events and their European precursors over the past 60 ka BP: a multi-proxy ice-rafted debris provenance study in the North East Atlantic. *Quaternary Science Reviews* **26**: 862–875.

Peltier WR, Fairbanks RG. 2007. Global glacial ice volume and Last Glacial Maximum duration from an extended Barbados sea level record. *Quaternary Science Reviews* **25**: 3322-3337.

Pennington W, Haworth EY, Bonny AP, *et al*. 1972. Lake sediments in northern Scotland. *Philosophical Transactions of the Royal Society* **B264**: 191-294.

Peters JL, Benetti S, Dunlop P, *et al*. 2015. Maximum extent and dynamic behaviour of the last British-Irish Ice Sheet west of Ireland. *Quaternary Science Reviews* **128**: 48-68.

Peters JL, Benetti S, Dunlop P, *et al*. 2016. Sedimentology and chronology of the advance and retreat of the last British-Irish ice Sheet on the continental shelf west of Ireland. *Quaternary Science Reviews* **140**: 101-124.

Phillips FM, Argento DC, Balco G, *et al*. 2016. The CRONUS-Earth project: a synthesis. *Quaternary Geochronology* **31**: 119-154.

Phillips E, Cotterill C, Johnson K, *et al*. 2018. Large-scale glacitectonic deformation in response to active ice-sheet retreat across Dogger Bank (southern central North Sea) during the Last Glacial Maximum. *Quaternary Science Reviews*, **179**: 24-47.

Powell R, Dawber M, McInnes J, *et al*. 1996. Observations of the grounding-line area at a floating glacier terminus. *Annals of Glaciology* **22**: 217-223.

Praeg D, McCarron S, Dove D, *et al*. 2015. Ice sheet extension to the Celtic Sea shelf edge at the Last Glacial Maximum. *Quaternary Science Reviews*, **111**: 107-112.

Putnam AE, Schaefer JM, Barrell DJA, *et al*. 2010. In situ cosmogenic Be-10 production-rate calibration from the Southern Alps, New Zealand. *Quaternary Geochronology* **5**: 392-409.

Rasmussen SO, Seierstad IK, Andersen KK, *et al*. 2008. Synchronization of the NGRIP, GRIP, and GISP2 ice cores across MIS 2 and palaeoclimatic implications. *Quaternary Science Reviews* **27**: 18-28.

Rasmussen SO, Bigler M, Blockley SP, *et al*. 2014. A stratigraphic framework for abrupt climatic changes during the Last Glacial period based on three synchronized Greenland ice-core records: refining and extending the INTIMATE event stratigraphy. *Quaternary Science Reviews* **106**: 14-28.

Reimer PJ, Bard E, Bayliss A, *et al*. 2013. IntCal13 and Marine13 radiocarbon age calibration curves 0–50,000 years cal BP. *Radiocarbon* **55**: 1869-1887.

Ritchie JD, Ziska H, Johnson H, *et al*. 2011. *United Kingdom Offshore Regional Report: The Geology of the Faroe-Shetland Basin and Adjacent Areas*. HMSO for the British Geological Survey: London.

Roberts DH, Grimoldi E, Callard SL, *et al*. 2019. The mixed-bed glacial landform imprint of the North Sea Lobe in the western North Sea. *Earth Surface Processes and Landforms*, **44**: 1233-1258.

Roberts DH, Callard SL, Grimoldi E, *et al*. 2021. Deglaciation of the last British-Irish Ice Sheet in the North Sea Basin (Britice-Chrono: Transect 2). *Journal of Quaternary Science* (in press).

Robinson M, Ballantyne CK. 1979. Evidence for a glacial readvance pre-dating the Loch Lomond Advance in Wester Ross. *Scottish Journal of Geology* **15**: 271–277.

Scourse JD, Haapaniemi AI, Colmenero-Hidalgo E, *et al*. 2009. Growth, dynamics and deglaciation of the last British-Irish ice sheet: the deep-sea ice-rafted detritus record. *Quaternary Science Reviews* **28**: 3066-3084.

Scourse JD, Saher M, Van Landeghem KJJ, *et al*. 2019. Advance and retreat of the marine-terminating Irish Sea Ice Stream into the Celtic Sea during the Last Glacial: Timing and maximum extent. *Marine Geology* **412**: 53-68.

Seierstad IK, Abbott PM, Bigler M, *et al*. 2014. Consistently dated records from the Greenland GRIP, GISP2 and NGRIP ice cores for the past 104 ka reveal regional millennial-scale $\delta^{18}O$ gradients with possible Heinrich event imprint. *Quaternary Science Reviews* **106**: 29-41.

Sejrup HP, Larsen E, Landvik J, *et al*. 2000. Quaternary glaciations in southern Fennoscandia: evidence from southwestern Norway and the northern North Sea region. *Quaternary Science Reviews* **19**: 667-685.

Sejrup HP, Nygård A, Hall AM, *et al*. 2009. Middle and Late Weichselian (Devensian) glaciation history of south-western Norway, North Sea and eastern UK. *Quaternary Science Reviews* **28**: 370–380.

Sejrup HP, Hjelstuen BO, Dahlgren KIB, *et al*. 2005. Pleistocene glacial history of the NW European continental margin. *Marine and Petroleum Geology*, **22**: 1111-1129.

Sejrup HP, Clark CD, Hjelstuen BO. 2016. Rapid ice-sheet retreat triggered by ice stream debuttressing: Evidence from the North Sea. *Geology* **44**: 355-358.

Shennan I, Bradley S, Edwards R. 2018. Relative sea-level changes and crustal movements in Britain and Ireland since the Last Glacial Maximum. *Quaternary Science Reviews* **188**: 143-159.

Small D, Rinterknecht V, Austin W, *et al*. 2012. In situ cosmogenic exposure ages from the Isle of Skye, northwest Scotland: Implications for the timing of deglaciation and readvance from 15 to 11 ka. *Journal of Quaternary Science* **27**: 150-158.

Small D, Fabel D. 2015. A Lateglacial 10-Be production rate from glacial lake shorelines in Scotland. *Journal of Quaternary Science* **30**: 509-513.

Small D, Fabel D. 2016. Response to Bromley *et al*. "Comment on 'Was Scotland deglaciated during the Younger Dryas?' *Quaternary Science Reviews* **152**: 206-208.

Small D, Smedley RK, Chiverrell RC, *et al*. 2018. Trough geometry was a greater influence than climate-ocean forcing in regulating retreat of the marine-based Irish-Sea Ice Stream. *Geological Society of America Bulletin* **130**: 1981-1999.

© 2021 The Authors. *Journal of Quaternary Science* Published by John Wiley & Sons Ltd

Small D, Benetti S, Dove, D, *et al*. 2017. Cosmogenic exposure age constraints on deglaciation and flow behaviour of a marine-based ice stream in western Scotland, 21–16 ka. *Quaternary Science Reviews*, **167**: 30-46.

Smedley RK, Chiverrell RC, Ballantyne CK, *et al*. 2017a. Internal dynamics condition centennial-scale oscillations in marine-based ice-stream retreat. *Geology* **45**: 787-790.

Smedley RK, Scourse JD, Small D, *et al*. 2017b. New age constraints for the limit of the British-Irish Ice Sheet on the Isles of Scilly. *Journal of Quaternary Science* **32**: 48-62.

Smith DE, Barlow N, Bradley S, *et al*. 2018. Quaternary sea-level change in Scotland. *Earth and Environmental Science Transactions of the Royal Society of Edinburgh* **110**: 219-256.

Smith JA, Graham AGC, Post AL, *et al*. 2019. The marine geological imprint of Antarctic ice shelves. *Nature Communications* **10**: 5635.

Smith DE, Stewart IS, Harrison S, Firth CR. 2009. Late Quaternary neotectonics and mass movement in SE Raasay, Inner Hebrides, Scotland. *Proceedings of the Geologists' Association* **120**: 145–154.

Stern JV, Lisiecki LE. 2013. North Atlantic circulation and reservoir age changes over the past 41,000 years. *Geophysical Research Letters* **40**: 3963–3697.

Stoker MS. 1990. Glacially-influenced sedimentation on the Hebridean slope, northwestern United Kingdom. In *Glacimarine Environments: Processes and Sediments*, Dowdeswell JA, Scourse JD, eds. The Geological Society: London: 349-362.

Stoker MS, Holmes R. 1991. Submarine end-moraines as indicators of Pleistocene ice-limits off northwest Britain. *Journal of the Geological Society, London* **148**: 431-434.

Stoker MS, Bradwell T. 2005. The Minch palaeo-ice stream, NW sector of the British-Irish ice sheet. *Journal of the Geological Society* **162**: 425-428.

Stoker MS, Hitchen K, Graham CG. 1993. *United Kingdom Offshore Regional Report: The Geology of the Hebrides and West Shetland shelves, and adjacent deep-water areas*. HMSO for the British Geological Survey: London.

Stoker MS. Bradwell T, Wilson C, *et al*. 2006. Pristine fjord landsystem revealed on the seabed in the Summer Isles region, NW Scotland. *Scottish Journal of Geology* **42**: 89-99.

Stoker MS, Bradwell T, Howe JA, *et al*. 2009. Lateglacial ice-cap dynamics in NW Scotland: evidence from the fjords of the Summer Isles region. *Quaternary Science Reviews* **28**: 3161-3184.

Stoker MS, Balson PS, Long D, *et al*. 2011. *An overview of the lithostratigraphical framework for the Quaternary deposits on the United Kingdom continental shelf*. British Geological Survey Research Report, RR/11/03: London.

Stone JO, Ballantyne CK, Fifield LK. 1998. Exposure dating and validation of periglacial weathering limits, northwest Scotland. *Geology* **26**: 587-590.

Stone JO, Ballantyne CK. 2006. Dimensions and deglacial chronology of the Outer Hebrides Ice Cap, northwest Scotland: implications of cosmic ray exposure dating. *Journal of Quaternary Science* **21**: 75-84.

Stone JO, Ballantyne CK. 2012. Did ice caps exist on low ground in north-west Scotland during the Lateglacial Insterstade? *Journal of Quaternary Science* **27**: 297-306.

Stroeven AP, Hattestrand C, Kleman J, *et al*. 2016. Deglaciation of Fennoscandia. *Quaternary Science Reviews* **147**: 91–121.

Sutherland DG. 1984. The Quaternary deposits and landforms of Scotland and the neighbouring shelves: A review. *Quaternary Science Reviews* **3**: 157-254.

Sutherland DG. 1986. A review of Scottish marine shell radiocarbon dates, their standardization and interpretation. *Scottish Journal of Geology* **22**: 145-164.

Sutherland D, Walker M. 1984. A late Devensian ice-free area and possible interglacial site on the Isle of Lewis, Scotland. *Nature* **309**: 701-703.

Svensson A, Andersen K, Bigler M, *et al*. 2006. The Greenland Ice Core Chronology 2005, 15-42 ka. Part 2: comparison to other records. *Quaternary Science Reviews* **25**: 3258–3267.

Thomsen KJ, Murray AS, Bøtter-Jensen L. 2005. Sources of variability in OSL dose measurements using single grains of quartz. *Radiation Measurements* **39**: 47-61.

Whittington G, Hall AM. 2002. The Tolsta Interstadial, Scotland: correlation with D–O cycles GI-8 to GI-5? *Quaternary Science Reviews* **21**: 901-915.

Xu S, Dougans AB, Freeman SPHT, *et al*. 2010. Improved 10-Be and 26-Al AMS with a 5 MV spectrometer. *Nuclear Instruments and Methods in Physics Research, Section B: Beam Interactions with Materials and Atoms* **268**: 736-738.

Yokoyama Y, Esat TM, Thompson WG, *et al*. 2018. Rapid glaciation and a two-step sea level plunge into the Last Glacial Maximum. *Nature* **559**: 603-607.

Young NE, Schaefer JM, Briner JP, *et al*. 2013. A 10-Be production-rate calibration for the Arctic. *Journal of Quaternary Science* **28**: 515-526.

© 2021 The Authors. *Journal of Quaternary Science* Published by John Wiley & Sons Ltd